



# Sulfide to Sulfate Reaction Mechanism



### WATER POLLUTION CONTROL RESEARCH SERIES

The Water Pollution Control Research Reports describe the results and progress in the control and abatement of pollution in our Nation's waters. They provide a central source of information on the research, development, and demonstration activities in the Federal Water Quality Administration, in the U. S. Department of the Interior, through inhouse research and grants and contracts with Federal, State, and local agencies, research institutions, and industrial organizations.

A triplicate abstract card sheet is included in the report to facilitate information retrieval. Space is provided on the card for the user's accession number and for additional uniterms.

Inquires pertaining to Water Pollution Control Research Reports should be directed to the Head, Project Reports System, Planning and Resources Office, Office of Research and Development, Department of the Interior, Federal Water Quality Administration, Room 1108, Washington, D. C. 20242.

# ***Sulfide to Sulfate Reaction Mechanism***

A Study of the Sulfide to Sulfate Reaction Mechanism  
as it Relates to the Formation of Acid Mine Waters

by

Ohio State University  
Research Foundation  
Columbus, Ohio 43210

for the

FEDERAL WATER POLLUTION CONTROL ADMINISTRATION

DEPARTMENT OF THE INTERIOR

Program Number  
FWPCA Grant No. 14010 FPS

February 1970

This report has been reviewed by the Federal Water Pollution Control Administration and approved for publication. Approval does not signify that the contents necessarily reflect the views and policies of the Federal Water Pollution Control Administration.

## ABSTRACT

### THE SULFIDE TO SULFATE REACTION

by E. E. Smith and K. S. Shumate

A detailed study of the mechanisms and kinetics of the chemical reactions responsible for acid mine drainage has been made.

The mineralogical features of the solid phase reactant (pyrite) that determine its reactivity were described. The rate-limiting reactions and variables affecting the rate of these reactions were identified.

It was found that two basic oxidation modes are important: oxygenation, in which oxygen is the immediate oxidizing agent; and ferric ion (or microbiologically catalyzed) oxidation, in which ferric ions are the oxidants. From a knowledge of the dissolved oxygen, ferric/ferrous ratio, and total iron ion content at the reaction site, the reaction regime can be determined.

Kinetic equations were derived for both reaction modes. From these basic relationships the oxidation rate in real pyritic systems can be accurately predicted when conditions at the reaction site are known.

For a given pyrite surface, oxygenation rate is, for all practical purposes, dependent only on the oxygen concentration in the aqueous phase surrounding the reactive site on the pyrite surface. Ferric ion oxidation rate is determined by the ferric/ferrous ratio and free ferric ion concentration in solution, and is not affected by dissolved oxygen.

In a real system, the ferric/ferrous ratio is determined by a "relative" microbial activity; i.e., the number of bacteria per exposed pyrite surface. Bacterial activity is limited by pH and oxygen concentration as well as nutrient levels.

This report was submitted in fulfillment of Research Grant No. 14010 FPS between the Federal Water Pollution Control Administration and The Ohio State University Research Foundation.

---

Key Words: Mine Drainage/Coal Mine Drainage/Sulfides/Iron Sulfides/  
Pyrite/Ferrobacillus/Pollution Abatement/Industrial Wastes/  
Reaction Kinetics

# TABLE OF CONTENTS

	<u>Page</u>
Section 1      Conclusions and Recommendations	1
Section 2      Introduction	3
Section 3      Mineralogy	7
Classification of Pyritic Materials	7
Surface Area and Pore Size Distribution	10
Preparation of Sulfur Ball Samples	10
Identification of Intermediate Products	12
Section 4      Oxygenation	13
Experimental Equipment	13
Results of Preliminary Runs	15
Discussion of Preliminary Runs	18
Role of Water	18
Oxygen Concentration	20
High Pressure Oxygenation	22
Effect of pH	27
Effect of Various Anions and Cations	29
Section 5      Microbiology	31
Preliminary Experimental Phase	31
Apparatus and Growth Media	32
Results	35
Conclusions	38
Warburg Respirometer Oxidation Experiments	38
Objectives	39
Materials and Procedures	39
Results	39
Section 6      Ferric Ion Oxidation	49
Experimental Equipment	49
Experimental Procedure	51
Experimental Results	52
Low pH, High Sulfate Runs	52
Treatment of Data	52
Interpretation of Data	58

# TABLE OF CONTENTS - (Continued)

	<u>Page</u>
Combined Oxygenation and Ferric Ion Oxidation	60
Varying pH, Type and Concentration of Anion	62
Ionic Composition of Reaction Solution	67
Iron Complexes in Sulfate Solution	67
Iron Complexes in Chloride Solution	68
Anion Concentration and pH Effect on Kinetics	69
Appendix I    Related Studies	73
Determination of Ferric and Ferrous Ion Adsorption	73
Direct Measure of Adsorption	73
Adsorption from Streaming Current Measurement	73
Equation for Streaming Current	74
Experimental	76
Conclusions	76
Application of the Potentiostat to Pyrite Oxidation Studies	76
Inhibition Studies	77
Adsorption of Oxygen, Nitrogen, and Water on Pyrite	80
Appendix II   Calculation of Experimental Data for Ferric Ion Oxidation	91
Appendix III   Calculation of Ionic Composition	93
Sulfate Solution	93
Determination of $H^+$ Concentration	94
Calculation of $HSO_4^-$ Concentration	94
Calculation of $Fe^{+++}$ , $Fe^{++}$ , and Their Complexes	97
Chloride Solution	98
Appendix IV   Run Data, Ferric Ion Oxidation	103
Appendix V    Characteristics of Pyrite Samples	107
Acknowledgements	109

TABLE OF CONTENTS - (Continued)

	<u>Page</u>
References	111
List of Publications	113
Glossary of Terms	115
Abstract Cards	



## FIGURES

<u>Figure</u>		<u>Page</u>
1	Pore Volume Distribution, Museum Grade Pyrite and Sulfur Ball	11
2	Vapor Phase Oxidation Apparatus	14
3	Liquid Phase Oxidation Apparatus	14
4	Variable Pressure Apparatus	14
5	Oxidation Rate vs. Partial Pressure of Water	19
6	Oxidation Rate vs. % Relative Saturation	19
7	Oxidation Rate vs. Temperature	19
8	Oxidation Rate vs. Oxygen Concentration in Aqueous Phase	19
9	Oxidation Rate vs. Oxygen Concentration	25
10	Oxidation Rate vs. Mole % Nitrogen in Liquid	26
11	Oxidation Rate vs. pH	28
12	Culture Apparatus	33
13	Bacterial Count and Oxygen Uptake Rate vs. Time	36
14	Oxygen Uptake Curve	40
15	Oxygen Uptake Rate	41
16	Change in Cell Population with Time	43
17	Change of Microbial Oxidation Rate with Time	44
18	Oxygen Uptake Rate vs. Total Cell Population	45
19	Oxygen Uptake Rate vs. Pyrite to Water Ratio	47
20	Ferric Ion Oxidation Apparatus	50
21	Reciprocal Rate vs. Reciprocal (Ferric Concentration) <sup>1/2</sup>	56
22	Rate vs. EMF, McDaniels Sulfur Ball	56

# FIGURES - (Continued)

<u>Figure</u>		<u>Page</u>
23	Rate vs. EMF for Three Pyrite Samples	59
24	Rate vs. EMF in Sulfate Solution	63
25	Effect of Sulfate Concentration	64
26	Comparison of Rates in Sulfate and in Chloride Solution	65
27	Comparison of Rates in Sulfate and in Chloride Solution	66
28	Reciprocal Rate vs. Reciprocal (Free Ferric Ion Concentration) <sup>1/2</sup>	70
29	Potentiometer Setting vs. Current	78
30	Pyrite to Reference Voltage vs. Potentiometer Setting	79
31	Nitrogen Adsorption Isotherm on Museum Grade Pyrite at 77.3°K	81
32	Nitrogen Adsorption Isotherm on Sulfur Ball at 77.3°K	82
33	Nitrogen Adsorption Isotherm on Museum Grade Pyrite at 25.0°C	83
34	Nitrogen Adsorption Isotherm on Sulfur Ball at 25.0°C	84
35	Water Adsorption Isotherm on Museum Grade Pyrite at 25.0°C	85
36	Water Adsorption Isotherm on Sulfur Ball at 25.0°C	86
37	Oxygen Adsorption Rate on Sulfur Ball at 25°C	87

# TABLES

<u>Table</u>		<u>Page</u>
I	Liquid Phase Runs	16
II	Vapor Phase Runs	16
III	Variable Pressure Runs at 25°C	17
IV	High Pressure Runs at 25°C	23
V	Oxidation Rate vs. pH	28
VI	Rate vs. Concentration at EMF = 0.700	53
VII	Rate vs. EMF (Museum Grade Pyrite)	53
VIII	Rate vs. Iron Concentration (Sulfur Ball No. 2)	54
IX	Rate vs. Iron Concentration (McDaniels Sulfur Ball)	54
X	Rate vs. EMF (Sulfur Ball No. 2)	55
XI	Combined Oxygenation and Ferric Ion Oxidation	60
XII	Chemical Inhibition Tests	77
XIII	Oxygen Adsorption, Absorption and Desorption on Sulfur Ball	89
XIV	Stability Constants for Sulfate Solutions	97
XV	Stability Constants for Chloride Solutions	101
XVI	Rate Data, Sulfate Solution	103
XVII	Rate Data, Sulfate Solution, Iron Concentration Varies	105
XVIII	Rate Data, Sulfate Solution, Sodium Sulfate Added	105
XIX	Rate Data, Chloride Solution	106
XX	Rate Data, Chloride Solution, Iron Concentration Varies	106

## Section 1

### CONCLUSIONS AND RECOMMENDATIONS

#### Conclusions

The following major conclusions may be drawn from information obtained during the course of this project:

1. The principal mineralogical form of naturally occurring iron disulfide materials in Eastern coal mining areas is pyrite.
2. The major factor influencing reactivity of various types of pyritic material is surface area (texture), not trace elements or included minerals.
3. The rate-determining reaction in "natural" systems, in the absence of mass transport limitations, is an electron transfer between the oxidizing agent (oxygen or ferric ion) absorbed on the surface of pyrite, and the pyrite itself.
4. There are two modes of pyrite oxidation as determined by the immediate oxidizing agent; i.e., oxygen or ferric ions. Each oxidation mode is independent of the other. For a given pyrite surface, oxygenation rate is, for all practical purposes, dependent only on the oxygen concentration in the aqueous phase surrounding the reactive site on the pyrite surface and independent of other solute concentration. Ferric ion oxidation is primarily determined by the ferric/ferrous ratio and free ferric ion concentration, and is not affected by dissolved oxygen.
5. Kinetics for the oxygenation of pyrite have been experimentally determined as a function of (a) temperature, (b) oxygen concentration, (c) pH, (d) water partial pressure, (e) surface area (or texture), and (f) concentration of iron, sulfate, and other ions.
6. Kinetics of pyrite oxidation by ferric ions have been determined as a function of (a) ferric/ferrous ratio, (b) total iron concentration, and (c) free ferric ion and hydrogen ion concentration (qualitatively). A mechanism has been proposed, based on the competitive adsorption of ferric and ferrous ions, which correlates experimental rate data.

7. Ferric ion oxidation of pyrite is the chemical analogy of microbial-enhanced pyrite oxidation.
8. Significant microbial catalysis will occur only if the water-to-pyrite ratio is sufficiently high to provide for the required population of organisms.
9. Those factors which determine the reaction regime, either chemical or microbiological, have been described.
10. Pyrite oxidation rates can now be accurately predicted in terms of known and measureable variables. Basic relationships are now available for calculating the oxidation rate under natural conditions, regardless of oxygen concentration, pH, bacteria, and other environmental conditions. Major variables have been identified, and measurements necessary to permit calculation of oxidation rates described.

#### Recommendations

With the information now available, kinetics of pyrite oxidation in well-defined laboratory systems are reasonably well known. Application of these basic data are hampered by lack of knowledge of the physical, chemical, and biological conditions at the reactive site in real pyritic systems. Continuation and extension of basic field or "pilot" scale studies in which the kinetics of formation, desorption, and dispersal of oxidation products in a natural environment are being examined, is recommended.

Several aspects of the work described in this report require further investigation. The reactive specie in ferric ion oxidation has not been positively identified. Considering the reliability of stability constants and experimental data, free ferric ions or one of the ferric hydroxide complexes may be the reactive specie; neither can be eliminated from consideration on the basis of available data.

Additional information on the effect of pH and oxygen concentration on microbial activity is needed. The water-to-pyrite ratio at which microbial catalysis becomes a significant factor in pyrite oxidation should be better defined. These data are needed in order to designate more precisely the regime (oxygenation or ferric ion oxidation) that is determined by environmental conditions.

## Section 2

### INTRODUCTION

Effective methods for alleviating acid mine drainage can best be found and developed if an understanding of the kinetics and reactions responsible for acid mine drainage is available. Therefore the objective of this study was to determine the basic rate-limiting mechanism(s) and kinetics of pyrite oxidation.

The significance of this simple statement of objective can be illustrated by assuming that the objective was achieved. If this were so, all the variables that influence the rate of oxidation would be known, logical approaches to inhibiting the reaction could be deduced, and evaluation of oxidation rates for different pyritic systems could be precisely calculated in terms of the environmental conditions which exist at the reaction site.

It must be noted that a complete evaluation of a pyritic system (i.e., strip mine, gob pile, drift mine, etc.) also requires a description of the environment and kinetics of the dispersal of oxidation products. This expresses the relationship between this project and the "pilot scale" or basic field studies of the type now being conducted at The Ohio State University in which the environmental conditions at the reaction sites are being examined. Neither project can be effective without the other. The necessity of more basic information to help plan experiments and evaluate field data has become more evident as analysis of pyritic systems becomes more sophisticated. For example, the ferric/ferrous ratio and its relation to the kinetics of microbial-catalyzed systems is an essential bit of basic information for interpreting data from a natural system.

The experimental work performed under this project was limited to laboratory-scale operations. Physical rate-limiting parameters (other than reactive surface area) were eliminated or controlled. Experimental conditions were varied to develop kinetics of pyrite oxidation, not necessarily to duplicate "natural" environments. Although not specifically related to any one real system, the data obtained from this project provide the necessary input data for analysis of real systems.

Chronologically, mineralogical investigations were performed concurrently with a preliminary kinetic study to identify the reactants as well as the physical, chemical, and biological parameters influencing rate of pyrite oxidation. Chemical (or direct oxidation by oxygen, hereafter termed "oxygenation") as opposed to microbiological (oxidation by ferric ions) reactions, were examined initially. As the kinetics of the oxygenation reactions were established, microbial-enhanced reactions were compared to the chemical reactions from both a mechanistic and kinetic reference.

Since we believe that systems having ferric ions as the oxidizing medium are chemically analogous to microbiologically controlled systems, the kinetics of ferric ion systems were studied in detail.

The following report is separated into sections arranged in the same order as emphasis developed in the course of the project. This is not to imply that these works are unrelated, but is presented in this manner in order to most clearly discuss the results and significance of these areas of research.

To assist in following the subsequent discussions, it may be helpful to keep in mind the purpose behind each major phase of the project.

Phase One (Mineralogy) was undertaken to describe the materials and their properties that influence the oxidation of pyrite.

Phase Two (Oxygenation) was an attempt to define the chemical kinetics of pyrite oxygenation; first, to determine the nature of the rate-limiting reaction, and second, to quantitatively evaluate the physical and chemical parameters that influence the oxidation reaction.

The third phase (Microbiological, Ferric Ion Oxidation) was a study of the kinetics of microbial-enhanced reactions, the development of an analogous chemical system, and a comparison of the rate-limiting reactions for chemical and microbiological systems.

## MINERALOGY

This phase of the study applied mineralogical concepts and techniques to the study of iron sulfide oxidation.

Iron sulfide exists in coal formations in two structural states -- pyrite and marcasite. Various authorities differ on which is the most common of the two types. Inasmuch as the oxidation rate is strongly dependent upon the structural state of the sulfide, the determination of the abundances of the two modifications was undertaken first. Representative sulfide samples were collected from coal beds of various ages in eastern and southeastern Ohio. Of the 30 samples collected and examined by x-ray diffraction, all but two were determined to contain pyrite as the major constituent. In the majority of the samples, marcasite was either not present, or was present in amounts less than five per cent. The details of this study are described by Birle.<sup>2</sup>

It has been shown that marcasite has a considerably higher oxidation rate than pyrite, and the high rate of oxidation of sulfides in coals has been commonly attributed to marcasite. Textural studies on pyrite samples indicate that this mineral may in some cases show extremely high reactivity as a result of textural features (such as grain size, distribution of impurities, grain shape, etc). Hence the oxidation rates obtained by various investigators show considerable differences, because of both textural and structural variations of the iron sulfides.

A survey of mineralogical literature reveals that the various crystal faces of pyrite have different oxidation resistances, the octahedron(III) being most susceptible to attack. A study was initiated to determine, quantitatively, the rates for different crystal faces.

Although most crystal faces consist of plane surfaces, it is generally necessary to polish these for detailed examination. A mechanical polish would, in almost every case, change the orientation of the surface; in order to avoid this, the metallurgical technique of electropolishing was used. The technique has been previously used only on metals, and this constituted the first such approach on sulfides. A proper choice of solutions compositions and concentrations with the proper electrical potential was established. It is possible to control the conditions under which pyrite can be made to polish or etch by varying the electrical potential. Inasmuch as this technique, if properly developed, may have considerable significance to ore microscopy, a report on this application was published by The American Mineralogist (see Ehlers and Birle, List of Publications, page 113).

Examination of polished and etched pyrite from Pennsylvanian-age coal beds by means of the electron microscopy has revealed the presence of fossil bacteria. Although there have been several reported instances of fossil bacteria, none has been discovered with such remarkably good



preservation. These bacteria, which lived approximately 200-million years ago in the coal swamps were instrumental in precipitating iron hydroxide (which was later converted to pyrite by  $H_2S$ ). A strong similarity can be seen between these and present-day swamp bacteria. A study of these bacteria types yields considerable information as to the precise conditions of formation of these ancient coal-forming environments. The interpretation of the various bacteria typed was aided considerably by Dr. James Schopf, of the Coal Petrography Branch of the U. S. Geological Survey.

A third aspect involved a study of the hydrated sulfates associated with exposed coal surfaces on, and adjacent to, coal mining areas. White, yellow, and greenish crusty or fibrous materials quite commonly are present on pyrite-containing material. These materials were collected at several localities and subjected to x-ray diffraction analysis. The most abundant mineral found was melanterite  $FeSO_4 \cdot 7H_2O$ . Halotrichite,  $FeSO_4 \cdot Al_2(SO_4)_3 \cdot 22H_2O$ , which had been found previously in several Ohio localities was also obtained. Another compound was identified as  $FeSO_4 \cdot 4H_2O$  by diffraction and polarizing microscopy. This material, although known as an artificially formed material, has never been obtained from a natural geological environment. Study of this material under laboratory conditions revealed that it was sensitive to changes in humidity.

Chemically pure samples were examined by x-ray diffraction at various fixed humidities. It was determined that above approximately 75% humidity this material exists as melanterite,  $FeSO_4 \cdot 7H_2O$ . Below this level, and to at least 35% humidity, the sample loses some of its combined water and exists as  $FeSO_4 \cdot 4H_2O$ . This transition appears to take place within about 30 minutes, although there is some variation as a function of grain size. This transition has been studied in some detail. This failure of previous investigators to observe the tetrahydrate form can probably be ascribed to the fact that most sample collecting is done during the summer months under conditions of relatively high humidity.

It is also known that the mineral szmolnokite,  $FeSO_4 \cdot H_2O$ , exists in nature. Attempts were made, without success, to synthesize this phase and determine its stability field at low humidities.

This aspect of the study is extremely interesting mineralogically, since the effect of humidity on such transitions has not been examined in any detail for most hydrated phases. The detailed results of this study can be found in a paper by Ehlers and Stiles.<sup>7</sup>

## Classification of Pyritic Materials

Naturally occurring pyrite found associated in coals and partings in coal beds were classified according to nature and sequence of deposition. The following classification has been proposed by David Stiles:

### A. Primary Pyrite

1. Sulfur Ball
2. Disseminated Pyrite
3. Primary Replacement Pyrite

### B. Secondary Pyrite

1. Secondary Replacement Pyrite
2. Fracture-filling Pyrite

Characteristics of each class may be described as shown below.

### A. Primary Pyrite

Primary pyrite was deposited contemporaneously with the peat that was converted into coal. Some of this pyrite could have been formed by bacterial metabolism as is shown by the bacterial remains within the "sulfur-ball." Part of the primary pyrite was deposited by replacement of plant fragments. It is certain that the replacement took place early in the coalification cycle because the fragments are only slightly distorted. Had the replacement occurred after coalification, the plant fragments would have been greatly flattened. Evidence of pyrite deposition and replacement was observed.

#### 1. Sulfur Ball

Sulfur ball is found as flattened circular masses ranging in size from 1 inch to 30 inches in diameter. The longer dimensions are always parallel to the bedding plane of the coal seam. It is found as lenses varying from 1/2 inch to 2 inches thick and 1 foot to 10 feet long and wide. These lenses had previously been thought to be different from the sulfur ball but their grain size and texture are very similar so they are grouped under the classification of sulfur ball. Pyrite comprises 90 to 98% of the sulfur ball, coal is the remaining percentage. Small amounts of quartz, clays, and clays, and calcite are also found in the sulfur ball masses.

The pyrite in the sulfur ball masses is found as small grains ranging in size from 2 to 5  $\mu\text{m}$  in diameter. Usually, these small grains agglomerate into spheres 10  $\mu\text{m}$  to 30  $\mu\text{m}$  in diameter. Individual grains are subhedral to anhedral with only a few good crystals for outlines apparent. These masses are a brassy-gray color. The grayish tint of the pyrite is caused by minute inclusions of coal, since pyrite is normally a bright brassy yellow.

It appears that these masses were formed at the same time the peat was being deposited. Bacteria nearly perfectly preserved are found within the "sulfur ball" masses. Had the masses been formed by replacement after compaction of the peat had started, the bacteria would have been distorted. Since the bacteria are only slightly distorted, it is thought that the pyrite containing the bacteria was deposited along with peat formation very early in the coal-forming process. For this reason sulfur ball has been placed in the category of primary pyrite.

## 2. Disseminated Pyrite

This type of pyrite is found mainly in the lower-grade coals at the bottom and top of the beds and also in shaley layers. Disseminated pyrite is seldom visible to the unaided eye because of the low percentage present and very small grain size. When seen, it is a brassy-gray color quite similar to the "sulfur-ball." As in "sulfur ball," the grayish cast of the pyrite is caused by minute coal inclusions.

The individual pyrite grains are 1 to 5  $\mu\text{m}$  in diameter and these are quite frequently agglomerated into masses 5 to 25  $\mu\text{m}$  in diameter. The coal inclusions are found along the grain boundaries of the pyrite. A few crystal faces are evident on some of the grains but none are apparent on most of the grains. These primary grains have fairly regular and smooth boundaries forming an equidimensional to slightly elongated body.

## 3. Primary Replacement Pyrite

This type is found replacing plant parts and is very frequently found associated with "sulfur ball." Some larger plant fragments, as tree trunks and branches, are found completely replaced by pyrite and completely isolated from other pyrite. Smaller pyrite-replaced plant parts (such as leaves, stems, and seeds) are frequently found in masses. These masses vary in size from 1/2 to 10 pounds and occur in no special shape. Pyrite comprises 25 to 50 per cent of the mass with coal as the remaining percentage.

The color of this pyrite is a bright brassy-yellow because little coal is found within the actual pyrite mass. The large percentage of coal in these masses is found between the actual pyrite-replaced

plant fragments. Pyrite grains of this type vary in size from 50  $\mu$ m to 1 mm. The shape of the grains depends somewhat upon the size of the material replaced; for example, plant cells that have been replaced contain pyrite grains the shape of the cell. But large plant fragments that are replaced by many pyrite grains contain some rather well-shaped crystals.

## B. Secondary Pyrite

Secondary pyrite was deposited after the coalification cycle was complete. A variety of secondary pyrite (i.e., fracture-filling pyrite) is found in fractures that could only be formed after the coal had been created. Peat and the intermediate products in the conversion to coal are all quite plastic and would give, rather than fracture, as coal does. Secondary pyrite is characterized by larger grain size than primary pyrite. Some fractures are found in primary pyrite that have been filled with the larger-grained secondary pyrite.

### 1. Secondary Replacement Pyrite

This type of replacement is commonly found replacing "sulfur balls" and associated with plant replacement. On "sulfur balls" the very small primary crystals are replaced with crystals up to 1 mm in diameter. Frequently, small "sulfur balls" are nearly completely replaced but the larger ones are replaced only near the surface. Fractures in the sulfur balls are filled with this same type of pyrite.

Plant fragments replaced by primary pyrite are found that have undergone secondary pyrite replacement. They are seldom recognized since the secondary replacement tends to destroy the original identity.

Secondary replacement pyrite appears much brighter and more brassy-yellow than the primary pyrite varieties because of the larger grain size and lower percentage of included coal particles. These crystals are 0.25 to 2 mm in diameter and usually have fairly good crystal shape.

### 2. Fracture-Filling Pyrite

As the name implies, this type of pyrite is found filling fractures in coal. Fracture-filling pyrite occurs randomly through a coal seam with the exception of the very top and bottom. This is true probably because the shale layers tend to keep the coal from fracturing and also they are quite impermeable to solutions. Quite frequently this type is found surrounding larger sulfur balls and pyrite lenses. As the coal is compressed, fractures are formed around the incompressible sulfur ball or pyrite lense. The fractures then are filled with pyrite and as the pyrite growth continues, the fractures are lengthened and branching fractures are formed. When a polished section is made of coal containing fracture-filling pyrite, it resembles a dineric pattern.

The pyrite grains in the form of flakes approximately 0.1 to 0.3 mm thick and 0.7 to 15 mm in diameter, are anhedral, bright brassy-yellow, seem not to incorporate any coal, and are of secondary origin. The larger surfaces of the flakes are fairly smooth, since they form against the coal fracture surfaces.

#### Surface Area and Pore Size Distribution of Pyrite

In order to determine significant differences between museum grade pyrite and the sulfur ball material, measurements of the surface area and pore volume distribution of both materials were made. Surface area was determined using the B.E.T. method. The pore volume distribution was obtained using nitrogen desorption and the method of calculation presented in Orr and Dallavalle.<sup>15</sup> The specific surface of museum-grade pyrite in the size range from 60 to 150 mesh was found to be  $0.12 \pm 0.01 \text{ m}^2/\text{g}$ , and that of the sulfur ball material in the same size range to be  $1.12 \pm 0.02 \text{ m}^2/\text{g}$ . The corresponding oxidation rates were 5 and 130  $\mu\text{g/hr/g}$  pyrite.

The pore volume distributions of the two materials are presented in Fig. 1, as the change in pore volume per unit change in pore radius in  $\text{cc}/\text{\AA}$  versus the pore radius in  $\text{\AA}$ . The curves show a much larger total pore volume for the sulfur ball material, and a fairly flat distribution of pore volumes, except near the lower limit of detection at about 25  $\text{\AA}$  radius.

The greater surface area and pore volume of the sulfur ball material as predicted from its structure definitely will account to some extent for its greater reactivity, since the rate-controlling step involves a solid surface.

#### Preparation of "Sulfur Ball" Samples

All coal and shale samples were crushed to pass a 1/4-inch screen. They were then separated in a mixture of carbon tetrachloride-bromoform (or tetrabromoethane) having a specific gravity of 2.00. The portion which sank to the bottom was removed, dried, and crushed to pass a 60-mesh screen. All particles smaller than 150 mesh were saved. The 60- to 150-mesh portion was placed in a bath of pure bromoform and allowed to stand overnight. The float portion was discarded and the sink dried at  $100^\circ\text{C}$ . The enriched pyrite was separated into closer-sized fractions for subsequent experimental work, and stored in tightly-stoppered bottles purged with nitrogen. Immediately prior to use, the samples were washed with warm 2% hydrochloric acid, then washed with distilled water, dried under vacuum, and weighed in the form it was charged to the reactor.

Characteristics of the several different pyrite samples used are given in Appendix V.

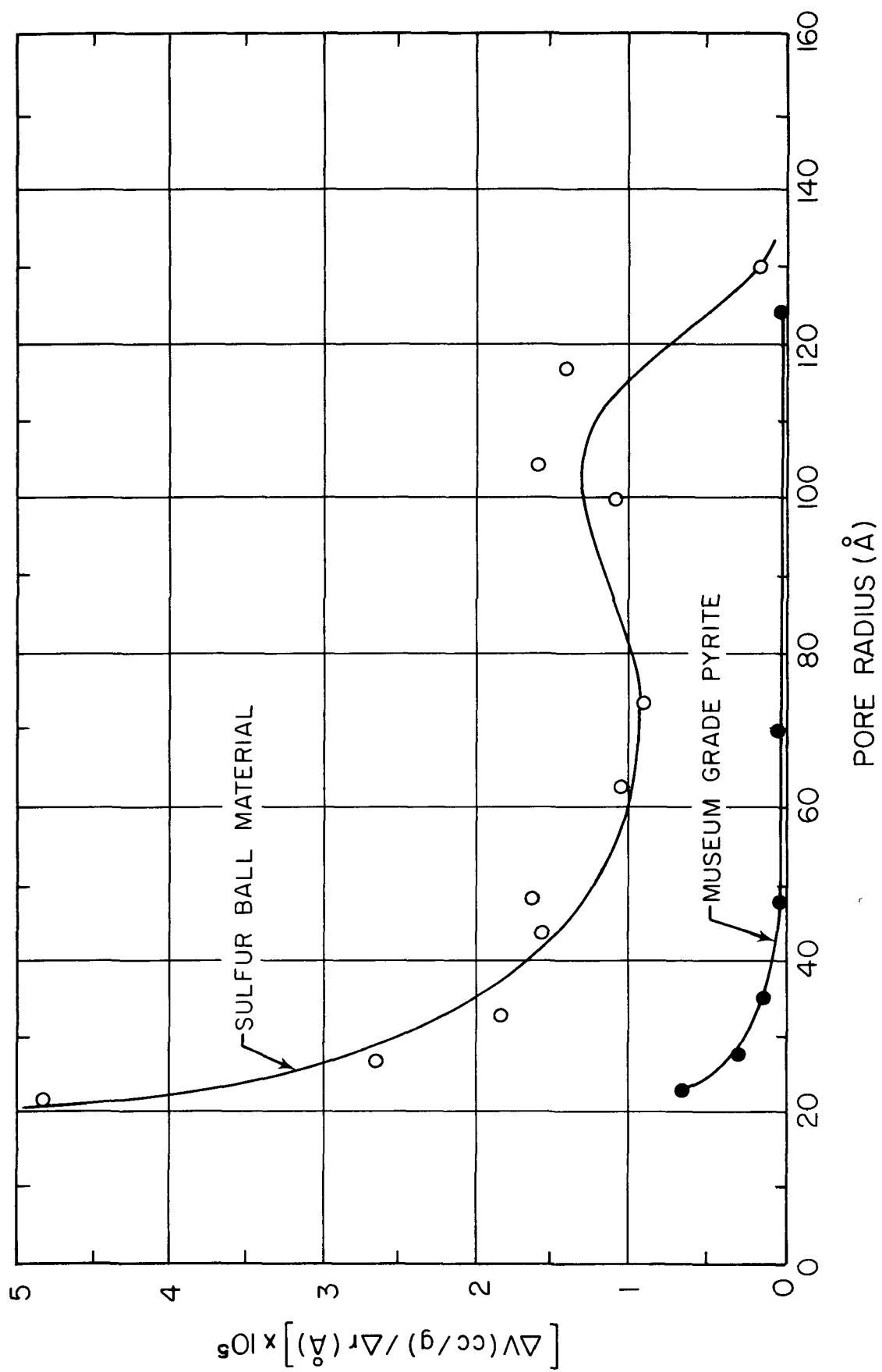


Fig. 1 - Pore Volume Distribution of Museum Grade Pyrite and Sulfur Ball

## Identification of Intermediate Products

With the equipment and facilities available, no mineralogical species, other than "final" products, were observed on the surface of pyrite. X-ray and electron diffraction studies failed to reveal any unexpected intermediates. It should be noted that no detailed microprobe analyses were made, nor was low-energy electron diffraction equipment available for use on this project.

It therefore appears that the rate-controlling step is an electron transfer reaction on the surface of pyrite itself (or through an absorbed ionic specie) since no other solid phase is present in identifiable quantities.

## Section 4

### OXYGENATION

The first oxygenation (i.e., oxygen as the immediate oxidizing agent) studies were designed to rationalize the conflicting reports on the effect of oxygen concentration and the role of water in the kinetics of pyrite oxidation. The influence of different anions and cations, as well as concentration of reaction products in the liquid phase, was then determined in order to establish a firm base for quantitative kinetic studies.

The kinetics of pyrite oxidation were evaluated in two types of environment: (1) liquid phase, in which the weight of aqueous solution in contact with the pyrite was 20 to 1000 times greater than the weight of pyrite; and (2) vapor phase, in which the pyrite was suspended in a gas phase of controlled humidity and oxygen concentration.

#### Experimental Equipment

In addition to standard Warburg equipment and techniques, equipment shown in Figs. 2, 3, and 4 were used. The apparatuses shown in Figs. 2 and 3 are similar in concept; i.e., recirculating the vapor phase (Fig. 2) and the liquid phase (Fig. 3) through a bed of pyrite. In each case, oxidation of pyrite was monitored by measuring the quantity of make-up oxygen required to maintain a constant pressure in the vapor space.

This type of equipment was used for several reasons: (1) to establish influence of diffusional resistances and desorption of reaction products on reaction rates, (2) to allow the control of concentration of various components in the recirculating fluid, and (3) to permit periodic sampling of streams to follow build-up of reaction products.

Figure 4 is a modified differential Warburg unit used to determine oxidation rates over comparatively wide pressure ranges. It consists of two identical flasks on either arm of a manometer. The same quantity of water was added to each flask; then pyrite was placed in the right-hand flask. A small amount of manometer fluid was added to the top of the mercury. To fill the system with vapor, the mercury column was lowered so that the water level was at the right-hand stopcock, the system was evacuated, and then the vapor was admitted through the vacuum line. The left stopcock was then closed and the mercury leveling bottle raised or lowered, depending on the pressure in the system, so that the water level rose half-way in the manometer. The entire assembly was agitated during liquid phase runs.

The pyrite sample used for these preliminary runs was a "sulfur ball" material collected from the Middle Kittanning No. 6 coal seam in Vinton County, Ohio. Several stages of float-and-sink separation were used to



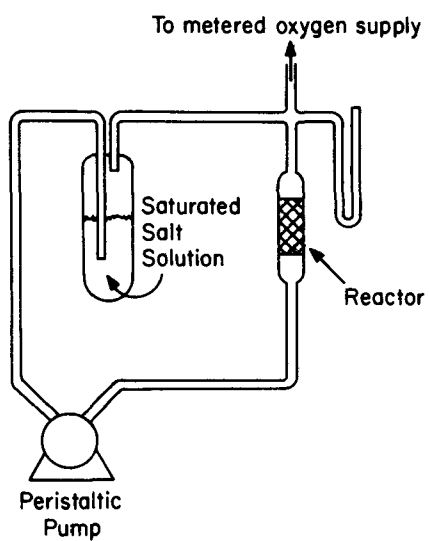


Fig. 2 - Vapor Phase Oxidation Apparatus

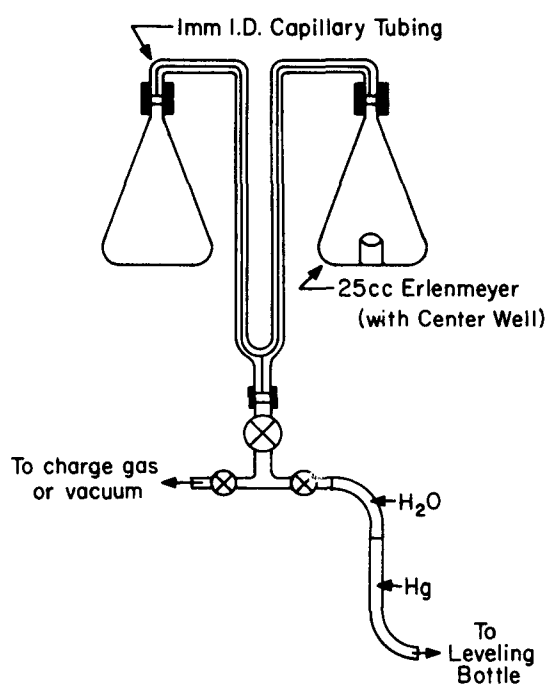


Fig. 4 - Variable Pressure Apparatus

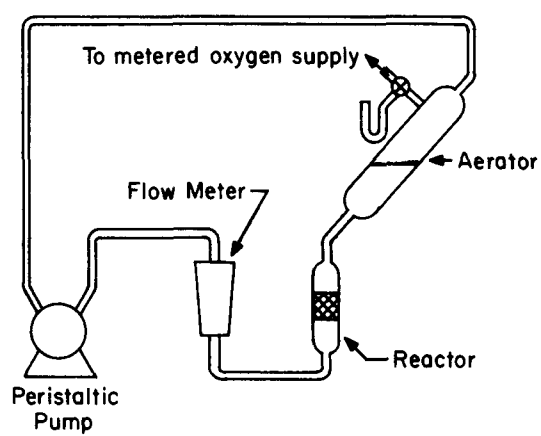


Fig. 3 - Liquid Phase Oxidation Apparatus

obtain an 85%  $\text{FeS}_2$  material. This was then carefully screened and the 70- to 100-mesh fraction used as the sample was designated "Sulfur Ball No. 1."

#### Results of Preliminary Runs

Data on liquid phase oxidation using equipment shown in Fig. 3 showed that flow rates from three or four ml/hr to 30 l/hr of fluid through the bed had no effect on rate of oxidation. Also, the rate remained constant for the duration of the runs (one to two weeks).

Two runs were made with a column of "Amberlite" IRA-120 in series with the reactor to remove all iron from the circulating fluid. With "zero" iron in solution, the rate remained the same.

The relation between the increase of iron in solution and oxygen absorbed was frequently checked and found to be approximately 3.5 moles oxygen consumed per mole of soluble iron produced. The relative ferrous-ferric ion concentration was found to vary between 85% and 95% ferrous for runs listed in Table I.

A series of liquid phase runs was made in which oxygen concentration in the vapor space and temperature were varied. The results of these runs, together with those obtained with the ion-exchange resin in the system, are listed in Table I.

A similar study was made using the vapor phase apparatus. As in the liquid phase runs, flow rates had no effect on the rate of oxygen absorption, which remained constant throughout the run periods of from several days to two weeks. Temperature and humidity of the recycled vapor were varied; the results are shown in Table II.

Since the other oxidation units were not capable of operating over wide pressure ranges, the equipment shown in Fig. 4 was constructed. Runs were made at different oxygen pressures and vapor compositions to study the effect of dissolved oxygen and nitrogen concentrations on oxidation rate. These data are shown in Table III.

All rate data in Tables I and III were recalculated to the same reference; i.e., 100  $\mu\text{gO}_2/\text{hr/g}$  of pyrite at 25°C and oxygen pressure of 760 mmHg. This was necessary in order to obtain consistent results from one column packing or washing to the next. The principal problem was the tendency of the sulfur ball particles to break down during agitation. For one continuous series of runs, the change from run to run was small. But after washing or repacking, a reference run was necessary to obtain comparative rates.

Table I. Liquid Phase Runs

Vapor Conc. (% O <sub>2</sub> )	Temp. (°C)	Oxidation Rate*
100	20	58
100	25	100
100	30	138
100	35	215
10	25	23
26	25	47
54	25	79
79	25	85
100	25	100
100	25	102**
100	35	210**

\*Rate =  $\mu\text{g O}_2/\text{g pyrite/hr}$

\*\*With "Amberlite"

Table II. Vapor Phase Runs

Temp. (°C)	Partial Pressure H <sub>2</sub> O (mmHg)	Relative Saturation (%)	Oxidation Rate*
25	22.8	96	85
	17.8	75	50
	12.6	53	25
	7.6	32	16
35	40.5	96	168
	31.2	75	90
	21.5	51	57
	13.1	31	33
45	69	96	400
	53.2	75	152
	33	46	70
	22.3	31	48

\*Rate =  $\mu\text{g O}_2/\text{g pyrite/hr}$

Table III. Variable Pressure Runs at 25°C

O <sub>2</sub> Pressure (cm Hg)	N <sub>2</sub> Pressure (cm Hg)	Liquid O <sub>2</sub> Concentration (ppm)	Oxidation Rate*
76	0	34.4	100
183	0	95	165
170	0	88	162
170	0	88	156
143	0	74	144
91	0	47	110
48	0	25	68
38	0	19.5	62
28	0	14.5	52
21.5	0	11.2	39.5
20	0	10.4	37
14	0	7.3	34
15	0	7.8	32
10	0	5.2	25
34	128	17.5	47
15	100	7.8	30.5
14	67	7.3	30
15.5	59	8.0	26.5
10	70	5.2	24.5
7.1	27	3.7	19

\*Rate =  $\mu\text{g O}_2/\text{g pyrite/hr}$

## Discussion of Preliminary Runs

Based on the observations that (1) flow rates of the recirculated fluid had no effect on oxygen absorption rates, (2) rates were constant throughout the test period, and (3) removal of iron from solution did not affect rates, it seems evident that reaction rates in the recirculating-type equipment, for the reaction periods used, are not influenced by diffusional resistances nor desorption of oxidation products. This conclusion is supported by the value of 14 kcal/g-mol for the activation energy determined from an Arrhenius plot of data presented in Table I. This value for activation energy is typical of a reaction-controlled, rather than a physically controlled, rate-limiting step.

### Role of Water

In studying the role of water, Kim<sup>11</sup> conducted a series of vapor phase oxidations using the equipment shown in Fig. 2. Over the limited temperature range studied, he observed that the rate varied linearly with absolute humidity (or partial pressure) of water in the vapor phase, apparently indicating that the rate of oxidation was first-order with respect to water and suggesting that water is a reactant.

When this study was extended to cover a wider temperature range, a distinct temperature dependence was observed, as shown in Fig. 5. It was also noted that in the temperature range covered by Kim both the oxidation rate and partial pressure of water vapor (over a saturated salt solution) doubled with a 10°C temperature rise. In other words, the influence on rate observed by Kim may be interpreted as a change caused by temperature at a constant relative humidity. The runs plotted in Fig. 5 are replotted as Rate vs. % Relative Saturation in Fig. 6. Note that at a given value of relative saturation, the rate nearly doubles with each 10°C increase in temperature, the same as observed in liquid phase oxidation. When curves in Fig. 6 are compared to the adsorption isotherms for water on sulfur ball and museum grade pyrite (see Figs. 35 and 36) the shapes of the curves are very similar, strongly suggesting that the rate is dependent on the quantity of water adsorbed or, in other words, the number of reactive sites which are covered by water. Note that even the so-called vapor phase oxidation really occurs in a liquid phase formed by adsorption of water condensed from the vapor phase.

When the isotherms of Fig. 6 are extrapolated to 100% Relative Saturation and the rates thus obtained plotted, together with those from the liquid phase runs (Fig. 7), the similarity of temperature effect in both vapor and liquid phase oxidations is apparent.

While it is not possible to describe the role of water in all phases of the reaction, for the rate-limiting reaction water is involved as a reaction medium rather than a reactant. If water were one of the

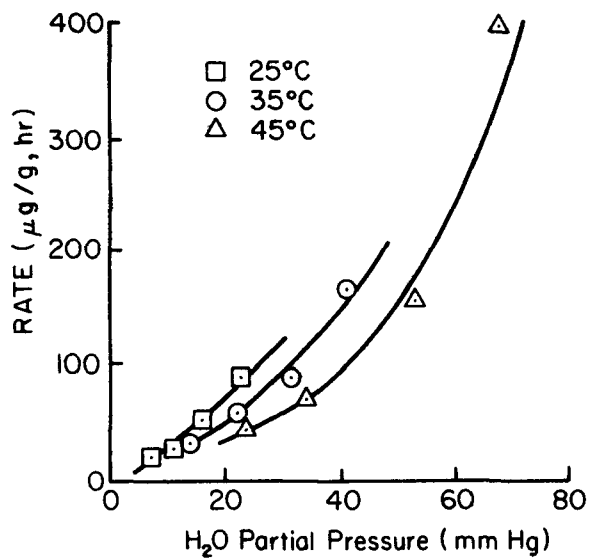


Fig. 5 - Oxidation Rate vs Partial Pressure of Water

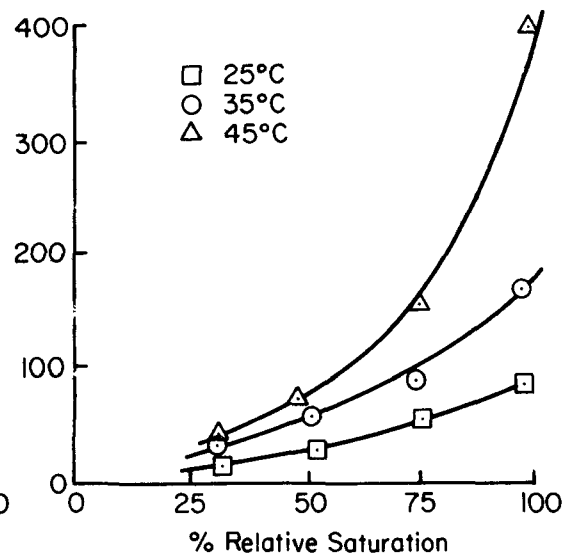


Fig. 6 - Oxidation Rate vs % Relative Saturation

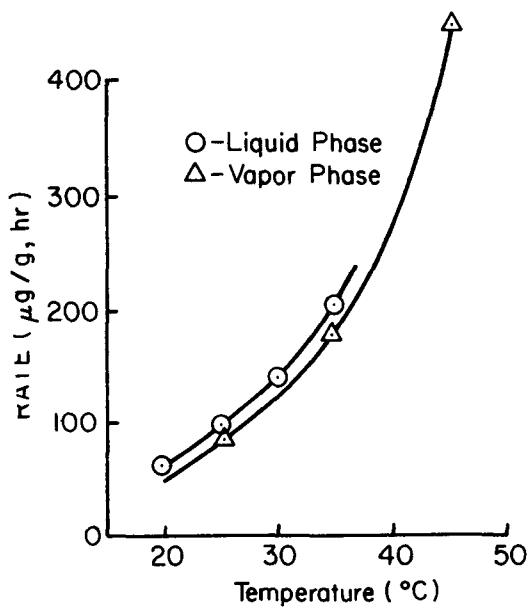


Fig. 7 - Oxidation Rate vs Temperature

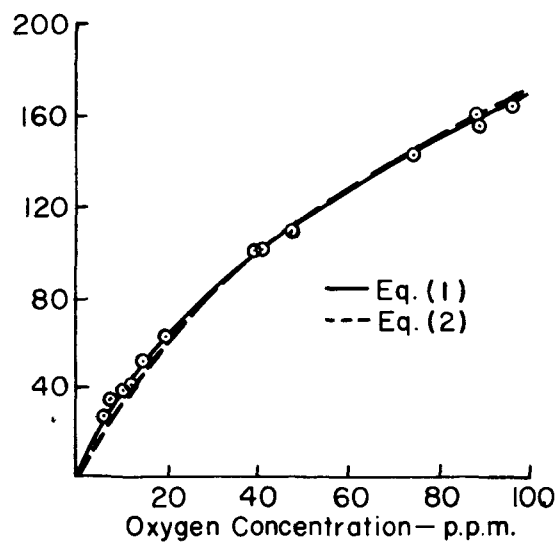


Fig. 8 - Oxidation Rate vs Oxygen Concentration in Aqueous Phase

reactants in the rate-limiting step, the rate of reaction would level off as the partial pressure of water approached saturation pressure (i.e., since water is no longer the limiting reactant). Instead, the rate of increase is greater as water concentration nears saturation, as seen in Fig. 7.

Even in vapor phase oxidation, rates remain constant over long periods of time. This can be explained by products "salting-out" of a condensed liquid phase as the content of dissolved reaction products reaches saturation. This process was qualitatively observed by Birle<sup>2</sup> from photomicrographs showing the build-up of salts around the edges of pores or etch marks which contained water.

The basic function of water at least for the rate-limiting<sup>+</sup> reaction, is to provide a means by which the oxidation products are desorbed (dissolved) for the pyrite surface. Normal oxidation, which may occur in the dry state on clean surfaces, can be stopped by build-up of products on the "reactive sites" of pyrite. Data for oxygen adsorption on dry pyrite can be interpreted in this manner (see Fig. 37 and Table XIII).

#### Oxygen Concentration

Possible kinetic mechanisms by which oxygen enters the rate-limiting reaction are suggested by the data presented in Table III.

These data show a quantitative relation between oxidation rate and oxygen concentration, and indicate that the concentration of inert gas (nitrogen) affects oxidation rate.

Using procedures and modifications suggested by Hougen and Watson,<sup>10</sup> rate equations for different assumed mechanisms can be derived. For the type of reaction under study, simplifications can be made. It has been shown that neither desorption of products nor diffusional resistances influence the rate of reaction under the laboratory conditions used in this study. Therefore, the experimental rates can be considered "initial rates" and derivations simplified by eliminating consideration of both product composition and concentration.

Data at low pressures (shown in Fig. 8) may be correlated by assuming the following mechanism:

- (1) oxygen is adsorbed on "reactive site" of pyrite;
- (2) oxygen is dissociated, forming an activated complex;
- (3) the activated complex decomposes to form an oxidation product; and
- (4) the oxidation product is desorbed, forming another reactive site.

If decomposition of the activated complex is the rate-limiting step, the adsorption and desorption step would be in equilibrium. The following rate equation can be derived:

$$r = kC_A / (1 + \sqrt{K_A C_A} + K_I C_I)^2 \quad (1)$$

or

$$r' = k'C_A / (1 + K_A C_A + K_I C_I) \quad (2)$$

where

$r$  = reaction rate for "dual site" adsorption,

$r'$  = reaction rate for "single site" adsorption,

$C_A$  = concentration of dissolved oxygen,

$C_I$  = concentration of dissolved inert gas,

$K_A$  = adsorption equilibrium constant for oxygen, and

$K_I$  = adsorption equilibrium constant for inert gas.

Plotting the data of Table III together with the derived equations (Fig. 8) indicates that the adsorption mechanism is consistent with experimental data. However, it must be emphasized that this does not prove the validity of the mechanism. It merely indicates that the proposed mechanism is possible according to this set of experimental data. The single-site adsorption mechanism, although showing greater deviation, can not be eliminated on the basis of these data.

Oxidation rates in both vapor and liquid phase runs do not appear to be limited by oxidation products. Rates are constant for long periods of time. Visible build-up of oxidation products in vapor-phase oxidations do not influence rate. The desorption of oxidation products by adsorbed water is a continuous and effective mechanism for renewing "reactive site" on the pyrite surface.

The presence of dissolved nitrogen reduces the rate of oxidation slightly as shown in Table III. The rate data are not so consistent that a reliable value for  $K_I$  can be calculated.

Since the adsorption of oxygen occurs in an aqueous medium and since the presence of nitrogen reduces oxidation rate, it is likely



that physical rather than chemical adsorption on "reactive sites" is involved. It is unusual for chemisorption to occur from highly polar solvents. Also, if oxygen were chemisorbed, nitrogen would have no effect on rate. At the same time it may not seem likely that nitrogen could compete with oxygen in an aqueous solution for physical adsorption on a relatively nonadsorptive material like pyrite. However, adsorption isotherms for nitrogen on sulfur ball pyrite (see Fig. 34) show a relatively strong adsorption, compared to adsorption on museum grade pyrite.

It was recognized that a more critical study was needed of the effect of nitrogen on the reaction since the manner in which nitrogen and oxygen are adsorbed is of fundamental importance to inhibition and mechanism studies. Therefore a high-pressure liquid-phase oxidation investigation was made to quantitatively evaluate the effect of nitrogen partial pressure on oxidation rate.

#### High Pressure Oxygenation

Equipment similar in concept to that shown in Fig. 4 was redesigned to operate at 25 atm. Instead of a leveling bottle to control the manometer liquid level, a displacement piston was used to position the manometer fluid.

The experiment was divided into two phases. During the first phase, oxidation rates as a function of oxygen dissolved in the liquid were determined. The second phase consisted of studying the effect of an inert gas (nitrogen) on the oxidation rate of pyrite.

All experimental runs were carried out at 25°C. The oxidation rates were recorded as  $\mu\text{gO}_2/\text{g/hr}$  consumed, where gram refers to one gram of pyritic material. The runs are numbered in the sequence in which they were performed.

First, the agitation rate which would eliminate the diffusional resistance was determined. No direct measurement was taken of the degree of agitation, but it was set at a rate such that an increase in agitation did not change the oxidation rate. The agitation rate, which was determined at the highest oxidation rate, was then held constant throughout the remainder of the experimental runs.

Table IV lists the experimental runs and the resulting oxidation rates expressed in  $\mu\text{gO}_2$  consumed/hr/g pyrite. One should notice the two columns of oxidation rates; i.e., Oxidation Rate and Recalculated Oxidation Rate. Since the base rate runs indicated that the oxidation rate changed slowly over a period of weeks, because of a loss of pyrite and attrition of pyrite particles, the series of runs (Runs #3 - #17 and #21 - #27) involving pure oxygen were recalculated to the same reference. The reference used was the rate of 335  $\mu\text{gO}_2$  consumed/hr/g pyrite at 25°C and 384 cm Hg oxygen pressure. Once the material was contaminated with nitrogen the recalculation was not made because the original base rate could not be duplicated.

Table IV. High-Pressure Runs at 25°C

Run #	Oxygen Pressure (cm Hg)	Nitrogen Pressure (cm Hg)	Liquid O <sub>2</sub> Conc. (ppm)	Oxidation Rate*	Recalculated Oxidation Rate**
3	384	0	186	285	335
4	596	0	284	394	450
5	74.5	0	40	93	104
11	384	0	186	334	335
12	1574	0	626	711	711
13	384	0	186	325	325
14	384	0	186	320	320
15	384	0	186	332	332
16	596	0	284	404	404
17	1068	0	460	590	590
17a	1068	241	460	530	
18	1068	536	460	498	
20	849	0	382	340	
new sample					
21	384	0	186	313	335
22	849	0	380	565	564
23	1574	0	626	827	811
25	188	0	118	193	186
26	240	0	142	251	236
27	384	0	186	362	334
28	384	69	186	355	
29	380	212	184	349	
31	380	707	184	316	
32	380	1245	184	273	
33	384	0	186	318	
34	384	1024	186	292	
35	229	0	138	202	
36	384	0	186	300	
37	1600	0	636	612	
38	384	0	186	362	
39	384	0	186	328	
40	384	1240	186	298	
41	304	0	186	319	
42	384	1240	186	285	

\*  $\mu\text{gO}_2$  consumed/hr/g Pyrite\*\* Based on reference rate of 335  $\mu\text{gO}_2$  consumed/hr/g at 25°C and 384 cm Hg

A further calculation was necessary at the end of Run #38. Since some of the pyritic material was lost in the washing prior to this run, the rate was assumed to be equal to Run #27 and the amount of pyritic material left was back-calculated.

Figure 9 is a plot of the rate of oxygen consumption versus dissolved oxygen concentration. The points in the lower concentration region represent data shown in Fig. 8.

Figure 10 is a plot of the oxygen consumed per hour per gram pyrite versus mole percent of nitrogen in the total dissolved gas. Partial pressure and the dissolved oxygen concentration were held constant at 384 cm Hg and 186 ppm, respectively.

Attempts to check the original base rate, after each sample was contaminated with nitrogen, were not successful, but an equilibrium oxidation rate of a lower value was established. However, after this initial contamination and decrease in rate, there was still a definite reduction in rate with increased dissolved nitrogen concentration. This was established by making several repetitive runs (Runs #38 - #42) using pure  $O_2$  and  $N_2$  mixtures. The effect of nitrogen on the oxidation rate of pyrite is revealed to some degree in Fig. 10, where oxygen consumption is plotted versus mole % nitrogen in the dissolved gases for a fixed dissolved oxygen concentration. Runs at higher mole ratios of nitrogen to oxygen were restricted by pressure limitations of the equipment.

After the run at 61.5 mole % nitrogen, the system was evacuated and a base run was made. A comparison of the oxidation rate of the original base run, made before the sample was subjected to nitrogen (Run #38), and this run (Run #39) (362 and 318  $\mu g O_2$  consumed/g pyrite/hr, respectively) showed a significant difference. A certain amount of nitrogen contamination was apparent. This contaminating effect of nitrogen was also noted in the first sample used and was the reason for discarding the material.

Since the nitrogen could not be removed by an ordinary vacuum, it was reasoned that the nitrogen may be rather strongly adsorbed on the pyrite. In an effort to check this, the flask was cut off and the pyritic material was washed, dried, and heated to 100°C under vacuum in an attempt to drive off the absorbed nitrogen.

The results of Runs #38 and #39 made after the flask was rejoined to the apparatus indicates that nitrogen was desorbed upon heating under vacuum.

Although it was shown that nitrogen has an initial contamination effect, it is of interest to know the decrease in oxidation rate, if any, brought about by dissolved nitrogen alone. The consistent results of a series of runs (#39 - #42) indicate that an increase in dissolved

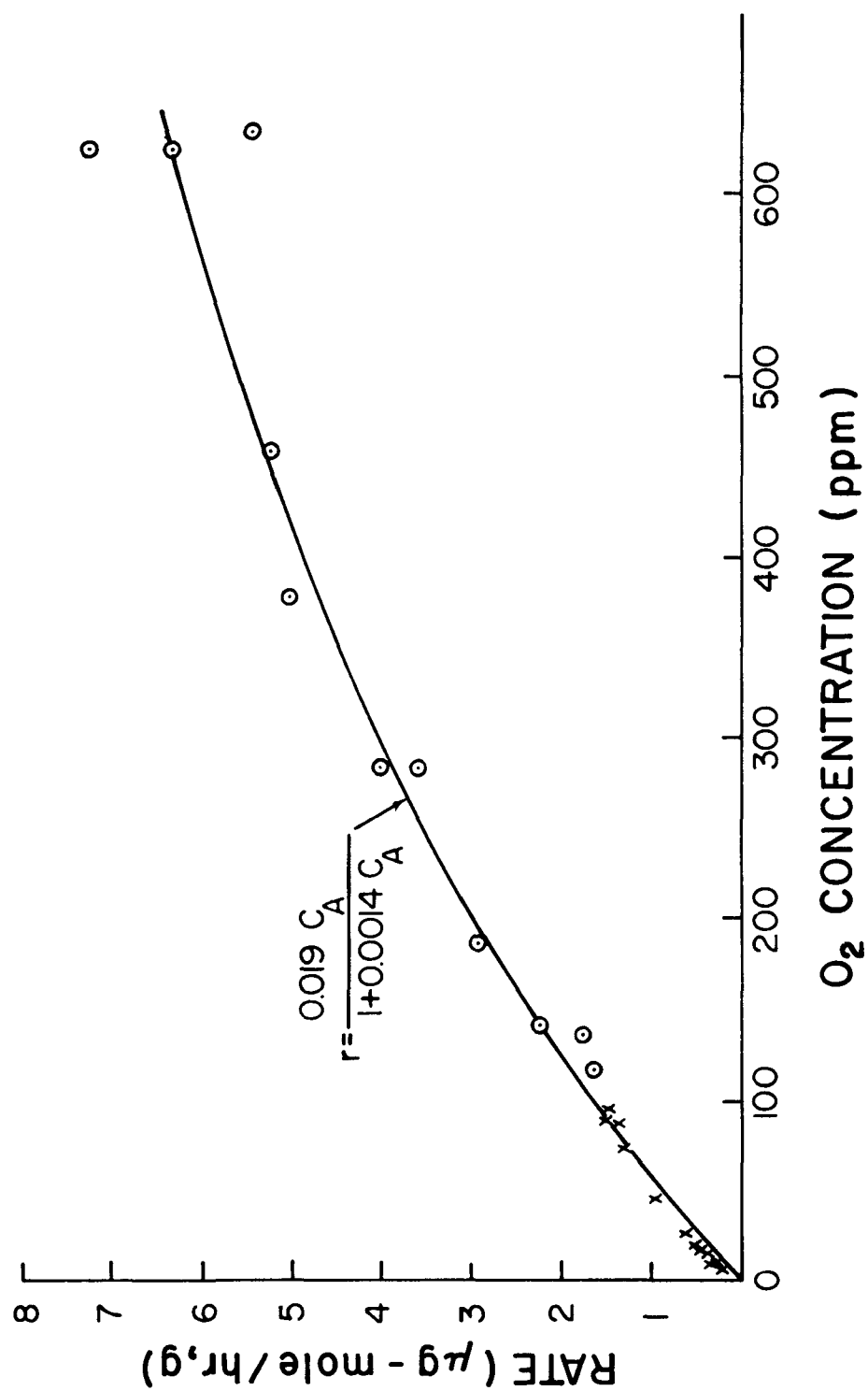


Fig. 9 - Oxidation Rate vs Oxygen Concentration

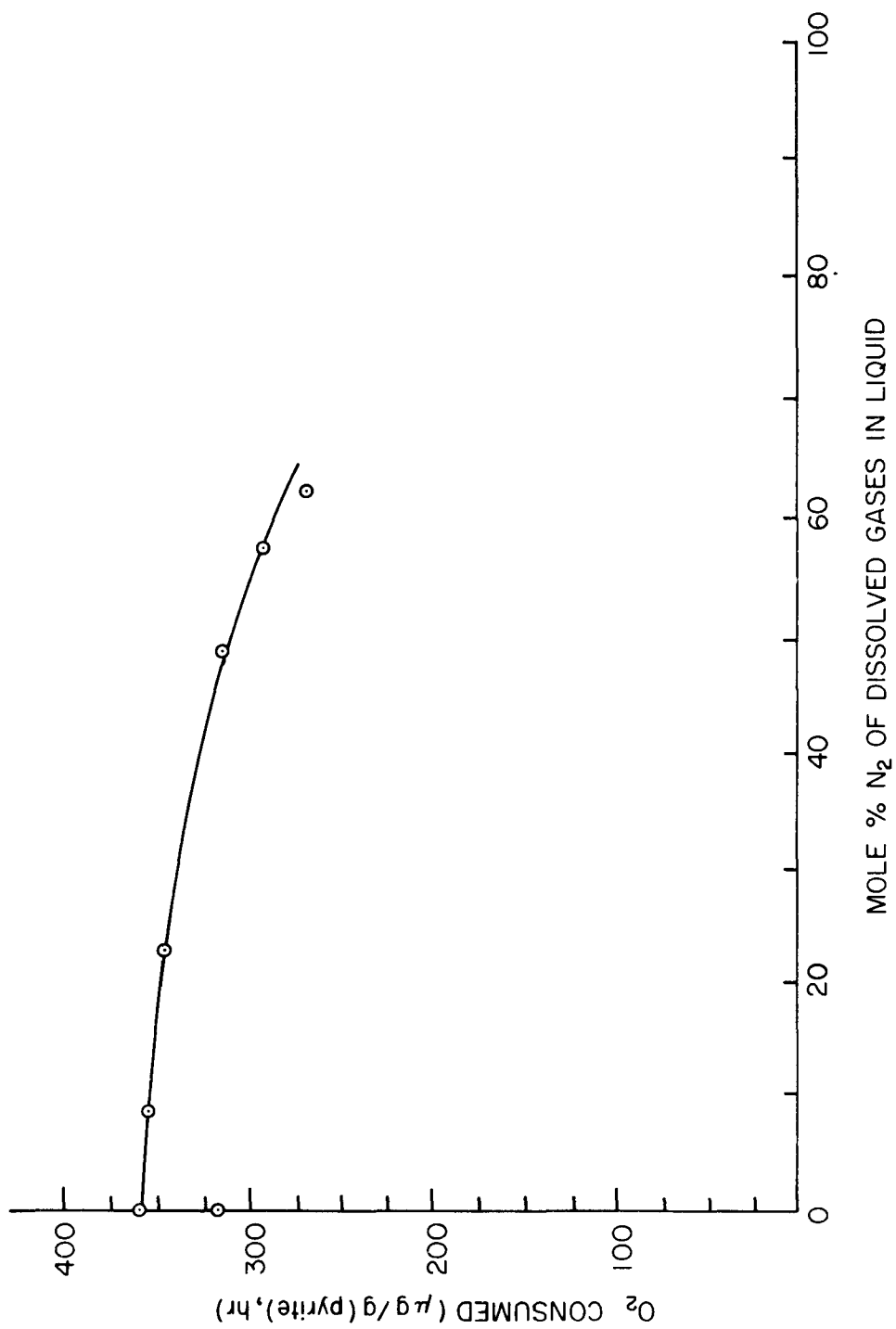


Fig. 10 -  $O_2$  Consumed vs Mole %  $N_2$  in Liquid Dissolved  $O_2$  is Constant at 186 ppm

nitrogen does decrease the oxidation rate over and beyond the first contamination effect.

It does not seem likely that an inert gas such as nitrogen would be strongly adsorbed. However, adsorption studies (see Fig. 34) indicate that the structure of sulfur ball pyrite is such that a significant number of reactive sites are found in small parting planes or ledges having a spacing or configuration that produces a relatively strong adsorption of nitrogen. The nitrogen adsorption isotherm (see Fig. 34) shows a decided hysteresis loop which can account for the nitrogen contamination observed. When nitrogen occupies the stronger reaction sites, reaction rate is decreased. Oxygen and nitrogen are in dynamic equilibrium in competition for the less active adsorption (reaction) sites.

#### Effect of pH

By controlling the pH of recirculated water in the apparatus shown in Fig. 3, the effect of pH on oxidation rate, as measured by oxygen consumption, was determined. As shown in Table V and Fig. 11, the reaction rate increases with pH -- slowly up to a pH 3 and rapidly as pH exceeds 6.

These results were surprising in view of the generally held opinion that the higher the acidity, the greater the oxidation rate. Exactly the opposite is true.

A proven explanation for this phenomenon is not available. It is not due to the increased rate of ferrous-to-ferric ion oxidation in solution. The concentration of ferric ion in solution above a pH of 3.5 is too small to account for the oxidation rates observed. Assuming the adsorption mechanism for oxygen is relevant, it may be that alteration of the pyrite surface with pH increases the number of adsorption sites, or the adsorption equilibrium constant for oxygen.

Table V. Oxidation Rate vs. pH;  
Sample: Sulfur Ball #2  
Oxygen Concentration = 39 ppm

pH	Oxidation Rate
1.5	2.10
2.0	2.2
4.0	3.2
6.0	4.1
6.0	4.2
7.0	5.5
8.0	7.9
9.0	11.4
10.0	13.5

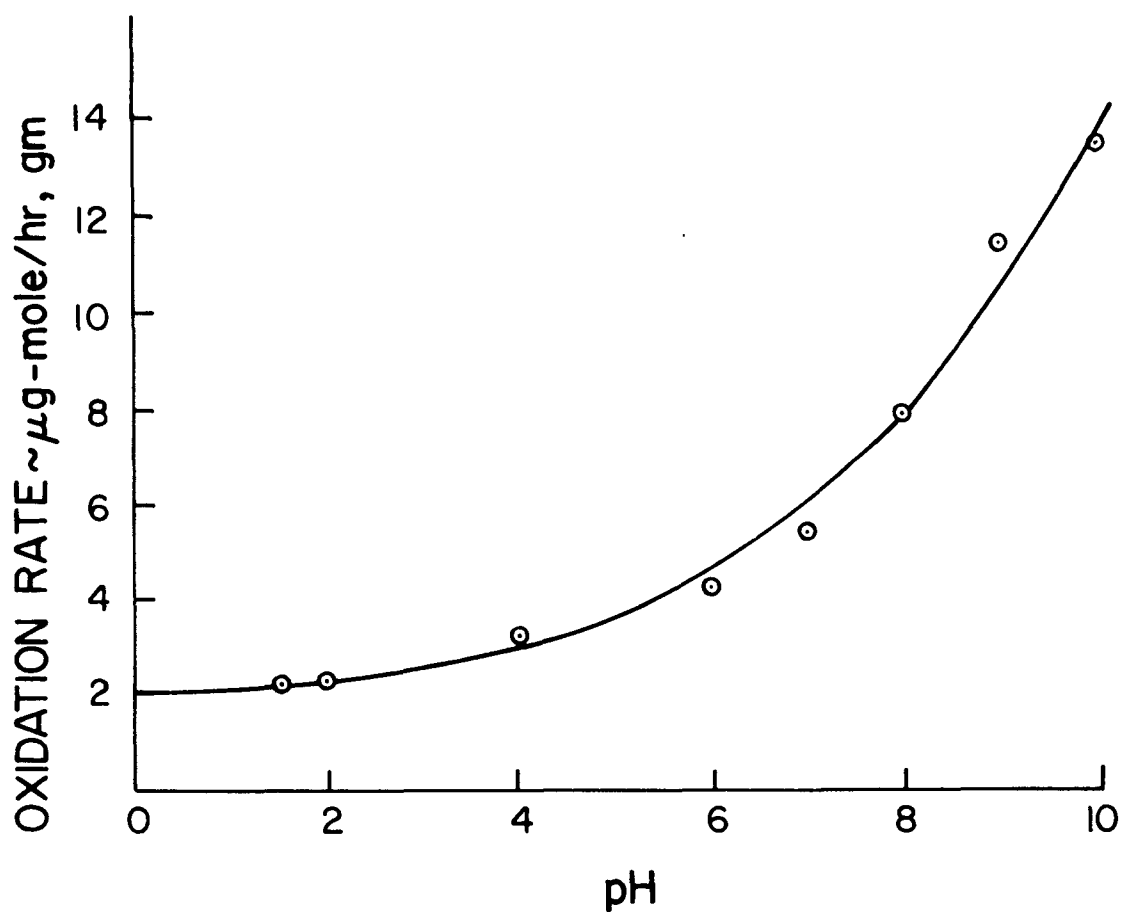


Fig. 11 - Oxidation Rate vs. pH

## Effect of Various Anions and Cations

Varieties of materials have been added to the circulated water to study their effects on oxidation rate. Concentration of sulfate and iron has a negligible effect at normal pH's. Humic acids; chromium; copper; manganese; nickel cations; and nitrate, chloride, and phosphate anions had no effect on rate when added to the solution in concentration many times greater than could be expected in natural conditions. High concentrations of phosphates did have an inhibitory effect, but negligible inhibition was noted in concentrations of less than 200 ppm. The oxygenation reaction is remarkably insensitive to concentration of material other than oxygen.

There is no evidence that trace impurities or features, other than those that can be described by texture of the pyrite agglomerate, have a major effect on reactivity of pyritic materials.



## Section 5

### MICROBIOLOGY

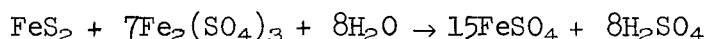
The role of autotrophic bacteria of the Ferrobacillus-Thiobacillus group in the kinetics of pyrite oxidation has been a subject of conjecture for many years, but little quantitative kinetic information applicable to pyrite oxidation in field environments has been available. The possible implication of the various species of organisms belonging to this group in pyrite oxidation kinetics is based on several observations. First, these organisms have the ability to oxidize reduced inorganic sulfur and/or iron species, particularly elemental sulfur, ferrous iron, and thiosulfate as their sole source of energy for the support of their metabolic processes. Second, they generally tolerate an environmental pH of less than 2, and appear to be almost universally found in acid coal mine drainages and in association with pyritic-containing materials in and around mines. Third, the presence of iron-oxidizing strains in growth media containing ferrous iron has been shown to greatly increase the rate of iron oxidation, as compared to sterilized controls.<sup>3</sup>

Although several of the strains which have been isolated and studied have been identified as separate species, there appears to be increasing opinion that these strains may be, in fact, variants of a single species<sup>8</sup> and the organisms are collectively referred to in this report as the Ferrobacillus-Thiobacillus group. Recent literature relating to the Ferrobacillus-Thiobacillus group are available<sup>6,21</sup> and such information will not be repeated here. In this study, the intent has been to investigate the kinetic effect of organisms from this group on the oxidation of pyrite under simulated natural environmental conditions. In all of the experiments described below, the only source of ferrous iron and reduced sulfur available to the organisms was pyritic material, and the aqueous salt solution used in the various runs was a simulated ground water. Possible carbon sources were carbonaceous materials in the pyritic, carbonate species in the simulated ground water, and CO<sub>2</sub> in the atmosphere of the various apparatuses. Simulation of a natural flow of water past the pyrite underwent a progressive development during the course of the experimentation, and will be discussed for each specific apparatus used.

#### Preliminary Experimental Phase

At the time this phase of the project was begun, most of the data available in the literature on the various strains of the Ferrobacillus-Thiobacillus group were derived from experiments in which the organisms were grown in media containing elemental sulfur, thiosulfate, or ferrous iron as the energy source; little work had been published in which pyritic material was described as the sole energy source. Braley<sup>3</sup> grew organisms on pyritic material, as well as on the above materials, and found the sulfur-oxidizing strains to produce appreciable amounts of

sulfuric acid from elemental sulfur, but to have little effect on the rate of oxidation of the iron sulfides of coals. The iron-oxidizing bacteria increased the rate of acid production from the iron sulfides to more than three times the rate in the sterile solution, and together the iron oxidizing bacteria and the sulfur oxidizing bacteria increased the rate ten-fold. Braley postulated that the role of the bacteria was to catalyze the oxidation of ferrous ions to ferric ions, which in turn oxidized the pyrite to ferrous and sulfate ions, in accordance with the reactions first presented by Stokes<sup>24</sup>:



Since these organisms are strict aerobes, oxygen is the only electron acceptor which will support the bacterial oxidation of ferrous to ferric iron in this scheme. If this bacterial oxidation of ferrous iron occurs in solution, then there is no necessity for the bacteria themselves to come into physical contact with the pyrite. This mechanism will be referred to as the indirect mechanism.

In contrast to the indirect mechanism model, other researchers<sup>5,19</sup> have presented evidence that the bacteria exert their catalytic effect while absorbed on the pyrite surface. From a practical standpoint, the important difference between these two conceptual models lies in the fact that in the former case the total number of bacteria in a given system is potentially a rate-determining factor, while in the latter model, only those bacteria absorbed on the pyrite surface will directly affect oxidation rates.

The specific objectives of this preliminary phase of research were to develop a culture apparatus which would simulate field conditions, and to quantitatively measure pyrite oxidation rates and bacterial growth under controlled environmental conditions with pyritic material as the sole source of iron in the system. Hopefully, the experimental results would tend to confirm one of the above mechanistic models. The apparatus development and experimental results are described in detail in the M.S. thesis by Bailey.<sup>1</sup> The pertinent procedures and results are given below.

#### Apparatus and Growth Media

The final apparatus design used by Bailey is shown in Fig. 12. Essentially, this apparatus is a respirometer in which the gas and water volumes are kept constant during a run, and oxygen uptake is calculated from observed changes in the gas pressure within the system, with due regard to exterior pressure and temperature changes. The entire apparatus could be autoclaved, all liquid additions and removals could be made aseptically, and gas inlets and outlets were protected by sterile filters. During an experimental run, a measured sample of pyrite was

1. Leveling bottle
2. Burette tube
3. Manometer
4. Flushing intake
5. Pyrite bed
6. Conduit for recirculated media
7. Salt solution intake
8. Air intake and filter
9. Measurement device for replacement volumes
10. "Top" sampling port
11. Thermometer
12. Intake to recirculation pump
13. "Bottom" sampling port
14. Main culture vessel
15. Magnetic stirrer

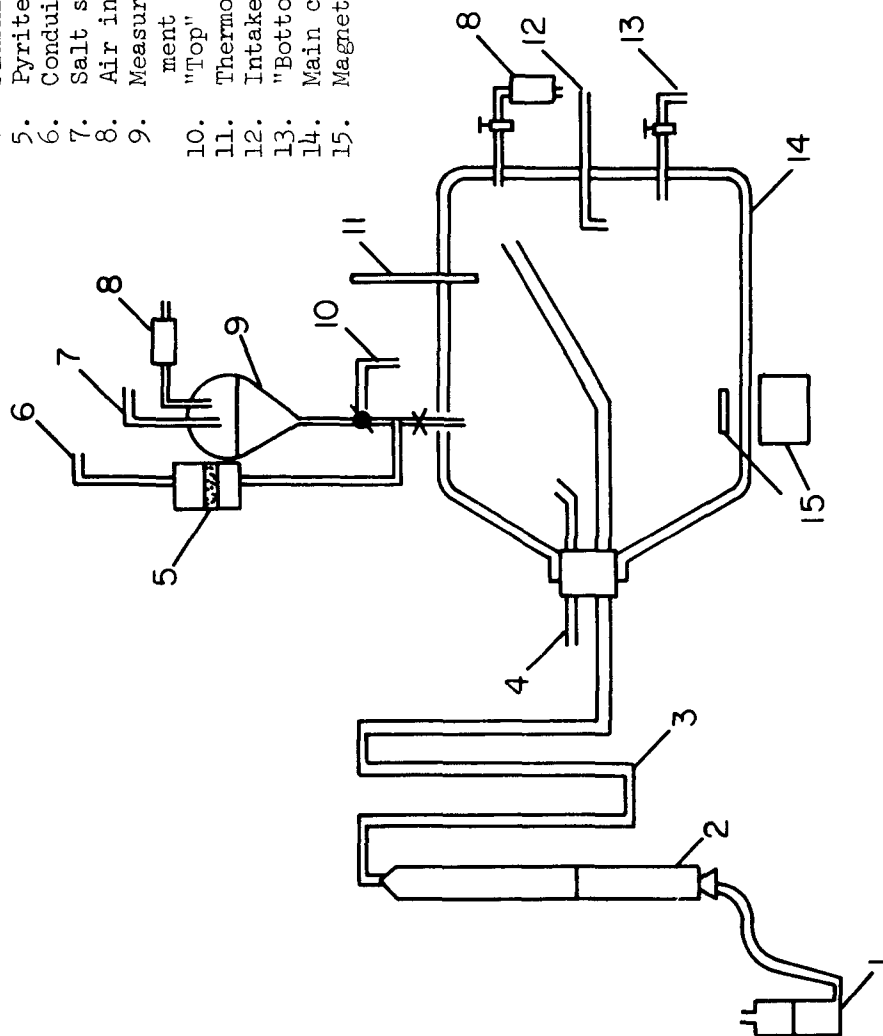


Fig. 12 - Culture Apparatus

placed in the pyrite bed, and ten liters of simulated ground water (iron free) were placed in the main culture vessel, which is a 20-liter carboy. A recirculating pump passed the water intermittently through the pyrite bed, at one-minute cycles, and the bed was allowed to drain freely between cycles. The recirculation rate used gave a retention time in the carboy of approximately 28 hours. The magnetic stirrer insured complete mixing and oxygen saturation of the water in the carboy.

The hydraulic design of this system was based on the belief that water entering an underground mine and traveling through many intricate passages at varying speeds will, at those points where the flow is relatively continuous, reach a steady-state chemical composition. Local pyrite oxidation rates and solute concentrations will differ depending on the distance traveled through the pyritic material. Thus, this laboratory simulation, in which an equilibrium will be attained between the reaction rates and dilution by daily replacement of sample volumes with an equal volume of the inorganic salt solution, should approximate the conditions at certain points in a mine.

The normal sequence for a run was to operate the system under sterile conditions for a period sufficient to give the base rate of pyrite oxidation due to oxygen alone, without bacterial catalysis. Then, the system was inoculated with a culture of bacteria, and oxidation rates, bacterial numbers, and iron concentration in the recirculated water were followed until the system reached steady state.

The system was difficult to operate, and only the results of the most meaningful run are reported herein. The operating parameters for this run were as follows:

Temperature - 20°C

Organism - Iron oxidizing organism of the *Ferrobacillus-Thiobacillus* group, isolated from acid drainage from the McDaniels Mine, Vinton Co., Ohio by serial dilution and growth in Silverman's 9-K medium.<sup>22</sup> Possibly a mixed culture.

Liquid Medium - Simulated ground water (iron-free), composition given in Appendix.

Pyrite - 25 grams of crushed sulfur ball, 35-48 mesh.  
Sulfur ball taken from McDaniels Mine, Vinton Co., Ohio.

Atmosphere Composition - Normal atmosphere (~ 21% O<sub>2</sub>).

The apparatus was operated for 150 hours under sterile conditions, at which time an inoculum containing approximately 10<sup>5</sup> cells was introduced into the system, and the run was continued for a total of

1030 hours. During the entire course of the run, oxygen uptake rate and soluble ferrous and ferric iron concentrations in the recirculated ground water were monitored, as well as pH of the water. Following inoculation with the bacterial culture, bacterial numbers in the recirculated water were monitored. Iron determinations were made colorimetrically with a Beckman DU spectrophotometer, using a modification of the phenanthroline method as described in Standard Methods.<sup>23</sup> The procedure was modified by omitting the boiling step in the sample preparation procedure. Bacterial populations were determined by the use of a multiple-tube serial dilution method, with population estimates based on the Most Probable Number tables given in Standard Methods. The medium used was Silverman's 9-K, with positive growth being indicated by a color change to rust-red. Incubation of the tubes was at 20°C for a period of two weeks.

### Results

For the run described above, plots of oxygen uptake rate and cell concentration versus time are shown in Fig. 13. Referring to Fig. 13, it is seen that following inoculation with the organisms at 150 hours, the oxygen uptake rate remained at the base (chemical oxidation) rate until about 325 hours, at which time it began to increase, ultimately leveling off at about 825 hours.

In regard to the growth of bacteria following the inoculation at 150 hours, the cells appeared to increase in a relatively constant logarithmic manner until reaching a population of about  $4.3 \times 10^6$  organisms/ml, as indicated by the Most Probable Number test. During the entire course of the run, the pH of the recirculated water dropped from an initial value of 4 to a terminal value of 2.7. Thus, it is improbable that limitation of the bacterial numbers resulted from an excessively low pH. Since the air space of the apparatus was flushed with fresh air daily, and approximately 100 ml of fresh ground water medium containing  $\text{NaHCO}_3$  was added daily to make up sampling volume losses, the availability of  $\text{CO}_2$  for autotrophic cell growth was far in excess of the amount used, based on observed population increases. The limitation of bacterial population may have resulted from a deficiency of available nitrogen, although trace element availability, or the buildup of metabolic products are other possible limiting factors. It is interesting to note that the bacterial population reached a level of about  $10^4$  per ml before there was any appreciable effect on oxygen uptake rate. If the rate increase at 325 hours is interpreted as evidence of the beginning of biological catalysis, then the catalysis may be related to the number of organisms in the recirculated water. If the indirect model for bacterial catalysis is correct, then the observed level of  $10^4$  organisms per ml may represent the population required to supply ferric ions at a sufficient rate to support a detectable oxidation of pyrite by ferric ions, as compared to the base rate for oxygenation. On the other hand, if the bacterial catalysis is due to bacteria adsorbed on the pyrite particles, then this level of  $10^4$  organisms per

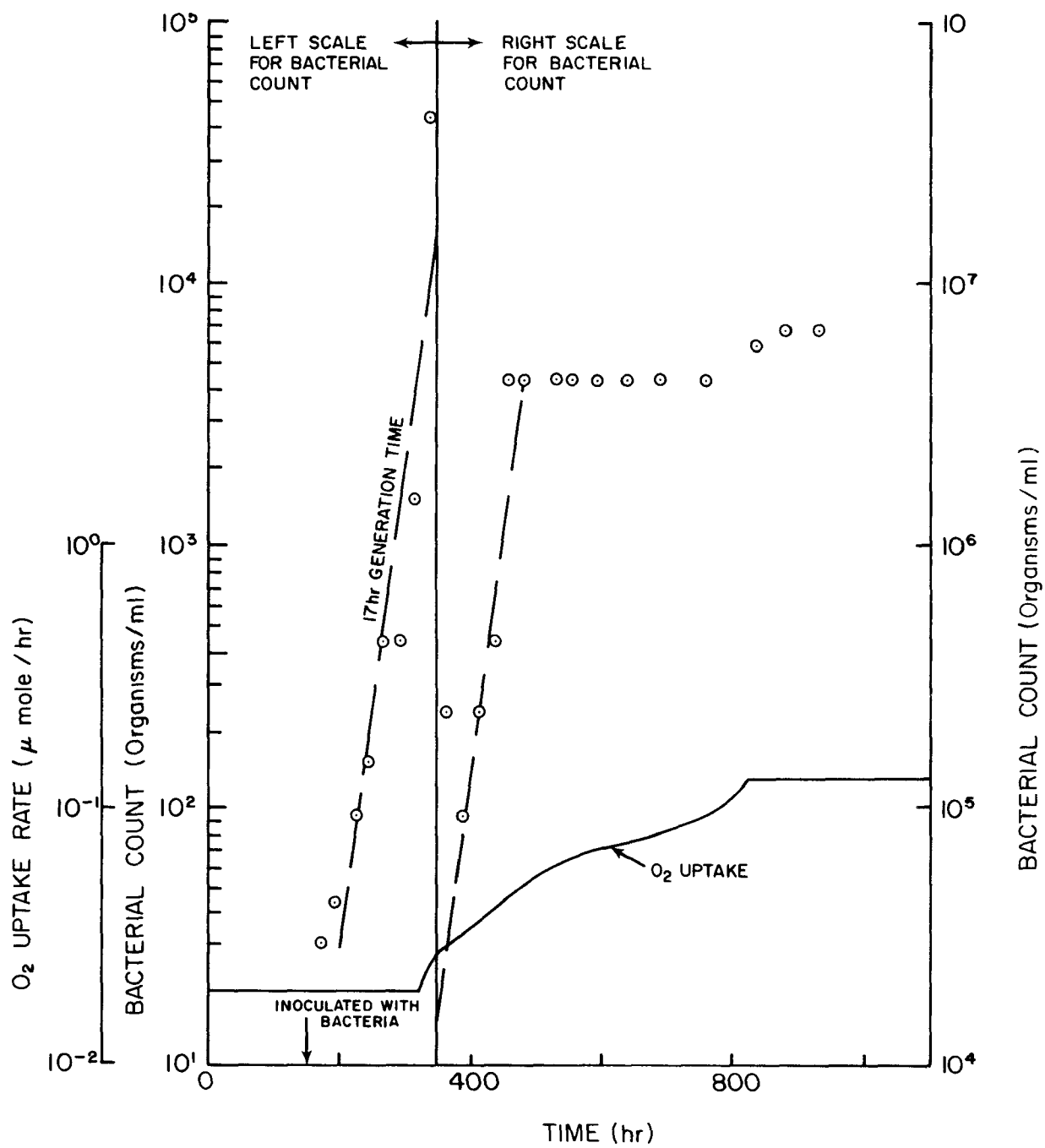


Fig. 13 - Bacterial Count and  $O_2$  Uptake Rate vs Time

ml would be the concentration of bacteria necessary to provide an equilibrium with a minimum critical population adsorbed on the pyrite surfaces.

Other observations may provide an indication of which model is more likely to be correct. The soluble iron in the recirculated water was predominately in the ferrous form until about 320 hours, at which time the ferric-ferrous ratio began to rise continuously for the remainder of the run. This suggests that the increase in pyrite oxidation rate may be related to the increase in ferric-ferrous ratio in solution. The application of the indirect model, in light of the ferric ion oxidation kinetics discussed in Section 6, would require a sufficient population of organisms in the recirculated water to increase the ferric-ferrous ratio to the point (at any given total soluble iron concentration) at which the rate of oxidation of iron by organisms is equal to the rate of reduction of ferric iron at the pyrite surface. Further, the ferric ion oxidation kinetic model predicts a maximum rate of pyrite oxidation when the ferric-ferrous ratio approaches infinity. The presence of a population of organisms in excess of the number required to keep all iron in the ferric state would result in no further increase in pyrite oxidation rate. The data shown in Fig. 13 could be explained in terms of the indirect model and ferric ion oxidation kinetics, if the continued increase in oxygen uptake rate between 460 and 820 hours could be accounted for. Since the bacterial population leveled off at about 460 hours, and since an increase in specific oxidative capacity per bacterial cell would be unlikely during this stationary phase of the bacterial culture, it is likely that the increasing oxidation rate is related instead to the total iron concentration. For the data gathered during this run, a plot of  $\log(\text{Fe}^{+++})$  versus pH yields a straight line with a slope of -2, indicating that the ferric iron solubility was controlled by the equilibrium of  $\text{Fe}(\text{OH})^{++}$  with  $\text{Fe}(\text{OH})_3$ , with  $\text{Fe}(\text{OH})^{++}$  being the principal ferric specie in solution. Since pyrite oxidation rate by ferric ions is a function of both ferric-ferrous ratio and total ferric ion concentration, the gradual lowering of the pH during the course of the run, and the consequent increase in soluble ferric iron, could have resulted in an increased pyrite oxidation rate.

The above interpretation of the data in terms of the indirect model does not prove this model to be correct. Presumably, the data could possibly be explained in terms of the model in which it is assumed that the bacteria responsible for the catalysis action are adsorbed on the pyrite surface. The coincidence of increasing the ferric-ferrous ratio in solution with observation of the beginning of the catalyzed oxidation rate, and the continued increase in oxidation rate after the bacterial population became stabilized, are, however, more difficult to explain if one assumes that adsorbed bacteria are the primary catalytic agent.

## Conclusions

The conclusions of this preliminary work are:

1. The iron-oxidizing autotrophs can be very satisfactorily grown in an environment in which the only iron source is pyrite, and at sufficiently high bacterial populations, will significantly increase the rate of pyrite oxidation over the base chemical rate.
2. Bacteria may function catalytically by merely oxidizing ferrous iron in solution. The ferric iron produced then oxidizes pyrite in accordance with the anaerobic pyrite oxidation kinetics presented in Section 6.

## Warburg Respirometer Oxidation Experiments

The preliminary work described above showed that it is practical to work with organisms grown only in a mixture of pyrite and simulated ground water, and that the culture under study could be grown directly in the respirometer. However, a decision was made to alter the method of experimentation for two reasons. First, when considering water and oxygen transport mechanisms in natural systems such as underground mines and gob piles, both the continuous flushing of the pyrite bed and the water-pyrite ratio inherent to the apparatus used by Bailey appear to be far out of proportion compared to probable natural conditions. In any natural environment, continuous flushing of pyrite surfaces with large volumes of water would, in general, require that the pyrite be completely inundated. Because of the low diffusivity of oxygen in water, this would effectively block the availability of oxygen in quantities sufficient to support commonly observed pyrite oxidation rates. It is much more likely that the rate of flow of water past actively oxidizing pyrite in natural systems is very slow, or that there is no continuous flow at all other than the seepage induced by the water condensed by hygroscopic salts of pyrite oxidation under the high humidities present in underground systems. Intermittent flushing of surfaces will occur by changing ground water levels in underground mines, and by infiltration of rain water or snow melt in the case of gob piles. Thus, a natural environment is more accurately approximated by a batch system, readily obtainable in a simple Warburg respirometer. The water-pyrite ratio, which is determined in a natural system by the nature and permeability of the mineral matrix surrounding the pyrite, can also be readily varied in the Warburg apparatus.

The second major problem encountered in the preliminary work was with the analytical methods. The nature of the carboy respirometer made accurate oxygen uptake rate determinations difficult, and results tended to be erratic. Further, bacterial counts by serial dilution were time-consuming, and results were subject to a two-week incubation delay. Use of the Warburg eliminated the former problem; to cope with



the bacterial count problem, it was decided to employ direct counts, using phase contrast microscopy and a standard Lineweaver-Burke counting chamber.

### Objectives

The specific objectives of this phase of the work were to describe the growth of organisms of the Ferrobacillus-Thiobacillus group in a system consisting of varying amounts of crushed pyrite and simulated ground water, to determine the relationship between bacterial activity and overall pyrite oxidation kinetics, and to determine whether the indirect model or the bacterial adsorption model is more likely to be a satisfactory model of the bacterial catalysis mechanism in natural systems.

### Materials and Procedures

All Warburg runs were made at 20°C, using 140 ml flasks and a shake rate of 80/min, with a 1-1/2 inch stroke measured at the manometer stopcock. No CO<sub>2</sub> absorbent was used, and carbon uptake due to cell growth was estimated to be insignificant compared to the gross gas uptake observed. Thus, gross uptakes were taken to be equal to oxygen uptakes.

The seed bacterial culture used was obtained by incubating acid drainage from the McDaniels Mine in Vinton Co., Ohio, with a mixture of simulated ground water and crushed pyrite.

The pyrite used was 80-100-mesh crushed sulfur ball, taken from the McDaniels Mine and washed with dilute HCl and distilled water before use to remove fine carbonaceous material and iron salts.

In all experiments, the initial gas phase in the flask was air, and care was taken to assure that the partial pressure of oxygen did not drop below 0.2 atm during the course of a run. Daily flushings with fresh air ensured both a constant oxygen content and the continued availability of atmospheric CO<sub>2</sub>.

### Results

Figure 14 is a typical cumulative oxygen uptake versus time curve for a mixture of 0.4 g pyrite and 20 ml of ground water, inoculated with bacteria at zero time. For the first 100 hours of the run, the rate of oxygen uptake was 10.4 µg/hr. Between 100 and 180 hours, the rate increased steadily, leveling off at 180 hours at a rate of 150 µg/hr. An indication of the significance of this type of curve is seen in Fig. 15. Here, the first 180 hours of data from Fig. 14 are replotted, together with data from an identical reaction mixture which was not inoculated with bacteria. Thus, it is seen that the 10.4 µg/hr base rate is apparently the rate due to chemical oxidation by oxygen.

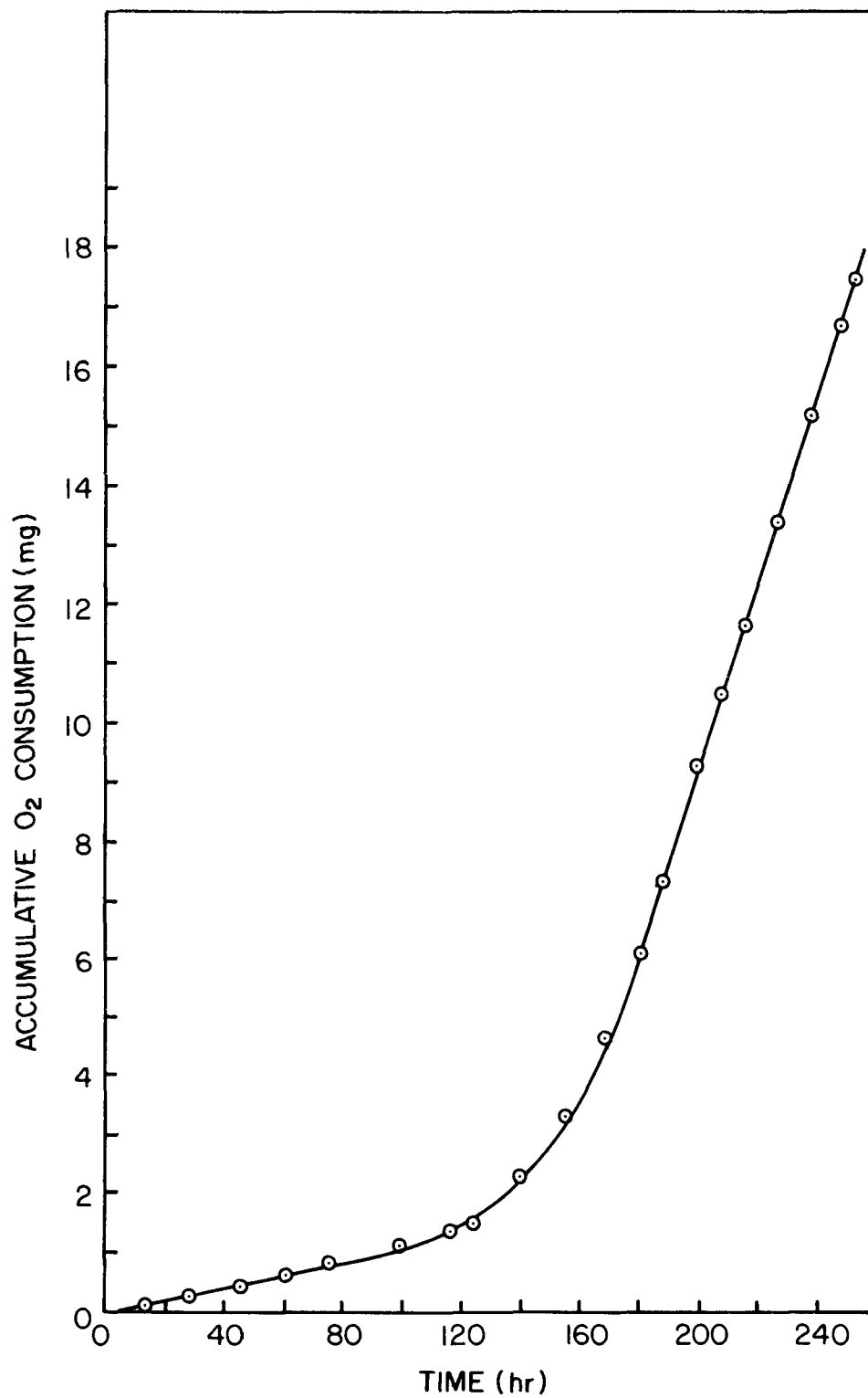


Fig. 14 - Oxygen Uptake Curve  
(0.4 g pyrite in 20 ml solution)

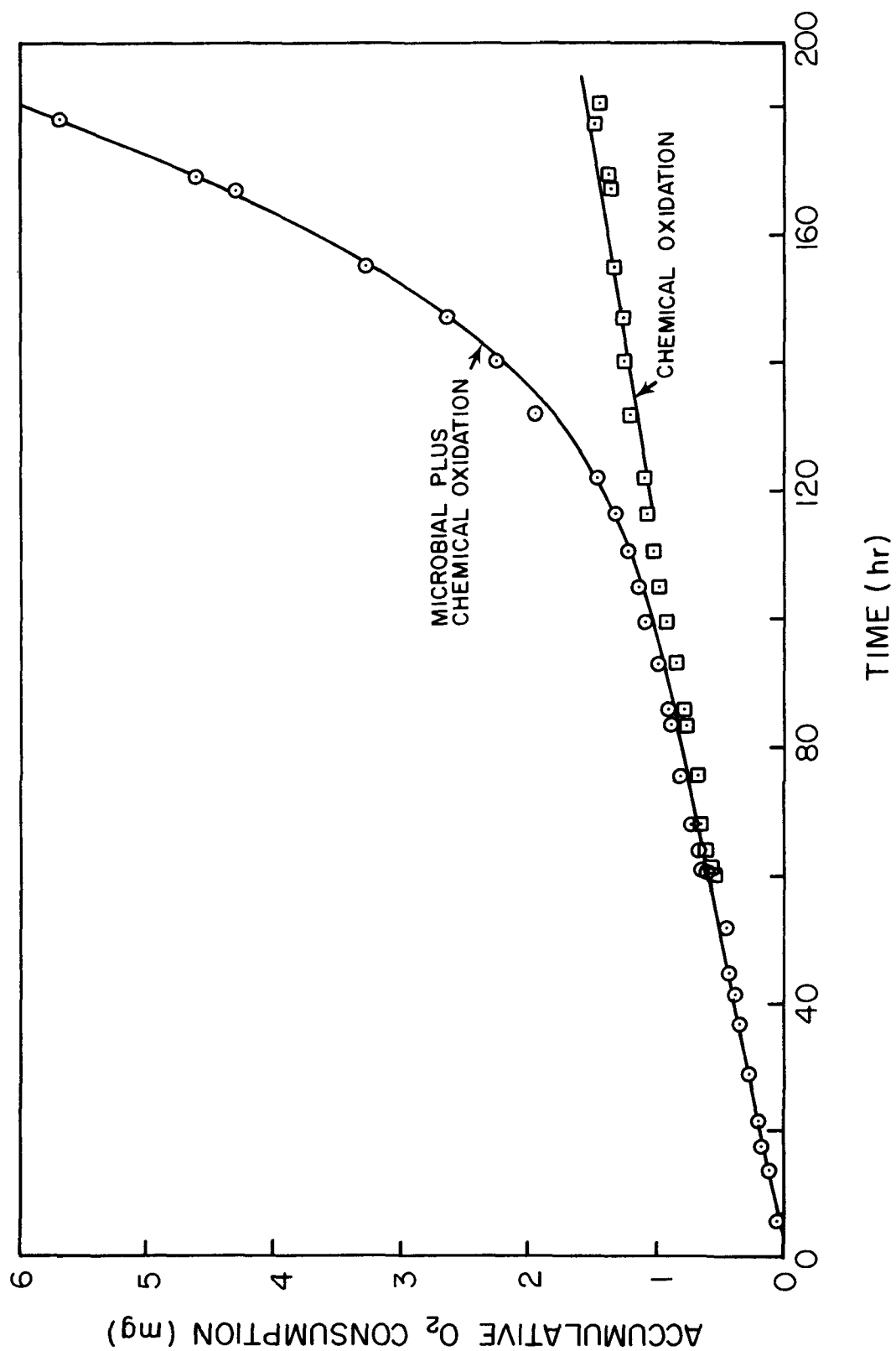


Fig. 15 - Oxygen Uptake Rate  
(0.4 g pyrite in 20 ml ground water)

The increase in rates past 100 hours must then be due to bacterial activity. Figure 16 is a semilogarithmic plot of bacterial concentration versus time. Bacterial growth appears to follow a normal first-order relationship up to a bacterial concentration of about  $2 \times 10^8$  cells/ml, at which time the population appeared to reach its maximum limit. It is significant to note that the time at which the oxidation rate stabilized at 150  $\mu\text{g/hr}$  coincides with the time at which the bacterial population ceased to increase, indicating that the bacterial population was controlling the rate of pyrite oxidation in this case.

If one analyses these data in terms of the indirect model for microbial catalysis, then the chemical base rate (oxygenation rate) and the oxidation by bacterially produced ferric ions will proceed independently, with the total observed rate being the sum of the two. Figure 17 shows a plot of bacterial oxygen uptake rate versus time, obtained from the data of Fig. 15 by subtracting out the base chemical rate of 10.4  $\mu\text{g/hr}$ . Although the slope of the curve is not identical with that of Fig. 16, it is seen that the bacterial oxygen uptake rate is approximately proportional to the population of bacteria. In regard to the limiting bacterial population of  $2 \times 10^8$  per ml, this value was a characteristic maximum population when the simulated ground water was used. Growth of the organisms in a mixture of unwashed pyrite and distilled water gave about half this value, or  $5 \times 10^7$  per ml, and commonly quoted maximum populations in Silverman's 9-K media are on the order of  $10^8$  per ml. Whether this limiting population is due to limited nitrogen source, or to toxic product buildup or to some other limitation, is not known. It should be mentioned, however, that if the nitrogen source in Bailey's groundwater medium is increased by a factor of ten, the limiting population is increased by a factor of approximately ten.

Further insight into the relationship between bacterial population and the catalyzed oxygen uptake rate may be gained by evaluating the rate versus population data in light of a simple model. If it is assumed that catalyzed oxygen uptake rate is first-order with respect to cell population, then

$$dO_2/dt = kN \quad (N = \text{bacterial population})$$

and

$$\log dO_2/dt = \log N + \log k.$$

Thus, oxygen uptake versus total cell population should plot on log-log paper as a straight line with a slope of unity. Figure 18 is a plot of oxygen uptake rate versus total cell population in the flask. While the data show considerable scatter, there is a distinct tendency toward a unit slope at lower cell populations, where the organisms are still in the log growth phase. During the 1:1 section of the curve in Fig. 18, the oxygen uptake rate per cell is from 2.5 to  $5 \times 10^{-7}$   $\mu\text{g O}_2/\text{cell-hr}$ , depending on whether the upper or lower envelope is used

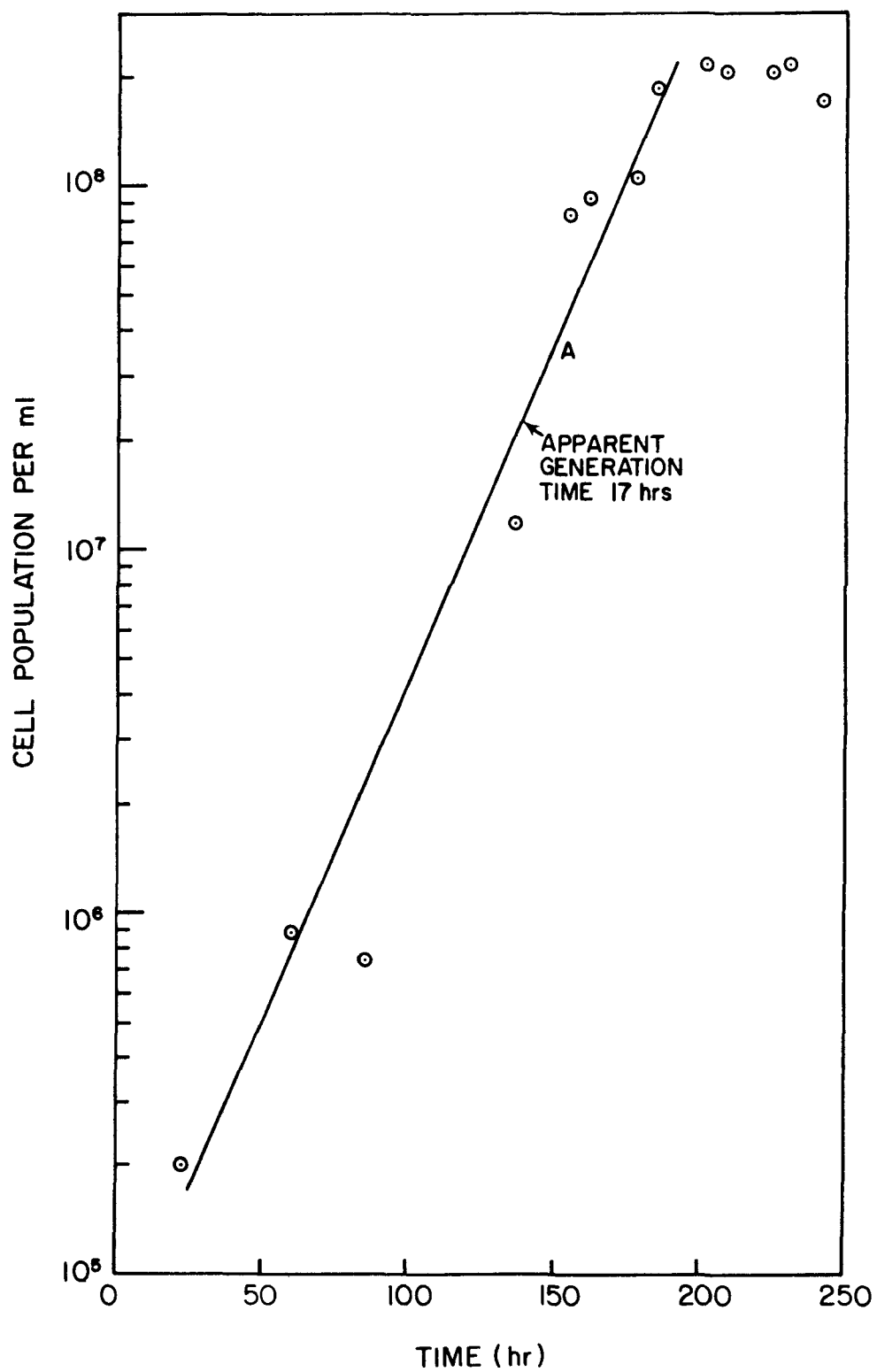


Fig. 16 - Change in Cell Population with Time

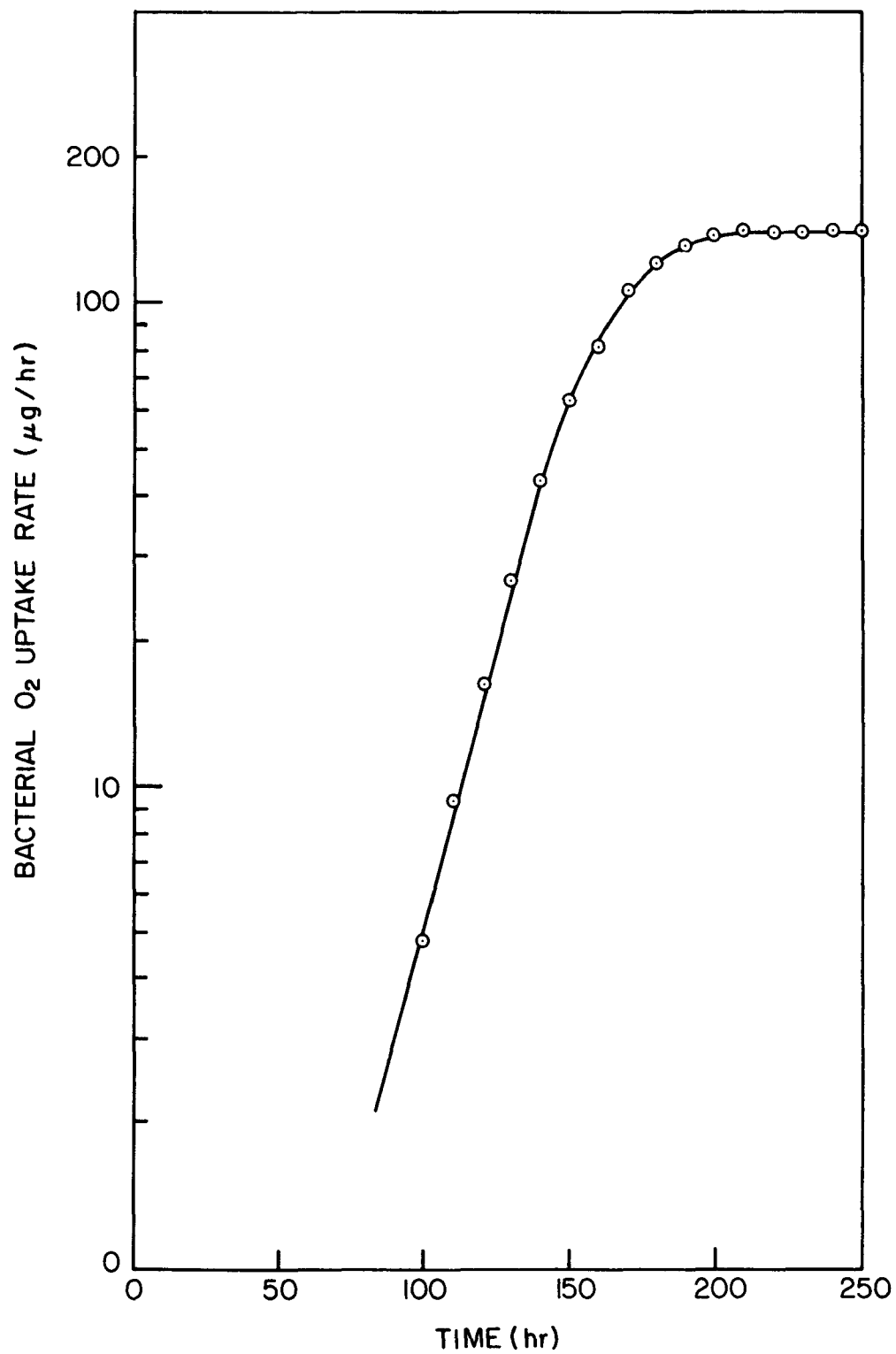


Fig. 17 - Change of Microbial Oxidation Rate with Time

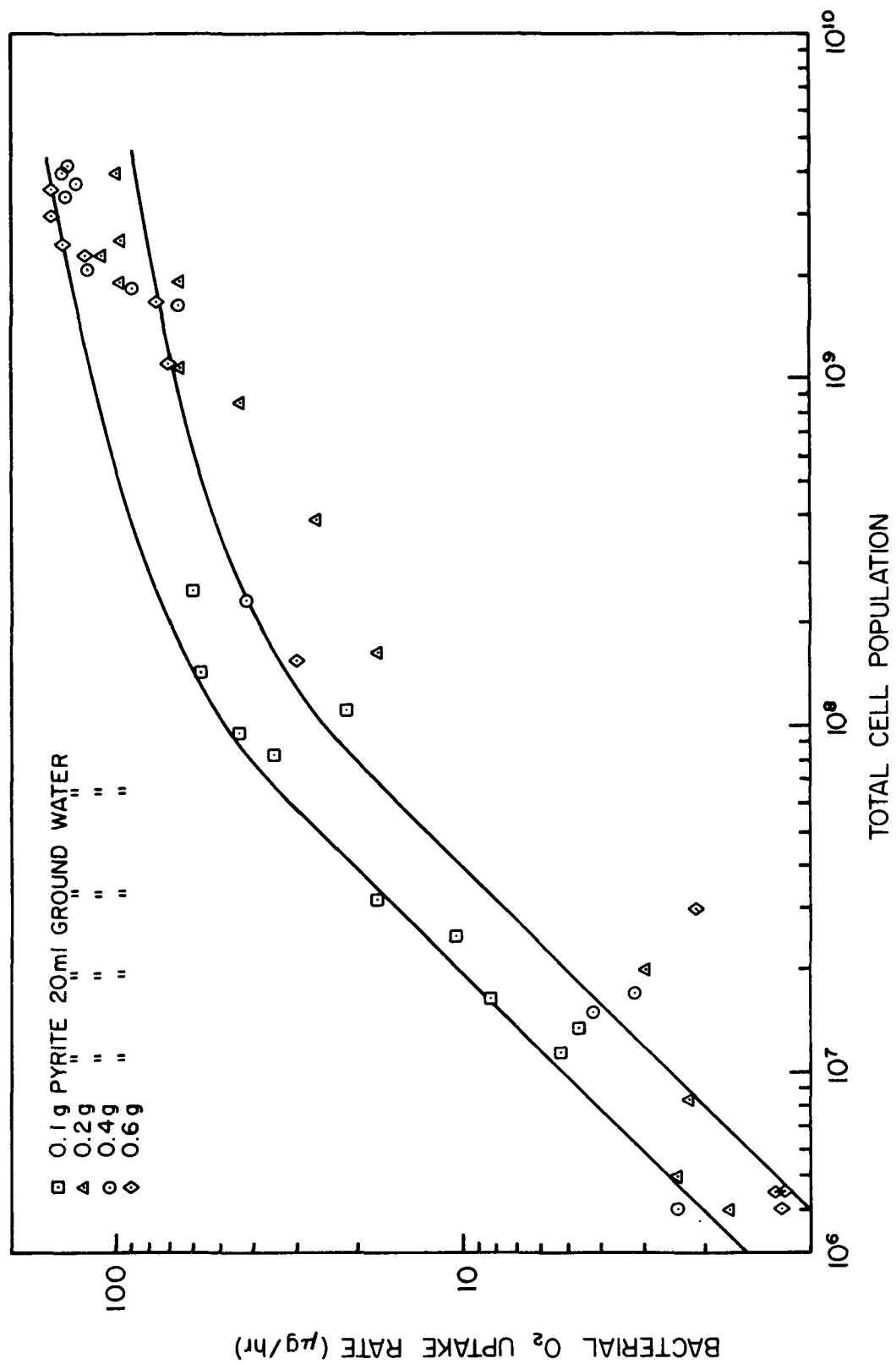


Fig. 18 - Bacterial Oxygen Uptake Rate vs Total Cell Population

for the calculation. At the higher cell populations, when the organisms are approaching the stationary phase of growth, the apparent respiratory activity per cell decreases considerably below these values.

The above data give some insight into the nature of growth of autotrophic iron-oxidizing organisms in a pyrite-ground water system, but they do not definitely prove whether bacterial catalysis is indirect through the oxidation of ferrous iron in solution, or direct through adsorption of the cells on the pyrite surface. Figure 19 presents evidence that the catalysis is through the indirect mechanism. Here, the chemical and the maximum biological oxygen uptake rates are plotted against the pyrite-to-water (wt = volume) ratio in the Warburg flask. The water volume was held constant at 20 ml in each flask, and the pyrite samples were 0.1, 0.2, 0.4, and 0.6 g. While the chemical rate increases linearly with pyrite weight increase in the flask, the biological rate shows a linear increase initially, but a tendency to approach a constant limiting rate at the higher pyrite-to-water ratios. While this phenomenon cannot be explained readily in terms of an adsorption mechanism, it is entirely compatible with the indirect mechanism. At a constant volume of water in the four flasks, and a limiting bacterial population of about  $10^8$  per ml, the total bacterial population and hence the total oxidative capacity of the bacteria has a specific maximum limit. In accordance with the ferric ion kinetics presented in the following section of this report, a given type and grain size of pyrite has a maximum specific oxidation rate by ferric iron. If the oxidative capacity of the available bacteria surpasses this rate, then the weight of pyrite limits the oxygen uptake rate. As the weight of pyrite increases, however, the ferric ions cannot be supplied rapidly enough by the available bacteria, and the maximum rate of pyrite oxidation is equal to the maximum rate of ferrous iron oxidation by the bacteria. The chemical rate of pyrite oxidation by oxygen will continue to climb, however, and at some pyrite-to-water ratio the chemical rate will surpass the biological rate. From the available data this ratio is calculated to be about 400 grams pyrite to one liter of water. This, of course, depends on the type and grain size of the pyrite.

The implications of bacterial catalysis through the indirect mechanism are very significant. In a natural system having a low pyrite-to-water ratio, the overall oxidation might be due primarily to bacterial catalysis. However, in case of a high pyrite-to-water ratio, there will be insufficient water to support the necessary bacterial population, and the reaction will be essentially chemically controlled. Oxygen transport considerations indicate that this is probably the case in underground mining systems.



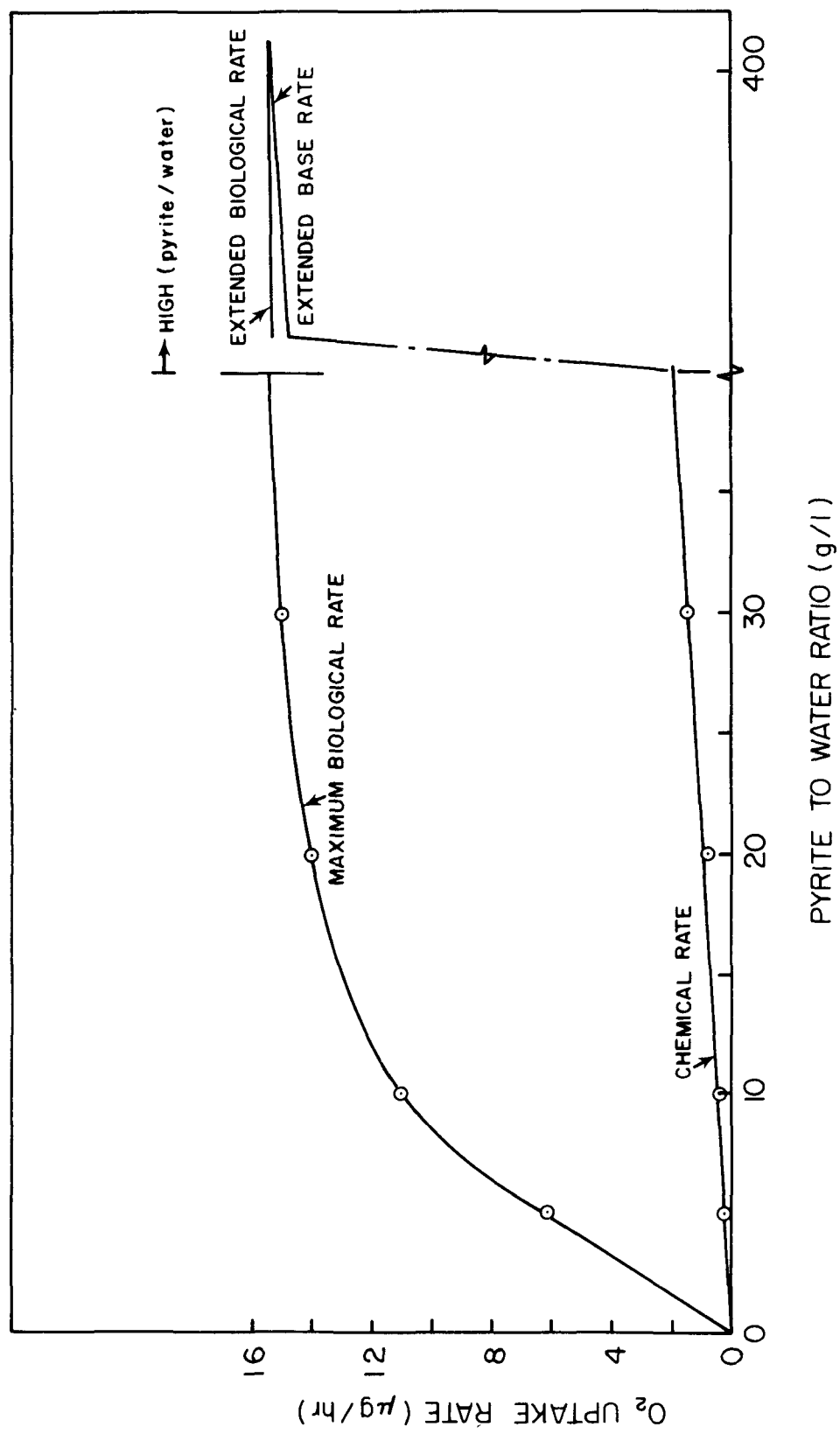


Fig. 19 - Oxygen Uptake Rate vs Pyrite to Water Ratio

## Section 6

### FERRIC ION OXIDATION

In the preceding section, microbial catalysis is shown to operate through a mechanism involving the oxidation of ferrous ions to ferric. The ferric ions then become the immediate oxidizing agent for pyrite. These experimental data also show that indirect oxidation is of primary importance, although they do not rule out a minor contribution by direct oxidation. If the indirect mechanism is the major microbial rate-determining mechanism, then ferric ion oxidation is the chemical analogy of microbial-enhanced oxidation.

From a kinetic point of view, the overall reaction rate is a steady-state value determined by the relative rates of two reactions: (a) oxidation of ferrous ions to ferric ( $\text{Fe}^{++} - e \rightarrow \text{Fe}^{+++}$ ) and (b) reduction of ferric ions by the pyrite oxidation reaction ( $14\text{Fe}^{++} + \text{FeS}_2 \rightarrow 15\text{Fe}^{+++} + 2\text{S}^{6+}$ ).

In the microbiological system, the rate of ferrous ion oxidation to ferric, and therefore the ferric-ferrous ratio reached, is determined by microbial activity. In the experimental chemical system, the oxidation of ferrous ions is controlled chemically by addition of an oxidizing agent at such a rate to maintain a constant ferric-ferrous ratio.

The real system is self-regulating. The higher the microbial activity (or higher the ferrous ion oxidation rate) the higher the ferric-ferrous ratio becomes. With an increase in ferric-ferrous ratio, the rate of ferric ion reduction by pyrite increases.

The ferrous-to-ferric oxidation is a solution reaction. The ferric ion reduction reaction is a heterogeneous reaction so that the reduction rate is a function of surface area of pyrite. Therefore the ferric-ferrous ratio reached in a given pyritic system depends on the exposed surface area of pyrite.

The chemical (as compared to microbiological) system is much more reproducible and easily controlled. It is possible to evaluate the microbial oxidation rate in a real system from a knowledge of the rate of ferrous oxidation or ferric reduction. Therefore a study has been made of the kinetics of the ferric ion oxidation reaction to help evaluate the relative effectiveness of microbial and oxygenation systems. Results of this study are given below.

#### Experimental Equipment

The equipment shown in Fig. 20 was developed to measure oxidation rate at any selected value of EMF (or  $E_h$ ).

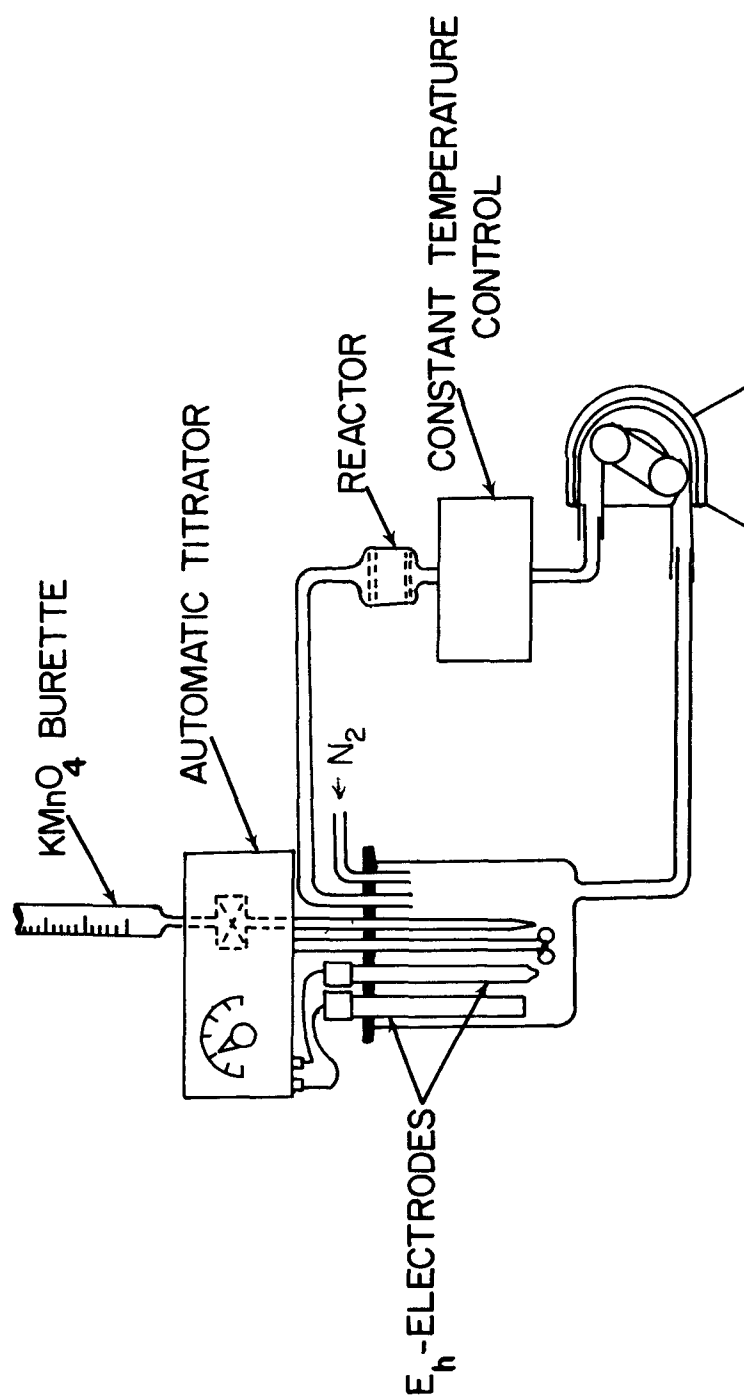


Fig. 20 - Ferric Ion Oxidation Apparatus

A mixing vessel contained the  $E_h$  electrodes (platinum, and calomel reference cell), stirrer, automatic titrator delivery tube, inlet and outlet lines for the recirculated fluid, and a nitrogen purge line. The liquid to the bed of pyrite (reactor) was recirculated by a peristaltic pump. The EMF of solution was controlled by an automatic titrator which added either  $\text{Fe}_2(\text{SO}_4)_3$  or  $\text{KMnO}_4$  to maintain a constant ferric-ferrous ratio in solution.

When combined oxygenation and ferric ion oxidation runs were made, all lines and electrodes to the mixing vessel were sealed in a tight-fitting cover, the stirrer was removed since adequate agitation was obtained by directing the flow of inlet recirculated solution, and the nitrogen purge line was replaced by a line to a metered supply of oxygen. The top of the burette of the automatic titrator was connected to the vapor space above the solution so the total vapor volume of the system remained the same as the titrant was added to the mixing vessel. In this way the oxygen consumed could be determined by the quantity of oxygen added to maintain a constant pressure on the system.

#### Experimental Procedure

Initial ferric ion oxidations were run at low pH's or, put in another way, at high sulfate concentrations since the low pH values were reached by addition of sulfuric acid. In light of more recent work, the important point to be made is that these initial runs were made at essentially constant sulfate concentration and constant ionic strength. Later studies were made to determine the effect of pH on ferric ion oxidation rates. Interpretation of these data indicate that the major variable involved is anion concentration, not pH.

Experimental results are therefore presented in several data sets:

- I. For high sulfate concentration, low pH, and constant ionic strength as a function of
  - A. EMF or ferric-ferrous ratio,
  - B. total iron concentration at high ferric-ferrous ratios, and
  - C. type of pyrite.
- II. Combined oxygenation and ferric ion oxidation runs.
- III. At varying pH and anion concentration as a function of
  - A. EMF or ferric-ferrous ratio and
  - B. total iron concentration.

All rates for ferric ion oxidations are based on the observed rate of ferric ion reduction and a stoichiometry of 14 moles of ferric

ions to oxidize one mole of pyrite (with iron ion as ferrous). The stoichiometry was checked experimentally and found to agree with the theoretical value of 14, within limits of experimental error. Rates are calculated in terms of  $\mu$  mole pyrite oxidized per hour per gram of pyrite. It should be noted that oxidation rates expressed as  $\mu\text{gO}_2$  consumed per hour per gram of pyrite multiplied by 0.0098 is equivalent to micromoles of pyrite oxidized per hour per gram of pyrite (when a stoichiometry of 3-1/2 mole of oxygen per mole of pyrite oxidized is assumed).

## Experimental Results

### Low pH, High Sulfate Runs

Several series of runs at low pH and high sulfate concentrations were made, using three different pyrite samples. Experimental data are given in Tables VI-X.

For some as yet unknown reason, data on the museum grade pyrite could not be consistently reproduced. Consistent data were obtained on a set of runs (e.g., a series of runs at different ferric-ferrous ratios) if operated continuously. But if the reactor were shut down overnight, the rate the following day would often be higher or lower by 25 to 50%. Sulfur ball material was much more predictable; the overall rate decreased slowly and regularly with reaction time as the pyrite was consumed.

Two consistent sets of data for the museum grade pyrite are given in Tables VI and VII.

Similar data for McDaniels Sulfur Ball sample and Sulfur Ball No. 2 are given in Tables VIII and X and graphically in Figs. 21 and 22.

The ferric-ferrous ratio was calculated from the equation  $\text{EMF} = 0.430 + 0.059 \log (\text{Fe}^{+++}/\text{Fe}^{++})$  as determined experimentally for these series of runs at low pH and high sulfate concentrations.

All rates within a series were recalculated to the same base rate for this series because of a small but consistent change in base rate during the course of the series. The change was determined experimentally by periodically performing a base rate run under base conditions and noting the change in rate over the operating period from one base run to the next. The change was assumed to be due to consumption of pyrite through oxidation. In some cases, more than 25% of the original pyrite charge was consumed.

### Treatment of Data

A simple "dual-site" adsorption model gives a rate equation that correlates experimental data within limits of experimental error.

Table VI. Museum Grade Pyrite

Rate vs. Conc. at EMF = 0.700

Total Iron (g/l)	r	$\frac{1^*}{\sqrt{\text{Fe}^{+++}}}$	$\frac{1}{r}$
0.125	0.83	21.1	1.21
0.250	1.25	14.9	0.80
0.500	1.6	10.6	0.63
1.00	2.2	7.45	0.45
2.00	3.1	5.3	0.34
4.00	4.0	3.73	0.25
8.00	4.9	2.64	0.20
10.00	5.2	2.36	0.195

\*Fe<sup>+++</sup> in moles/literNote: "r" (rate) in units of  $\mu\text{g-mole FeS}_2$   
oxidized per hour per gram of sample.

Table VII. Museum Grade Pyrite

Rate vs. EMF; Iron Conc. = 10 g/l

EMF	$\frac{\text{Fe}^{+++}}{\text{Fe}^{++}}$	r <sub>exp</sub>	r <sub>calc</sub> *
0.700	37,700	5.2	5.2
0.650	5,360	3.8	2.6
0.600	760	1.36	1.35
0.550	108	0.54	0.59
0.500	15.4	0.23	0.23
0.477	6.3	0.15	0.14

$$*r_{\text{calc}} = \frac{20 - 6.7\sqrt{\text{Fe}^{++}/\text{Fe}^{+++}}}{\sqrt{\frac{1}{\text{Fe}^{+++}}} + 1.4 + 300\sqrt{\text{Fe}^{++}/\text{Fe}^{+++}}}$$

Note: "r" (rate) in units of  $\mu\text{g-mole FeS}_2$   
oxidized per hour per gram of sample.

Table VIII. Rate vs. Iron Concentration

EMF = 0.650 V, pH = 0.2; Sulfur Ball #2

Concentration (mg-mole/l)	Oxidation Rate	1/Conc.	1/Rate
0.097	1.4	10.3	0.72
0.15	1.9	6.7	0.52
0.21	2.4	4.7	0.42
0.28	2.6	3.6	0.39
0.42	3.2	2.4	0.31
0.75	3.96	1.33	0.25
1.41	5.4	0.71	0.19
2.06	6.3	0.48	0.16
2.76	6.6	0.36	0.15
3.28	7.7	0.31	0.13
4.4	8.9	0.23	0.11
5.3	9.3	0.19	0.1075
5.8	10.3	0.17	0.097
10.9	13.7	0.092	0.073

Note: "r" (rate) in units of  $\mu\text{g-mole FeS}_2$   
oxidized per hour per gram of sample.

Table IX. Rate vs. Iron Concentration

EMF = 0.650 V; pH = 0.5; McDaniels Sulfur Ball

Run 23		Run 50	
r	Fe Concentration (g/l)	r	Fe Concentration (g/l)
19.3	5.0	19.1	4.3
18.7	3.85	14.2	2.26
14.3	2.15	11.3	1.26
10.9	1.10	9.1	0.675
8.5	0.59	4.8	0.193
6.5	0.31	11.7	1.28
5.3	0.183	8.2	0.54
		6.2	0.29

Note: "r" (rate) in units of  $\mu\text{g-mole FeS}_2$  oxidized  
per hour per gram of sample.

Table X. Rate vs EMF, Sulfur Ball #2, Ref. 16

Iron Conc. = 1 g/l, pH = 0.2

EMF	r <sub>exp</sub>	r <sub>calc</sub> *
0.65	14	14
0.60	12.5	12.3
0.55	11	9.2
0.50	6.1	5.4
0.477	3.6	3.6
0.460	2.1	2.7
0.430	0.56	1.3

$$*r = \frac{165 - 55 \sqrt{\text{Fe}^{++}/\text{Fe}^{+++}}}{\frac{1}{\sqrt{\text{Fe}^{+++}}} + 2.3 + 70 \sqrt{\text{Fe}^{++}/\text{Fe}^{+++}}}$$

As one possibility, assume a ferric ion is adsorbed on two "reactive sites" of pyrite (dual-site adsorption). Also assume ferrous ions ( $\text{Fe}^{++}$ ) compete for these dual sites. The activated complex formed by ferric ion adsorption is decomposed by electron transfer from one of the reactive sites to the ferric complex, thereby forming an adsorbed ferrous ion, which is then desorbed.

Using Hougen-Watson<sup>10</sup> concepts, the following rate equation was derived:

$$r = \frac{k_{3f} \sqrt{K_1} - \frac{\sqrt{K_2}}{K} \sqrt{\frac{\text{Fe}^{++}}{\text{Fe}^{+++}}}}{\frac{1}{\sqrt{\text{Fe}^{+++}}} + \sqrt{K_1} + \sqrt{K_2} \sqrt{\frac{\text{Fe}^{++}}{\text{Fe}^{+++}}}} = \frac{k - k' \sqrt{\frac{\text{Fe}^{++}}{\text{Fe}^{+++}}}}{\frac{1}{\sqrt{\text{Fe}^{+++}}} + \sqrt{K_1} + \sqrt{K_2} \sqrt{\frac{\text{Fe}^{++}}{\text{Fe}^{+++}}}} \quad (3)$$

where

$k_{3f}$  = rate constant, electron transfer reaction

$K$  = equilibrium constant, electron transfer reaction

$K_1$  = adsorption equilibrium constant for ferric ions

$K_2$  = adsorption equilibrium constant for ferrous ions

$\text{Fe}^{++}, \text{Fe}^{+++}$  = concentration of ferrous and ferric ions



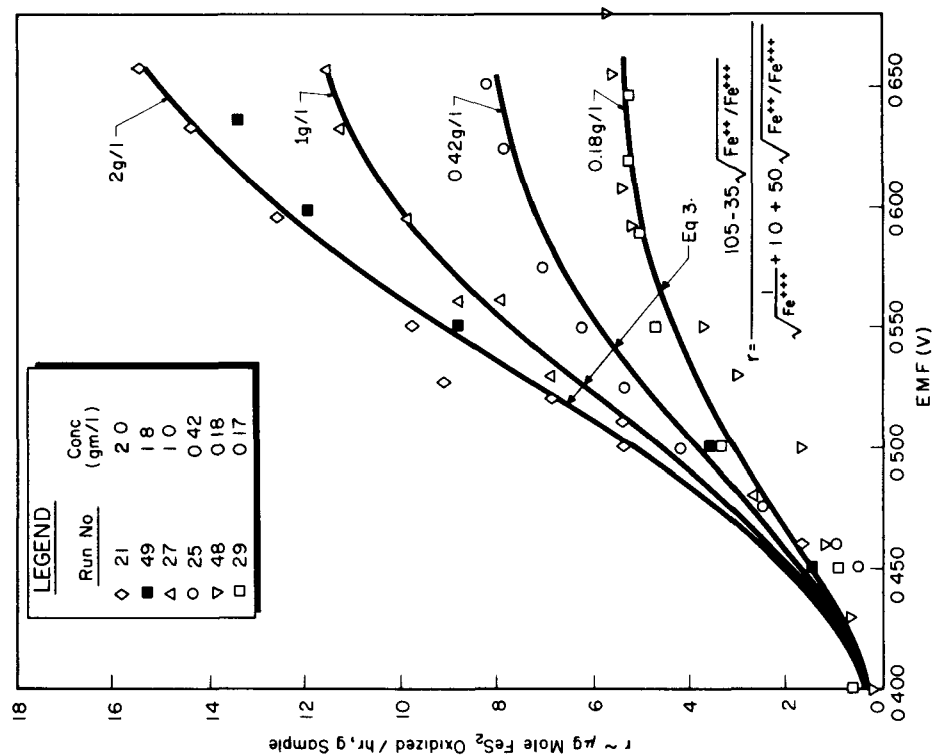


Fig. 21 - Reciprocal Rate vs Reciprocal (Ferric concentration)<sup>1/2</sup>

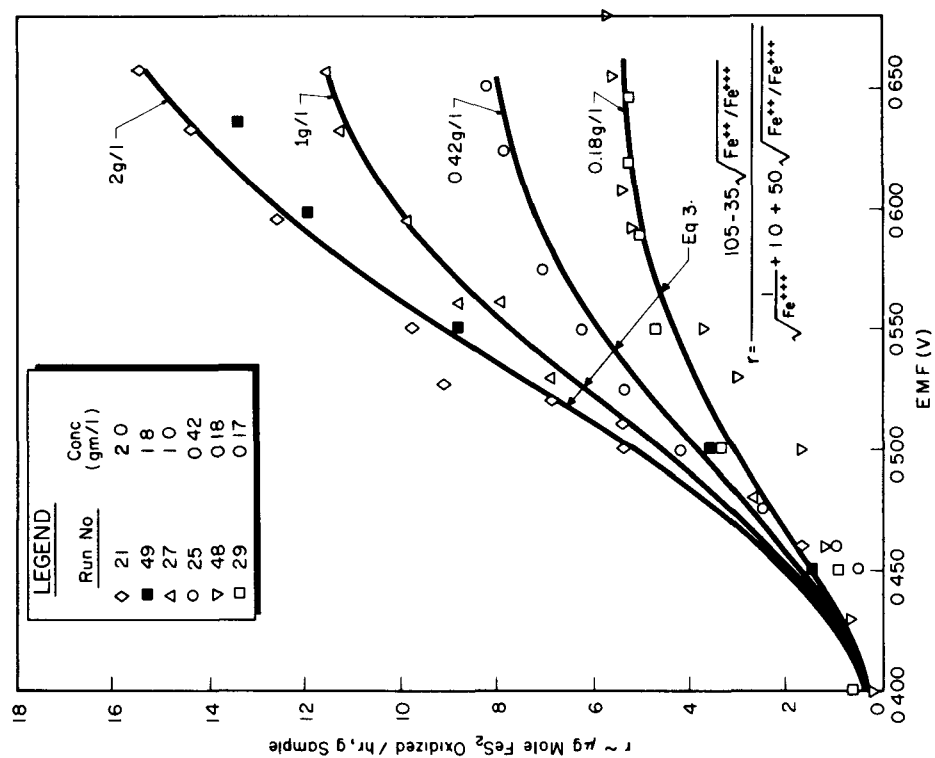


Fig. 22 - Rate vs EMF, McDaniel's Sulfur Ball

At high EMF's, where the square root of the ferrous-ferric ratio ( $\text{Fe}^{++}/\text{Fe}^{+++}$ ) is negligible, this equation may be written

$$r = \frac{k}{\frac{1}{\sqrt{\text{Fe}^{+++}}} + \sqrt{K_1}} \quad (4)$$

or

$$\frac{1}{r} = \frac{1}{k\sqrt{\text{Fe}^{+++}}} + \frac{\sqrt{K_1}}{k} \quad (5)$$

A plot of  $1/r$  vs.  $1/\sqrt{\text{Fe}^{+++}}$  for ferric ion oxidation at high EMF's should give a straight line with a slope equal to  $1/k$  and an intercept equal to  $\sqrt{K_1}/k$ .

These data for the three pyrite samples shown in Tables VI, VIII, and IX are plotted in Fig. 21.

After  $k$  and  $\sqrt{K_1}$  are calculated from the slope and intercept,  $k'$  and  $\sqrt{K_2}$  can be determined in the following manner: Assume that the reaction rate goes to zero as EMF approaches 0.370, or in other terms, as the ferrous-ferric ratio approaches 9.0. (note discussion of potentiostat measurements on page 79 regarding pyrite -- reference cell voltage as current goes to zero). These data were interpreted as an indication of a zero oxidation rate at some low oxidation-reduction potential rather than a means of determining the ferrous-ferric ratio when the rate drops to zero. The value of 3.0 for the ferrous-ferric ratio is taken as a single correlating factor to give best data fit (although potentiostat data indicate this value is a function of iron and sulfate concentration).

By setting the numerator of Eq. (3) equal to zero when  $\sqrt{\text{Fe}^{++}/\text{Fe}^{+++}} = 3.0$ ,  $k'$  is found to equal  $k/3$ .

$K_2$  can be determined from one value of the Rate vs. EMF data where the ferric-ferrous ratio is significant.

The data presented in Table VIII for Sulfur Ball #2 may be used to illustrate the calculation of the Rate Equation.

From Fig. 21, the slope of the line for Sulfur Ball #2 = 0.0061 and Intercept = 0.02, then

$$k = 1/0.0061 = 165$$

$$k' = 165/3 = 55$$

$$(\sqrt{K_1}) = \text{Intercept} \times k = 3.3$$

(Note: since  $\sqrt{\text{Fe}^{++}/\text{Fe}^{+++}}$  is not negligible at EMF = 0.650, the intercept value of 3.3 includes  $K_2$  times  $\sqrt{\text{Fe}^{++}/\text{Fe}^{+++}}$ . By trial and error,  $K_1 = 3.3 - 70 \times 0.0137 = 2.3$ , when  $K_2$  is calculated from rate at EMF = 0.477. Therefore the rate equation, as calculated using Fig. 21 and one point from Rate vs. EMF data is,

$$\frac{165 - 55 \sqrt{\text{Fe}^{++}/\text{Fe}^{+++}}}{\frac{1}{\sqrt{\text{Fe}^{+++}}} + 2.3 + 70 \sqrt{\frac{\text{Fe}^{++}}{\text{Fe}^{+++}}}} \quad (6)$$

Table X compares calculated and experimental rates for these data.

In like manner, the rate equations for the experimental points given in Fig. 22 can be calculated. The solid lines on Fig. 22 are loci of the calculated rates for different total iron concentrations. Calculated and experimental rates for museum grade pyrite are compared in Table VII.

#### Interpretation of Data

The excellent correlation of experimental data by Eq. (3) indicates that the form of the adsorption equation, if not the specific mechanism used to derive it, is relevant. It appears that the relative adsorption of ferrous and ferric ions is rate-determining in ferric ion oxidation. A comparison of adsorption equilibrium constants for ferrous and ferric ions is surprising. For sulfur ball pyrite the ratio of  $K_2/K_1$  (ratio of adsorption equilibrium constants for ferrous and ferric ions, respectively) is 900 for Sulfur Ball #2, 2500 for McDaniels Sulfur Ball, and 45,000 for Museum Grade pyrite. In other words, the relative adsorption of ferrous ions is much greater than ferric for all types of pyrite. The selective adsorption of ferrous ions is particularly great on museum grade pyrite; i.e., more than 20 to 50 times greater than on the sulfur ball. It is also interesting to note that the reactivity of the pyrite samples is inversely related to  $K_2/K_1$ . The rate curves for the three pyrite samples are compared in Fig. 23.

The data show that ferric ion oxidation rates are a function of total iron concentration, and are determined by the ferrous-ferric ratio, not  $E_h$ . As the  $E_h$  of the solution is raised to the point where all iron is ferric, the rate becomes constant. Further increase in  $E_h$  has a negligible effect on rate.

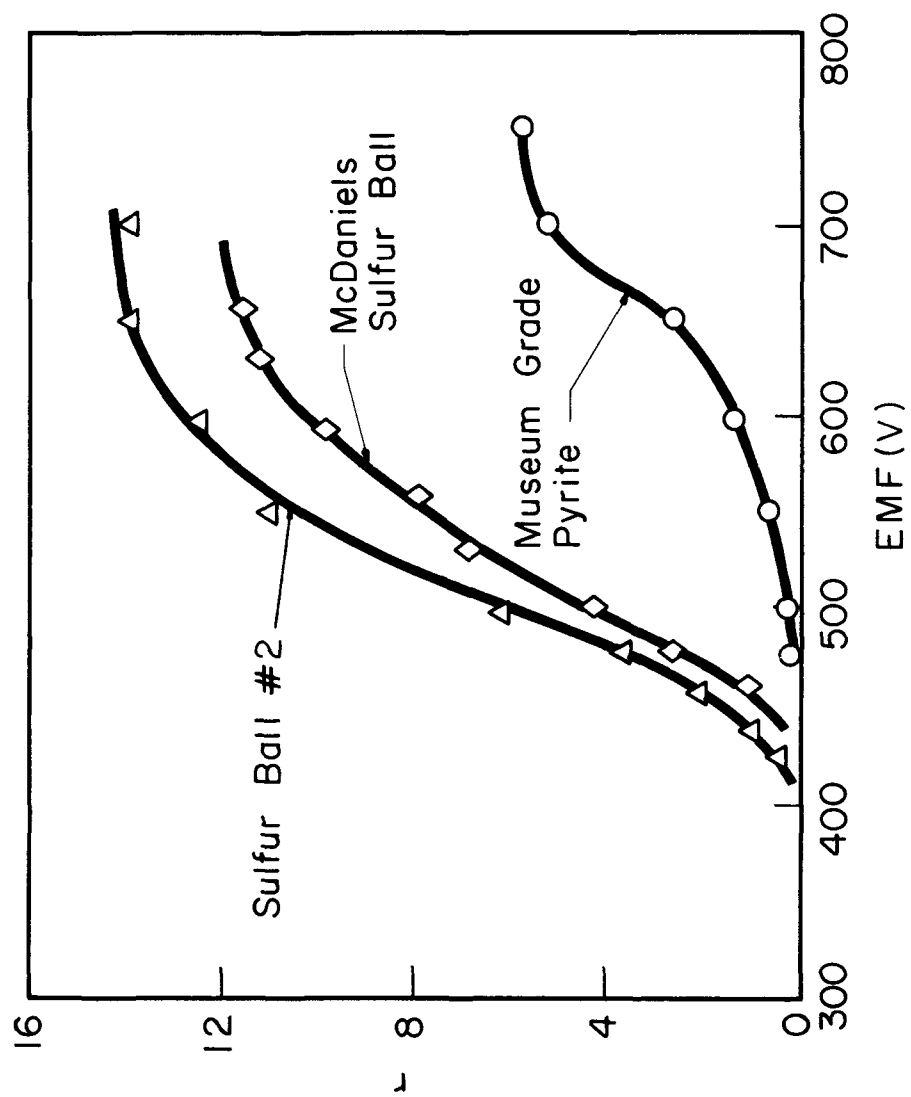


Fig. 23 - Rate vs EMF for Three Pyrite Samples

It should be again noted that all these runs were made at low pH (0.2 to 0.5) and similar sulfate content and ionic strength.

#### Combined Oxygenation and Ferric Ion Oxidation

Results of runs in which both oxygen and ferric ions were present are given in Table XI. The concentration of each oxidizing agent and, in the case of ferric ions, the ferric-ferrous ratio also were selected to give similar oxidation rates. McDaniels Sulfur Ball was the pyrite material used.

Table XI. Combined Oxygenation and Ferric Ion Oxidation:  
McDaniels Sulfur Ball

Run No.	EMF	Iron Conc. (g/l)	Rate (by 100% O <sub>2</sub> )	Rate (by Fe <sup>+++</sup> ions)
31	-	-	3.6	- (aerobic only)
33	500	1.00	3.6	4.5
34	-	-	3.5	- (aerobic only)
35	500	1.00	3.4	4.4
38	500	0.40	3.5	3.5
41	550	0.20	3.4	5.1
45	550	0.20	3.5	5.0

These combined oxygenation-ferric ion oxidation runs show the independence of the two reaction modes. The oxygenation rate is not influenced by solution EMF or ferric-ferrous ratio, and the ferric ion rate is not changed by the partial pressure of oxygen. This leads to the conclusion that the reactive sites for the two oxidation mechanisms are not the same.

It is interesting to note that the increase in oxidation rate, over the oxygenation rate, is approximately the same for samples heavily inoculated with *Ferrobacillus ferrooxidans*<sup>1,2</sup> and samples subject to ferric ion oxidation at high ferric-ferrous ratios. This observation, together with those discussed in the Microbiology section, leads to the conclusion that bacteria such as *Ferrobacillus ferrooxidans* function to generate a high ferric-ferrous ratio in solution. The rate of oxidation by ferric ions would then be the same in both a biological or chemical system, and determined by the ferric-ferrous ratio and total iron concentration. In real systems, the ferric-ferrous ratio is a steady-state value determined by the relative rates of (1) microbial oxidation of ferrous ions to ferric and (2) reduction of ferric ions by reaction with pyrite.

These data provide a basis for defining the reaction regime (i.e., oxygenation or ferric ion oxidation) if data on oxygen concentration, total iron, and the ferric-ferrous ratio at the reaction site are known. Oxygenation and ferric ion oxidation rates are approximately the same at oxygen partial pressures of 0.21 atm, when EMF = 0.450. This corresponds to a ferric-ferrous ratio of 2.2 or 70% of iron ions in the ferric state. At an EMF of 0.40, where 24% of iron is ferric, the ferric ion rate is one-fifth to one-tenth the oxygenation rate in air. Only with microbial-enhanced oxidation can ferric-ferrous ratios this high be attained. In other words, if the ferric-ferrous ratio is less than 0.3 (24% ferric) and the partial pressure of oxygen is 15 to 20%, the system is in an oxygenation regime; i.e., the oxidation rate is determined by the chemical oxygenation mechanism. If oxygen vapor concentration is less than 2% and 70% of the iron is in the ferric state, the system is in a ferric ion oxidation regime, generated by microbial activity. Although this last observation is true regardless of microbiological activity, it may have little practical significance. The observation is based on the premise that microbial rate is not influenced by oxygen concentration above a dissolved oxygen concentration of 0.1 ppm; that is, a 70% ferric concentration can be microbially generated at low oxygen levels. More recent data indicate that microbial activity may be limited by oxygen concentration at much higher levels than 0.1 ppm.

It seems evident that no significant amount of pollution is produced by microbial activity from a pyritic system which has an aerobic effluent with a ferric-ferrous ratio less than 0.2 (15% ferric ions).

Since ferrous ion oxidation is a solution reaction, the majority of bacteria will be found in solution. Even if the solution should pass through a section of highly pyritic material (i.e., where the number of bacteria per unit exposed pyrite surface is low because of large pyrite surface) the ferric-ferrous ratio would not drop much below 1.0 since the rate of ferric ion oxidation of pyrite (or ferric ion reduction) decreases rapidly as the ferric-ferrous ratio decreases. The bacterial ferrous ion oxidation would remain the same.

At the same time it is not necessarily true that acid effluents having high (more than 70% ferric ions) ferric-ferrous ratios were generated by microbial action. In underground mines for example, the effluent water may have a long residence time (ponding) after leaving the reaction site. The ferrous ions may be microbially oxidized after contacting pyrite so that the ferric ions are formed in a pyrite-free environment and do not contribute to the actual oxidation of pyrite.

In other words, significant microbial-enhanced pyrite oxidation may be discounted in pyritic systems having a low ferric-ferrous ratio aerobic effluent (less than 0.2). A high ferric-ferrous ratio in low-pH mine waters does not prove that microbial activity was important in the actual oxidation of pyrite. It only proves that microbial oxidation of ferrous ions to ferric has occurred. If a high ferric-ferrous ratio

is generated while the solution is in the presence of exposed pyrite, ferric ion oxidation will occur.

The controversy that has developed over the relative significance of oxygenation or ferric ion oxidation may lie in the difference between museum grade and sulfur ball pyrite.

As noted earlier, the ratio of adsorption equilibrium constants ( $K_2/K_1$ ) for museum grade and sulfur ball pyrite differ by a factor of 20 to 50, indicating the selective adsorption of ferrous ions is greater on museum grade pyrite. The difference in oxygenation rates for the same samples is equally significant. As given in Appendix V, the oxygenation rates for museum grade pyrite and McDaniels sulfur ball are 0.03 and 3.5  $\mu\text{g mole/hr,g}$ . The corresponding maximum ferric ion oxidation rates for museum grade pyrite and McDaniels sulfur ball are (from Fig. 23) 6 and 12  $\mu\text{g mole/hr,g}$ .

The ratio (maximum ferric ion oxidation rate/oxygenation rate) for museum grade pyrite is  $6/0.03 = 200$ . The same ratio for the sulfur ball sample is  $12/3.5 = 3.4$ . If one were to judge the relative importance of ferric ion oxidation and oxygenation on data obtained on museum grade pyrite, an erroneous conclusion could be reached in respect to relative rates which exists in real pyritic systems.

Also note that the maximum ferric ion oxidation rates quoted above are higher than could be reached in real systems even under ideal conditions.

#### Varying pH, Type and Concentration of Anion

Reports<sup>9</sup> on oxidation by ferric ions noted a negligible effect of pH on rate for pH's below 2.0. An investigation of the accuracy of this report has led to an interesting study involving effect of pH or anion concentration on the kinetics of ferric ion oxidation. Data are presented in Appendix IV.

As shown in Figs. 24-27, oxidation rate changes greatly in both sulfuric and hydrochloric acid solutions, as the pH is varied from 0.5 to 2.0. In both solutions, the rate is higher when the pH is higher. Since the pH was adjusted by adding either sulfuric acid or hydrochloric acid, a decrease in pH was accompanied by an increasing in anion concentration. Therefore, it is necessary to determine which of the two variables, pH or anion concentration, affects the rate or whether both variables are influential.

Figure 25 shows that at equal pH values the reaction rates are always lower when  $\text{HSO}_4^-$  concentrations are higher. In solutions having pH = 2.0 and  $\text{HSO}_4^-$  concentrations of 0.32 g-mole/l, the rates are comparable to those in solutions having pH = 0.5 and  $\text{HSO}_4^-$  concentration of 0.49 g-mole/l. It therefore appears that the sulfate concentration

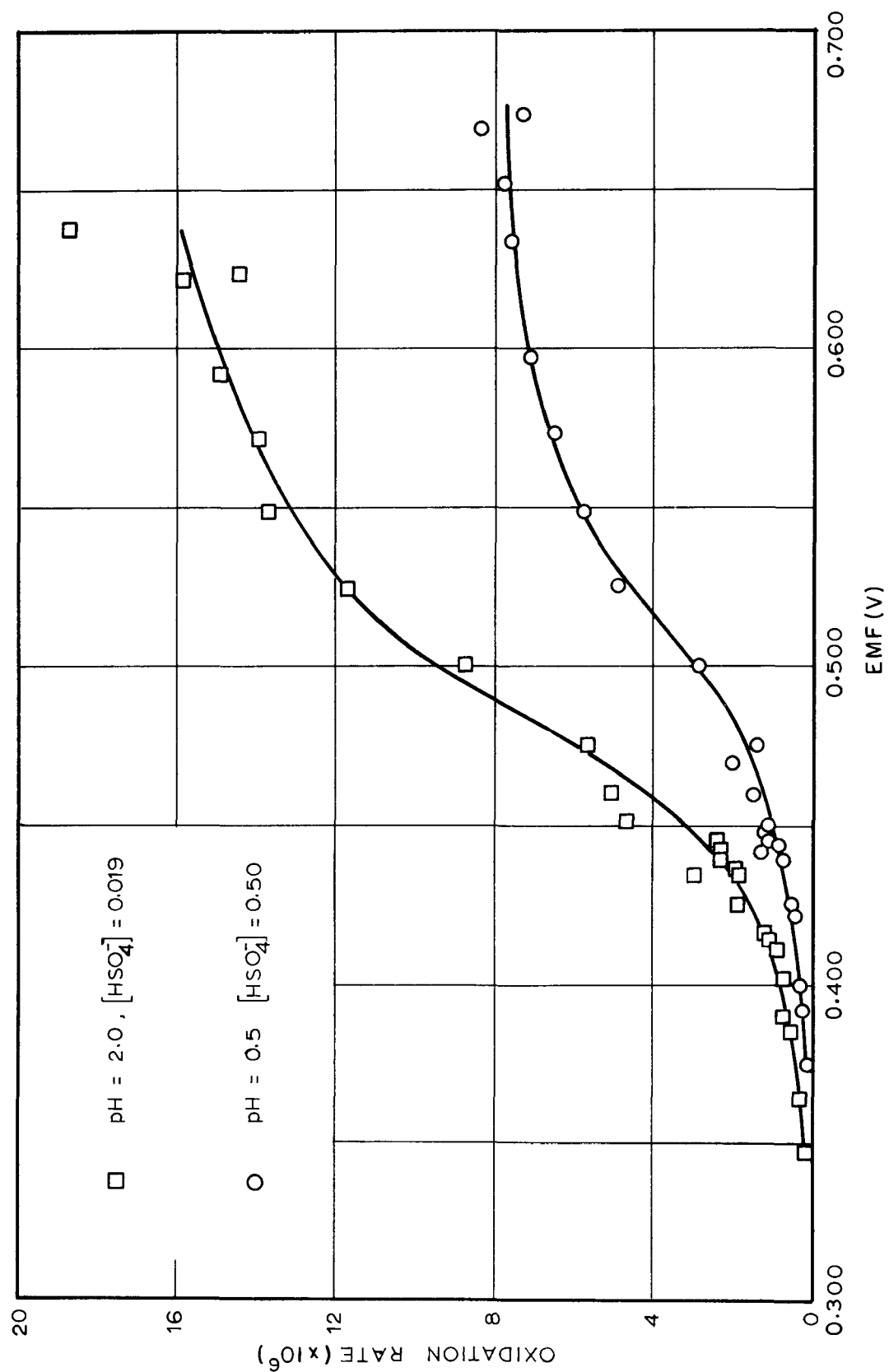


Fig. 24 - Rate vs EMF in Sulfate Solution



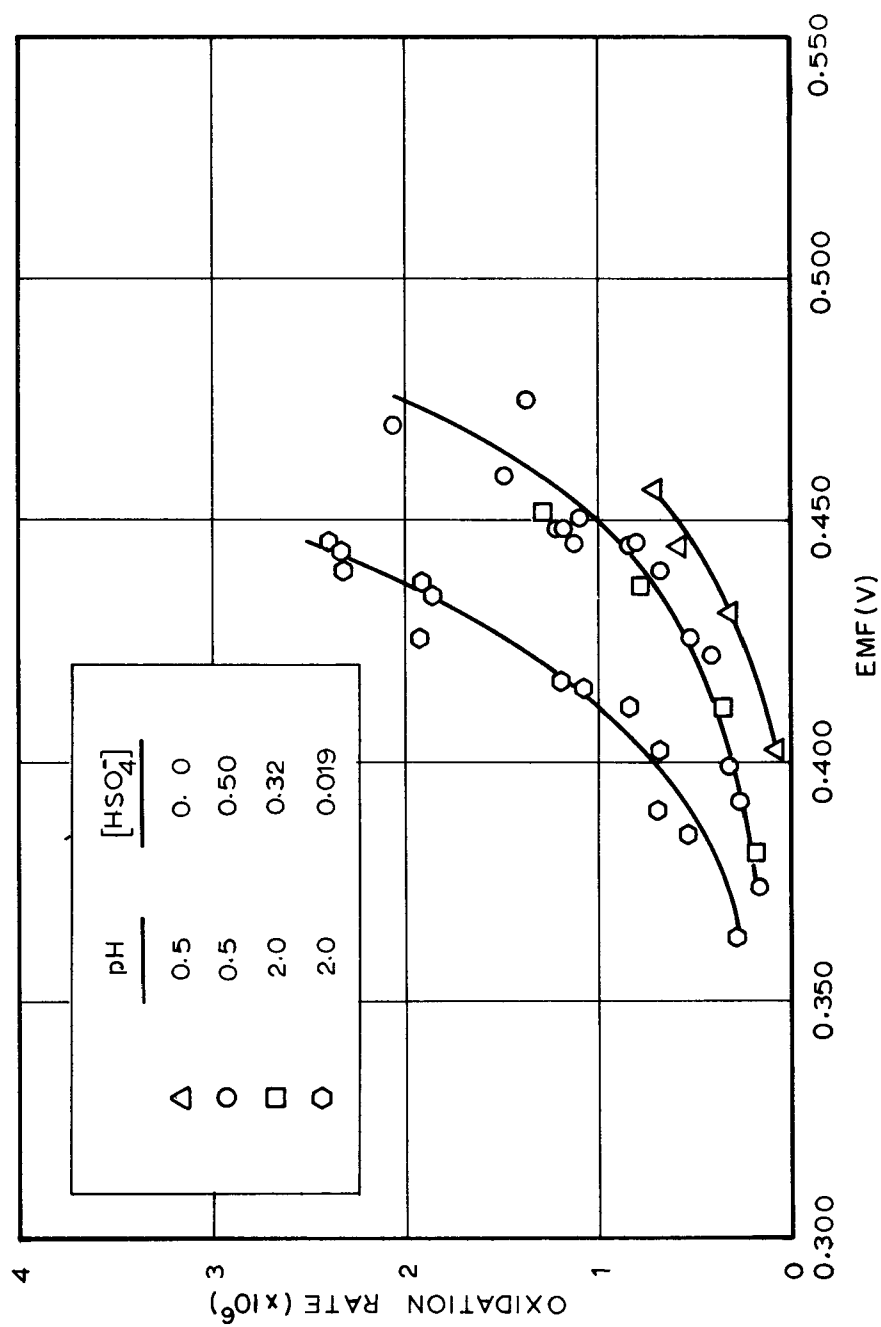


Fig. 25 - Effect of Sulfate Concentration

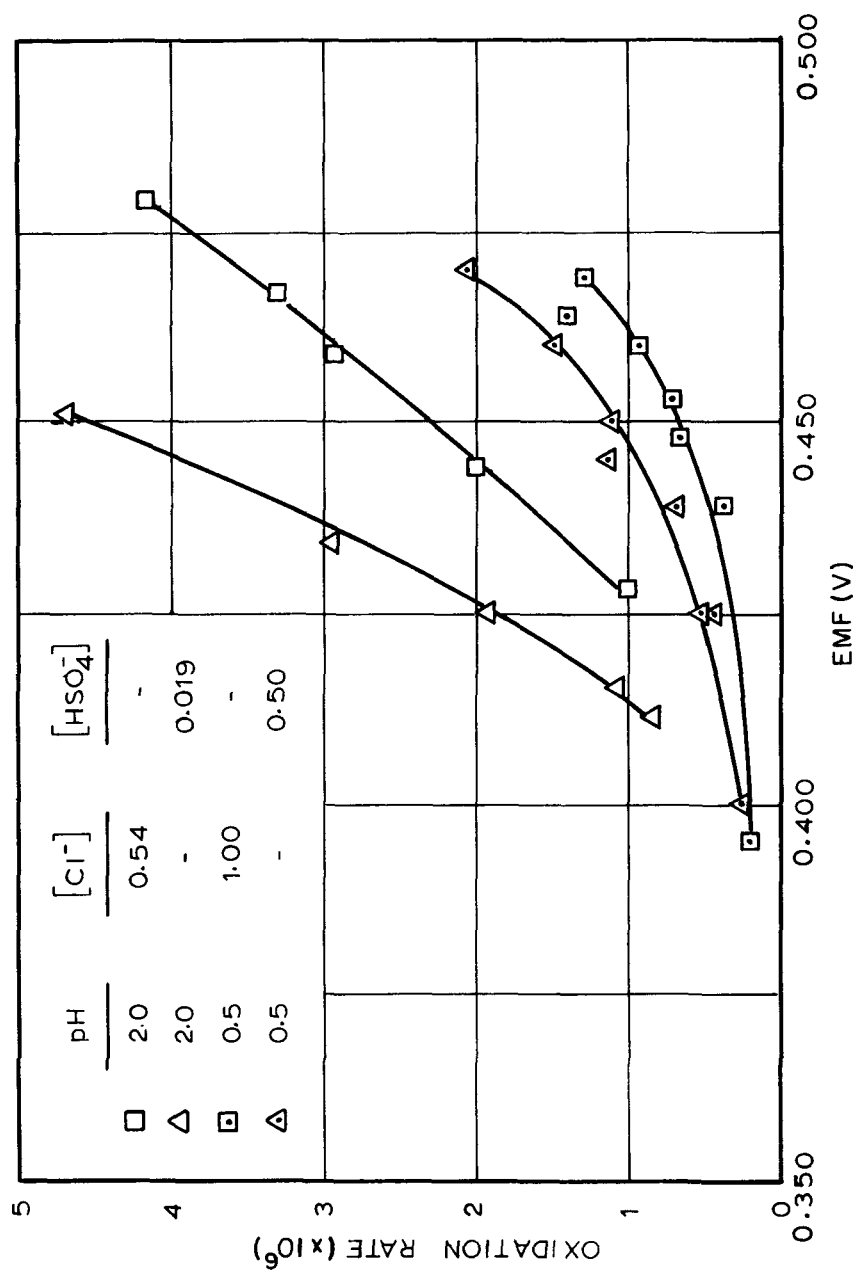


Fig. 26 - Comparison of Rates in Sulfate and in Chloride Solution

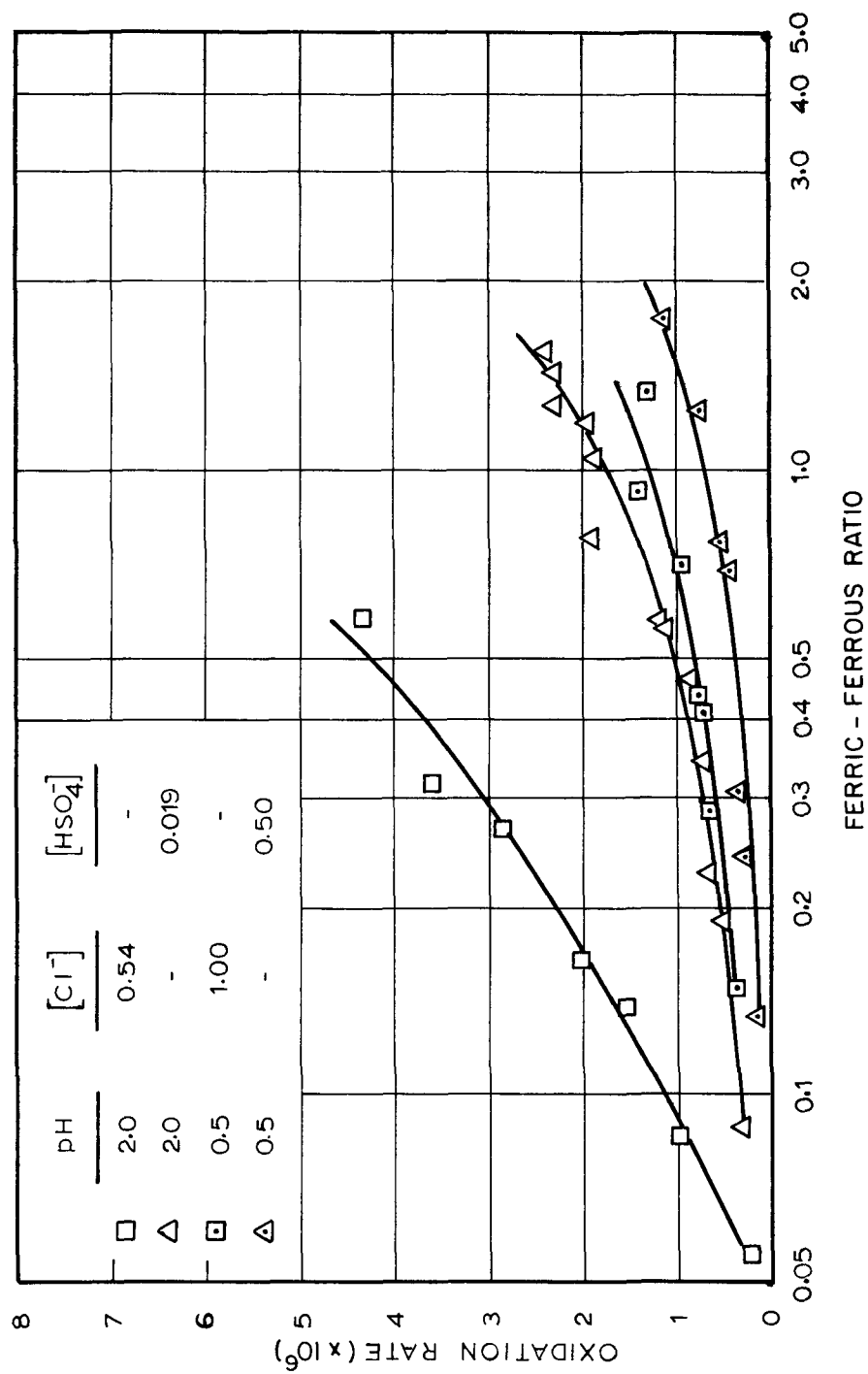


Fig. 27 - Comparison of Rates in Sulfate and in Chloride Solution

is the primary influence on rate and not pH. Following this premise further, it is probable that the increase in rate with increasing pH in chloride solutions actually results from the decrease in chloride concentration.

There are two possible mechanisms by which anion concentration can affect the oxidation rate; i.e., (1) the anions may be adsorbed on the pyritic surface, reducing the available sites for adsorption of ferric ions, or (2) complexes of ferric ions are formed with the anions, and the complexes are not as readily adsorbed on the pyrite surface.

It is possible that sulfate ions can be adsorbed on the pyrite surface since sulfate is an oxidation product of pyrite. It is unlikely that chloride ions would be adsorbed to the same degree, at least to the extent they need be considered in competitive adsorption for reactive sites.

In sulfate as well as chloride solutions, several complexes of ferric ions can be formed. Whatever form of complex the ions have with the anion, the formation of complexes cause a reduction in the net positive charge of the group. Since the reduction of ferric ions requires the transfer of an electron to the ferric ions, it is reasonable that such transfer will be retarded because of the negative charges of the complexed anion (or anions) surrounding the ferric ion. Furthermore, the diameter of the complexed ions would be larger than that of non-complexed ferric ions. In the case of sulfate complexes, the diameter of the complexed ferric ion would be even larger than that of hydrated ferric ion. This fact can very likely account for the difference in degree of adsorption of complexed ions compared to free ferric ion.

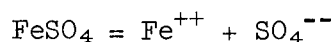
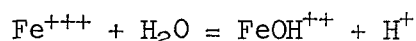
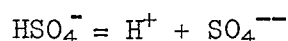
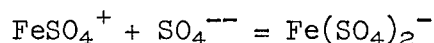
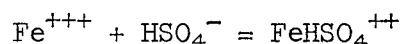
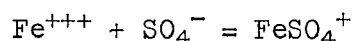
Based on the above conditions, one can postulate that the only ferric ions which are active in the reaction with pyrite are those that are not complexed. In order to evaluate this postulate, it is necessary to determine the composition of the ionic species in the reaction solution.

#### Ionic Composition of the Reaction Solution

To be able to determine the ionic composition of the reaction solution, we must know the type of iron complexes in the solution and the ionic equilibrium relationship between the species in the solution. A brief description of iron complexes in sulfate and chloride solutions is given below.

#### Iron Complexes in Sulfate Solution

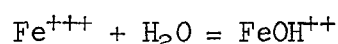
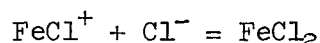
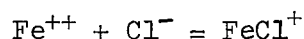
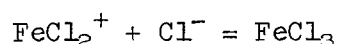
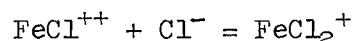
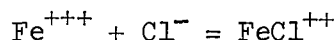
Several complexes of ferric and ferrous ions have been identified.<sup>13,25,27</sup> The equations below describe the complex formations and association reactions of the iron ion in sulfate solution in the pH range involved.



Considering the equilibrium relationship of each reaction, the composition of the ionic species in solution can be calculated. In Appendix III a detailed description of the calculation procedure is given. For the calculation, equilibrium constant values (also known as stability constants) were taken from the literature.<sup>20</sup> These values are also tabulated in Appendix III. To be used in the calculation, the values of the stability constants were corrected to values corresponding to the ionic strength of the reaction solutions. The equation proposed by Davies<sup>4</sup> for calculating activity coefficient was used for this purpose.

#### Iron Complexes in Chloride Solution

For the chloride solutions, the equilibrium reactions below were considered.



The complexes formed in the reactions listed above have been identified by Rabinowitz and Stockmayer.<sup>17</sup> Their stability constants are given in Appendix III.

Procedures similar to those used to calculate the ionic composition in sulfate solution were applied. A detailed description is given in Appendix III.

Comparing the free ferric ion concentration in chloride and sulfate solutions, it can be seen that at a given ferric-ferrous ratio and pH value the free ferric ion concentration is the same. As shown in Fig. 26, however, the rates in chloride solution are always higher than the rates in sulfate solution. This can be explained if it is further assumed that, in addition to forming complexes with ferric ions, the sulfate ions also directly inhibit the oxidation reaction. A possible explanation for this is that some sulfate ionic species are capable of being adsorbed on the reactive sites of the pyrite surface. Unfortunately the experimental data to evaluate this assumption directly are not available.

#### Anion Concentration and pH Effect on Kinetics

Based on present information, detailed evaluation of pH or anion concentration effects on ferric ion oxidation kinetics is not warranted.

In the first place the stability constants for the assumed complexes are only approximate. Literature values, in addition to being somewhat inconsistent, are not directly applicable to solutions of high ionic strength used in this work. Depending on the values used for the stability constants, wide variations in ion concentrations result from calculations.

In addition, most of the original experimental data did not include a direct analysis of anion concentration or ferric-ferrous ratio. For example, sulfate ions were added as sulfuric acid to control pH, not to provide a sulfate concentration. At the low pH's used, this is not a good quantitative method for determining sulfate content.

Considering these facts, the best quantitative interpretation can be made from sets of runs at fixed ferric-ferrous ratios, or constant ionic strengths. Under these conditions, actual changes in a variable will be (approximately) proportional to the calculated change of the variable being studied, even if the absolute value of the variable is in error. For example, we may not know the actual value of the free ferric ion concentration because of errors in stability constants, but the change in ferric ion concentration with change in total iron concentration (at a given ferric-ferrous ratio) will be in the same proportion as the actual value.

This is illustrated in Fig. 28 where the reciprocal of the free ferric ion concentration is plotted against the reciprocal oxidation rate; this is the same type of plot as Fig. 21. Here again an excellent correlation of experimental data is obtained. However, this

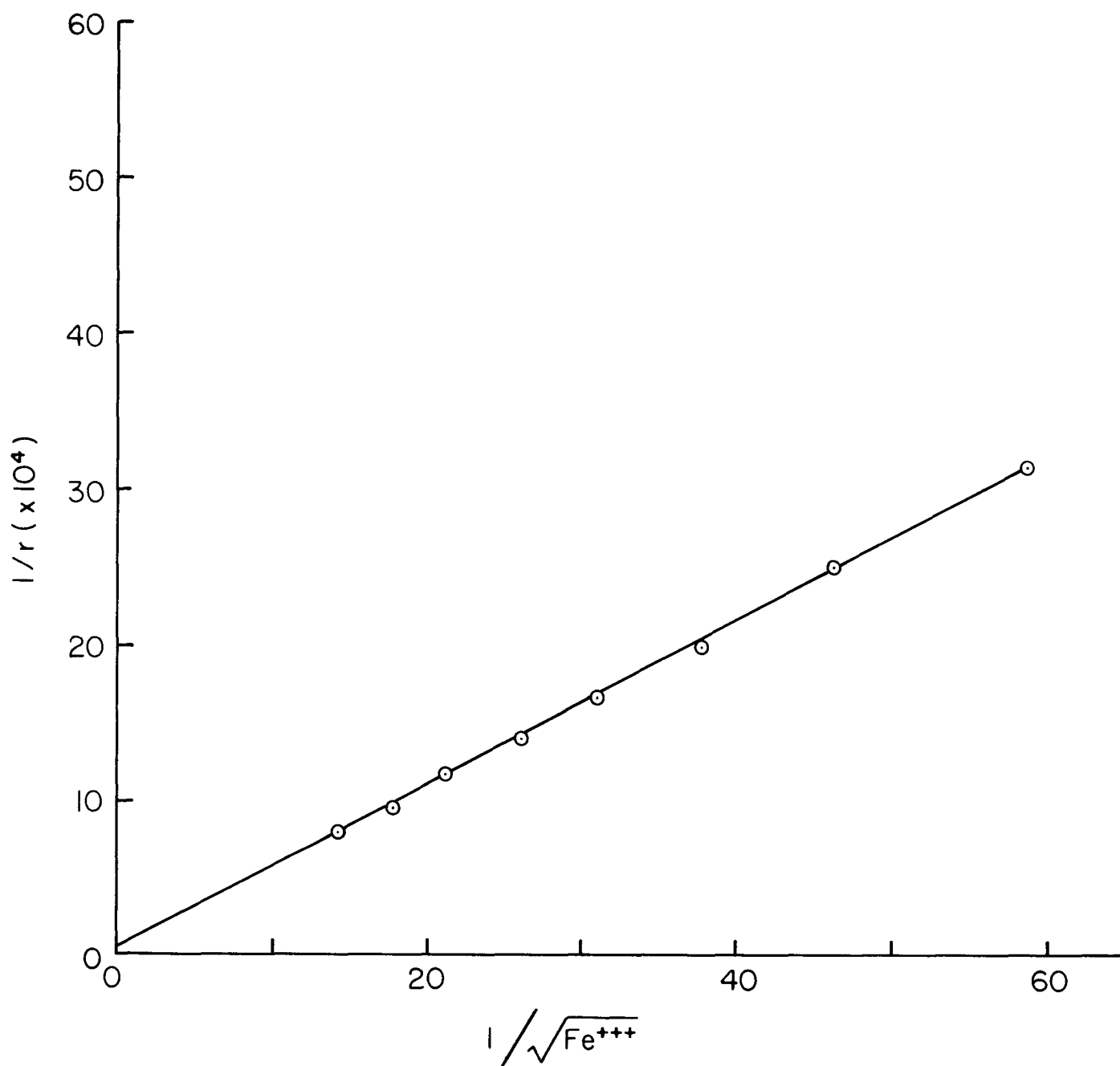


Fig. 28 - Reciprocal Rate vs Reciprocal of the Square Root of Free Ferric Ion Concentration

does not help to identify the active oxidizing ionic species because other ions would undergo a similar change in concentration with change in total iron concentration.

A series of ferric ion oxidation runs was made by Sasmojo<sup>18</sup> at pH = 4.0 in a solution saturated with ferric ions. The EMF was varied from 0.500 to 0.650. As may be expected from the kinetic model previously developed, the oxidation rate was much lower than rates for runs at lower pH and an iron concentration of 0.01 moles per liter. The obvious reason is the low ferric ion concentration that can exist in a solution of such a high pH. Because of the low iron concentration, it was difficult, experimentally, to maintain a reasonably constant EMF, but in runs where well over 99.9% of the iron was ferric, the maximum oxidation rate observed was 0.59  $\mu$ g mole pyrite oxidized per hour per gram pyrite. This is less than 3% of the maximum rate in sulfate solutions of 0.01 molar iron solutions. This rate is also approximately 10% of the oxygenation rate.

As the pH increases, the ferric ion oxidation rate becomes limited by the (free) ferric ion concentration in solution. For a solution of pH = 3.0 and above, it is highly unlikely that the microbial-enhanced reaction rate could be greater than the oxygenation rate simply because there can not be enough ferric ions in solution at high ferric-ferrous ratios to produce that significant an oxidation rate.



## APPENDIX I

### RELATED STUDIES

Specific research projects were undertaken on subjects directly related to the sulfide-to-sulfate reaction. In a few cases, no positive contribution to the overall project was obtained. These studies are reported to describe the difficulties encountered and, hopefully, to assist future researchers in avoiding the same pitfalls and "blind alleys."

#### Determination of Ferric and Ferrous Ion Adsorption

Kinetic data strongly indicate that competitive adsorption of ferrous and ferric ions is a factor determining the rate of ferric ion oxidation of pyrite. An attempt was made to measure directly the adsorption equilibrium constants for these ions to compare with the corresponding constants obtained from kinetic data using Eq. (3).

#### Direct Measurement of Adsorption

The attempt to determine the adsorption isotherm was first made by measuring the amount of ferrous and ferric ions adsorbed on pyrite surfaces. The experiment was conducted by equilibrating a ferric or ferrous solution with the pyrite particles. The amount of iron adsorbed was to be determined by the difference between iron concentrations before and after the solution was equilibrated with the particles.

This method was not successful because (a) the amount of ferric or ferrous ions adsorbed appeared to be very small, so that the change in iron concentrations before and after the solution was contacted with the pyrite particles did not show any change in iron concentration; and (b) complications arose because of reaction of the ferric ion with pyrite. Furthermore, there was always pyrite itself, from which iron could be desorbed upon contacting the pyrite particles with a solution.

Because of the difficulties encountered, the direct experimental approach to determining the adsorption of ferric and ferrous ion was discontinued.

#### Adsorption from Streaming Current Measurement

The adsorption of ions from a solution on solid surfaces in contact with the solution will result in the formation of an electrical double layer at the solid-liquid interface. The formation of such a double layer causes several phenomena to occur when there is a relative motion between the solid surface and the solution. Such phenomena are known as electrokinetic phenomena. One is the development of a streamin

current when a liquid is flowing past solid surfaces with large surface areas.

Based on the consideration that adsorbed ionic species could cause a streaming current, a method was developed to determine the adsorption of ferric and ferrous ions from measurements of streaming current.

The electrical double layer is an array of charged particles which exist at every interface. This array may consist of a layer of adsorbed ions, known as the compact layer, followed by a diffuse layer consisting of an ionic atmosphere, in which ions of one sign are in excess relative to those of the opposite sign. This excess charge will balance the electrical charges of the adsorbed ions. Therefore there is an unsymmetric distribution of charges in the neighborhood of the solid-liquid interface. Detailed discussion of the double layer theory can be found elsewhere<sup>16</sup> and will not be presented here.

If we let a solution in contact with solid particles flow while maintaining the solid particles at their fixed position, the diffuse layer will be carried away from the particles' surface. Since the diffuse layer contains excess charged particles of one sign, the flow of the solution causes transport of electrical charges; i.e., a current flow is developed. This transport of electrical charges due to the flow of a solution past solid surfaces is known as streaming current. If we can measure this streaming current, we would know the amount of charged particles in the diffuse layer that are transported by the flowing liquid. Since the charges in the diffuse layer are balanced by the charges of the adsorbed ions, the amount of the adsorbed ions can be determined if we know the valence of the adsorbed ions, and if there is only one type of adsorbed ion.

#### Equation for Streaming Current

The streaming current is the number of electrical charges of charged particles in an electrolyte solution transferred per unit of time attributable to the flow of the solution past solid surfaces. If we have a packed bed of solid particles, the streaming current can be expressed by the equation,

$$I_{str} = \eta_d \cdot a_i q \quad (7)$$

where

$I_{str}$  = streaming current (A),

$\eta_d$  = charge density in the diffuse double layer  
(C/cm<sup>2</sup> of interfacial area),

$a_i$  = interfacial area per unit volume of the packed bed ( $\text{cm}^2/\text{cm}^3$ ), and

$q$  = volumetric flow rate of the liquid ( $\text{cm}^3/\text{sec}$ ).

The charge density of the compact layer,  $\eta_c$ , is given by

$$\eta_c = -\eta_d \quad (8)$$

since the compact layer and the diffuse layer have charges of opposite sign.

In order to obtain the value of  $\eta_c$ , an expression for  $q$  should be known. For flow through a packed bed, we can use the Blake-Kozeny equation;

$$q = \frac{6}{25} \frac{\Delta P (\phi/a_i)^2 \phi A}{\mu L} \quad (9)$$

where

$\Delta P$  = pressure drop across the packed bed ( $\text{dyn}/\text{cm}^2$ ),

$\phi$  = void fraction of the packed bed,

$A$  = superficial cross-sectional area of the packed bed ( $\text{cm}^2$ ),

$\mu$  = viscosity of the solution (poise), and

$L$  = length of the packed bed (cm).

Combining Eqs. (7), (8) and (9), we obtain

$$\eta_c = \left[ \frac{25}{6} \cdot \frac{\mu L}{\phi^3 A q (\Delta P)} \right]^{1/2} I_{\text{str}}^{-1} \quad (10)$$

All the quantities on the right hand side of Eq. (10) can be determined experimentally, and therefore  $\eta_c$  can be calculated.

## Experimental

The equipment used to measure the streaming current consisted of a packed bed of pyrite particles, assembled in a constant head arrangement, so that liquid flow through the packed bed could be maintained constant. A stop-clock was provided in the flow line to regulate the liquid flow rate. A rotameter was used to measure the flow rate. The pressure drop across the packed bed was obtained from a prepared calibration curve, relating pressure drop to flow rate.

To measure the streaming current, a platinum electrode was provided at each end of the packed bed. Each electrode was constructed from platinum gauze welded to a platinum wire, which functioned as a frame and leads for external connections. Outside the packed bed the platinum electrodes were connected by a resistor having resistance much less than the resistance of the solution. The ratio of the solution resistance to that of the resistor was 1000:1. With this arrangement, most of the streaming current developed would be conducted through the external resistor. By using a resistor of known resistance, the streaming current can be determined from the potential drop across the resistor.

Preliminary measurement of the streaming current showed that its value was of the order of  $10^{-6}$  A. A consistent and reproducible result, however, could not be obtained. For an unknown reason, erratic results were always obtained. Since the cause of the erratic behavior could not be found, the experiment was discontinued.

## Conclusions

It is very possible that an extremely small number of adsorption sites make a direct determination of adsorption equilibrium constants difficult from an experimental point of view. Measurement of adsorption isotherms for liquid phase systems is difficult under the best conditions. Pyrite, with its low surface area, is an extremely difficult material to work with. We do not believe that the failure to experimentally observe adsorption of ferric or ferrous ions should in itself raise doubts as to the adsorption mechanism proposed to explain the kinetics of pyrite oxidation by ferric ions.

## Application of the Potentiostat to Pyrite Oxidation Studies

A potentiostat was used as a tool to study the sulfide-to-sulfate reaction. We hoped that it would prove to be an effective instrument that could quickly and accurately determine the oxidation rate of pyrite, and aid in finding the reaction mechanism.

Unfortunately, no relationship between current flow, pyrite-electrode potential, and conventional oxidation rates could be found. Only at, or approaching, equilibrium conditions were results reproducible and capable of rationalization.

A crystal of museum pyrite was the anode and the potential between the anode (pyrite) and reference cell (saturated KCl) was controlled by the potentiostat. The anodic current was determined as a function of the pyrite-to-reference cell voltage for different solution concentrations; results are plotted in Fig. 29. When the potentiometer setting of the potentiostat was plotted as a function of pyrite-to-reference cell voltage the data shown in Fig. 30 were obtained. Note that the voltage at which current flow goes to zero is the same in each case, as would be expected, but the extrapolation to the potential corresponding to zero current is much easier using Fig. 30.

A detailed discussion of the equipment and procedure used in this study is given by Wendschuh.<sup>26</sup>

### Inhibition Studies

An effort was made to find a chemical inhibitor for the pyrite oxidation reaction. Physical methods for preventing the reaction, such as impervious coatings, elimination of oxygen or water, etc., are dependent on the physical properties of the pyritic system itself and must therefore be examined on a pilot or field scale.

For the chemical oxygenation reaction, several ions are known to decrease oxidation rate; e.g., phosphate, thiocyanate, phenanthroline, and bipyridine. The plan was to evaluate these and other materials in an attempt to resolve the mechanism by which inhibition occurs. Hopefully, it would then be possible to specify a material which could be added to the pyritic system as a vapor, thereby reaching the majority of the reactive areas in an underground mine.

Other ions, as listed in Table XII, were selected on the basis of their adsorption characteristics, iron complexing ability, and oxidation-reduction values in solution.

Table XII. Chemical Inhibition Tests

Ion Studied	Effect on Rate
Fluoride	increase
Oxalate	-
Chloride	-
Sulfate	-
Thiocyanate	50% decrease
Phenanthroline	50% decrease
Bipyridine	50% decrease
Hydroxylamine	90% decrease
Nitrate	-
Iodide	-
Borate	-
Chlorate	increase
Phosphate	80% decrease

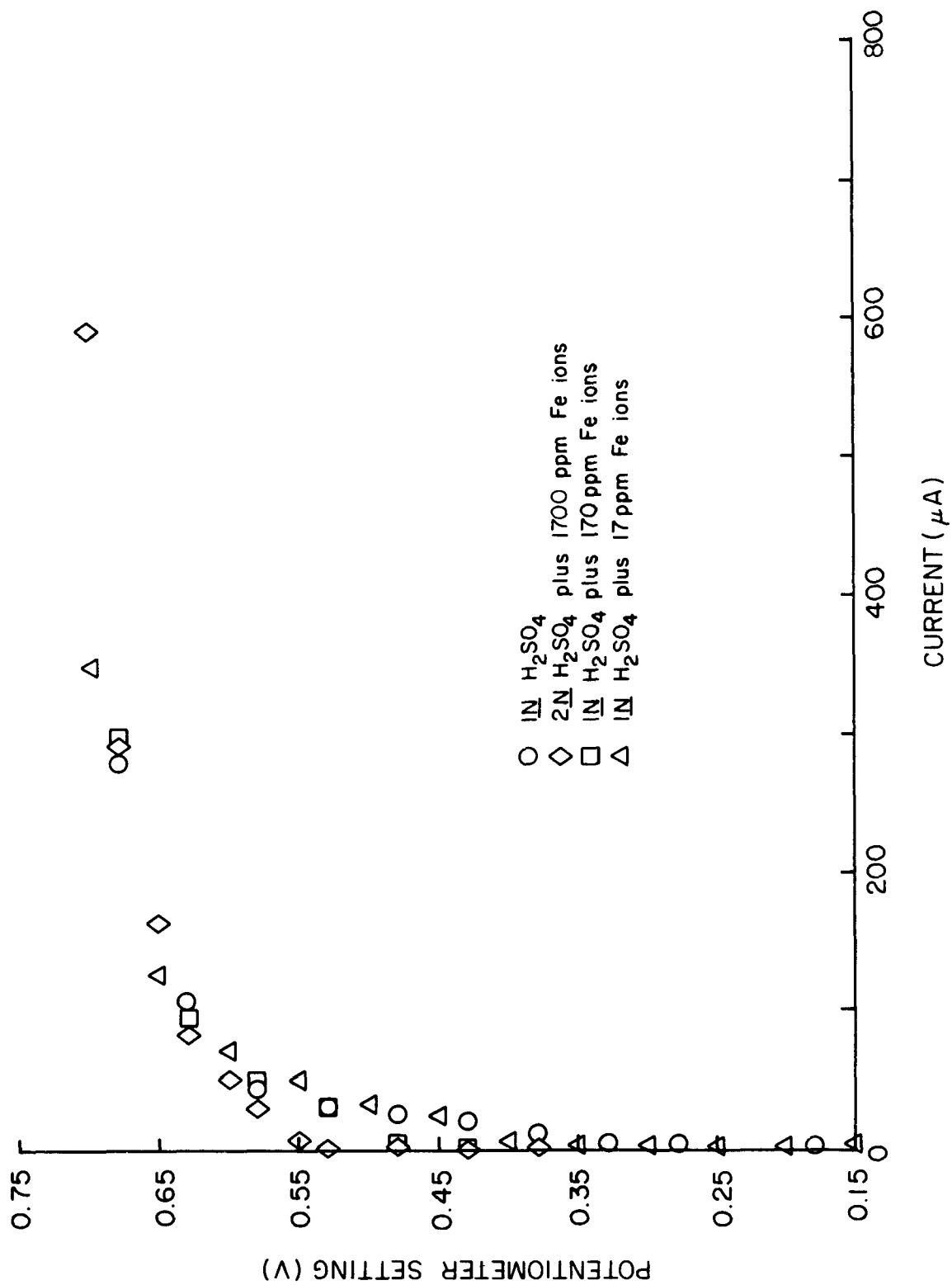


Fig. 29 - Potentiometer Setting vs Current

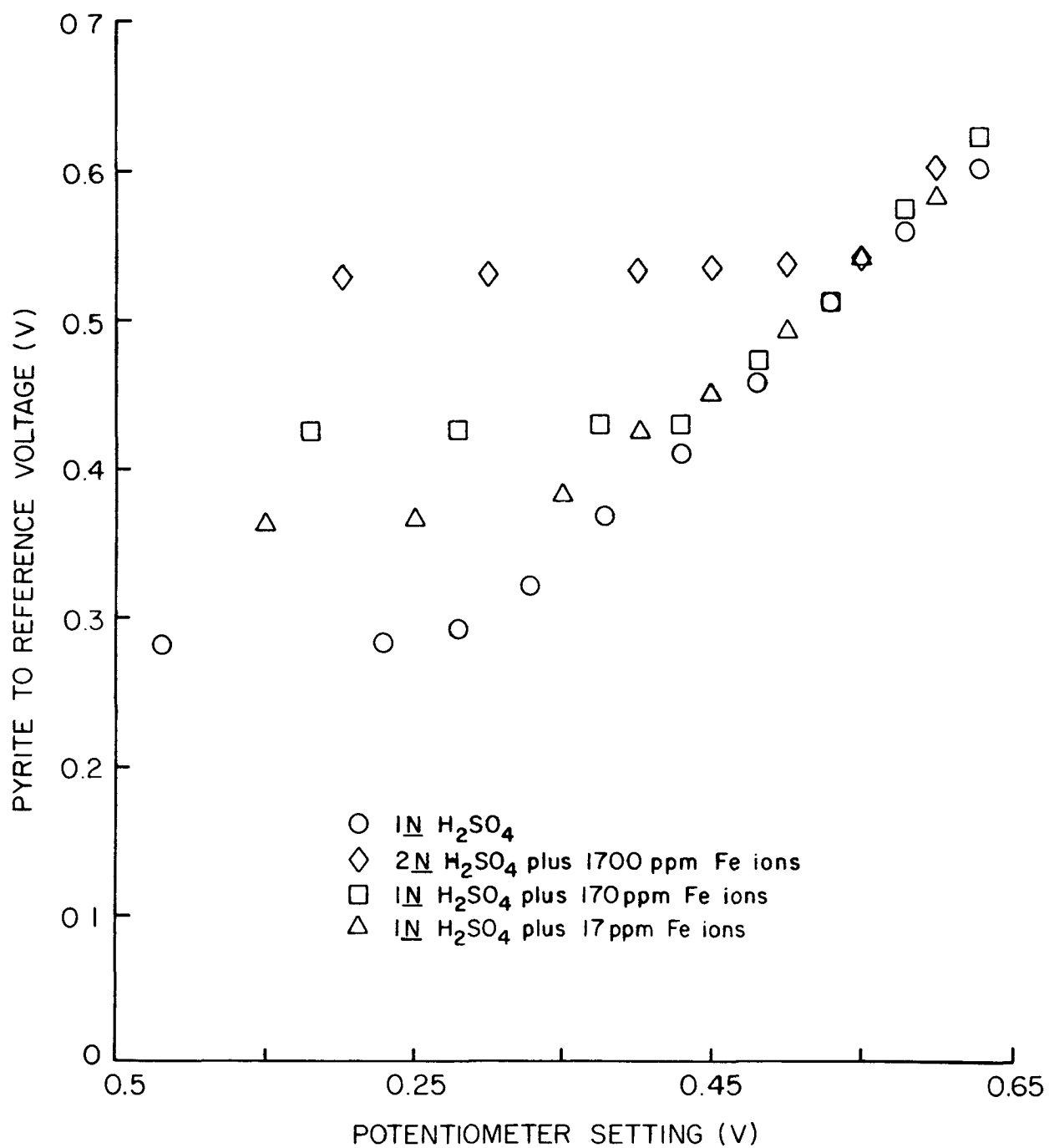


Fig. 30 - Pyrite to Reference Voltage vs Potentiometer Setting

It should be noted that all of the above ions had to be present in concentrations greater than 250 ppm before any appreciable effect on rate was observed. Rate was determined by change in iron concentrations of solution, not oxygen absorption. In several of the organic ions, oxidation of these ions consumed oxygen, and in the case of hydroxylamine hydrochloride, probably reduced the dissolved oxygen concentration to produce the low oxidation rate.

Since oxygenation rates are independent of iron and sulfate concentrations, it was not surprising to observe that there is no correlation between complexing strength for ferrous or ferric ions and change in oxidation rate.

No quantitative measure of adsorption was possible so that relative adsorption of the inhibitory ions is not known. However, based on structural considerations, relative adsorption does not appear to be a logical explanation for the observed data.

#### Adsorption of Oxygen, Nitrogen, and Water on Pyrite

The gas phase adsorption isotherms reported in this section were determined for two reasons: first, to evaluate that physical property of pyrite (or pyritic material) that determines adsorption capacity of the different gases; and second, to try to find an independent method of evaluating adsorption equilibrium constants previously determined from Eq. (1) or (2). Unfortunately the total adsorption of oxygen in relation to that adsorbed by the reaction was too small to obtain a reliable value as a difference.

Adsorption isotherms for oxygen, nitrogen and water were determined for both Museum Grade and Sulfur Ball pyrite at 25°C. Curves and data points are given in Figs. 31-37. Surface area was determined for each material by nitrogen adsorption at 77.3°K. The 100 - ∞ mesh Museum Grade sample had a surface area of 0.70 m<sup>2</sup>/g, and the 70-100 mesh Sulfur Ball material had an area of 0.82 m<sup>2</sup>/g as determined from a B.E.T. plot of nitrogen adsorption data.

The nitrogen adsorption curves at 77.3°K (Figs. 31 and 32) are normal for materials of low surface area.

The difference in the Museum Grade and Sulfur Ball samples is apparent in the nitrogen adsorption curves at 25°C. The adsorption of nitrogen on the Sulfur Ball is almost a hundred times greater than for Museum Grade pyrite. This is no doubt due in part to adsorption on the small quantity of carbonaceous and siliceous material included in the Sulfur Ball agglomerates. However, it is equally apparent, when considering the difference in reactivity of Sulfur Ball and Museum Grade pyrite, that a significant fraction of this increased adsorption is due to pyrite itself. The small-grained agglomerates composing Sulfur Ball would present many more adsorption sites per unit surface



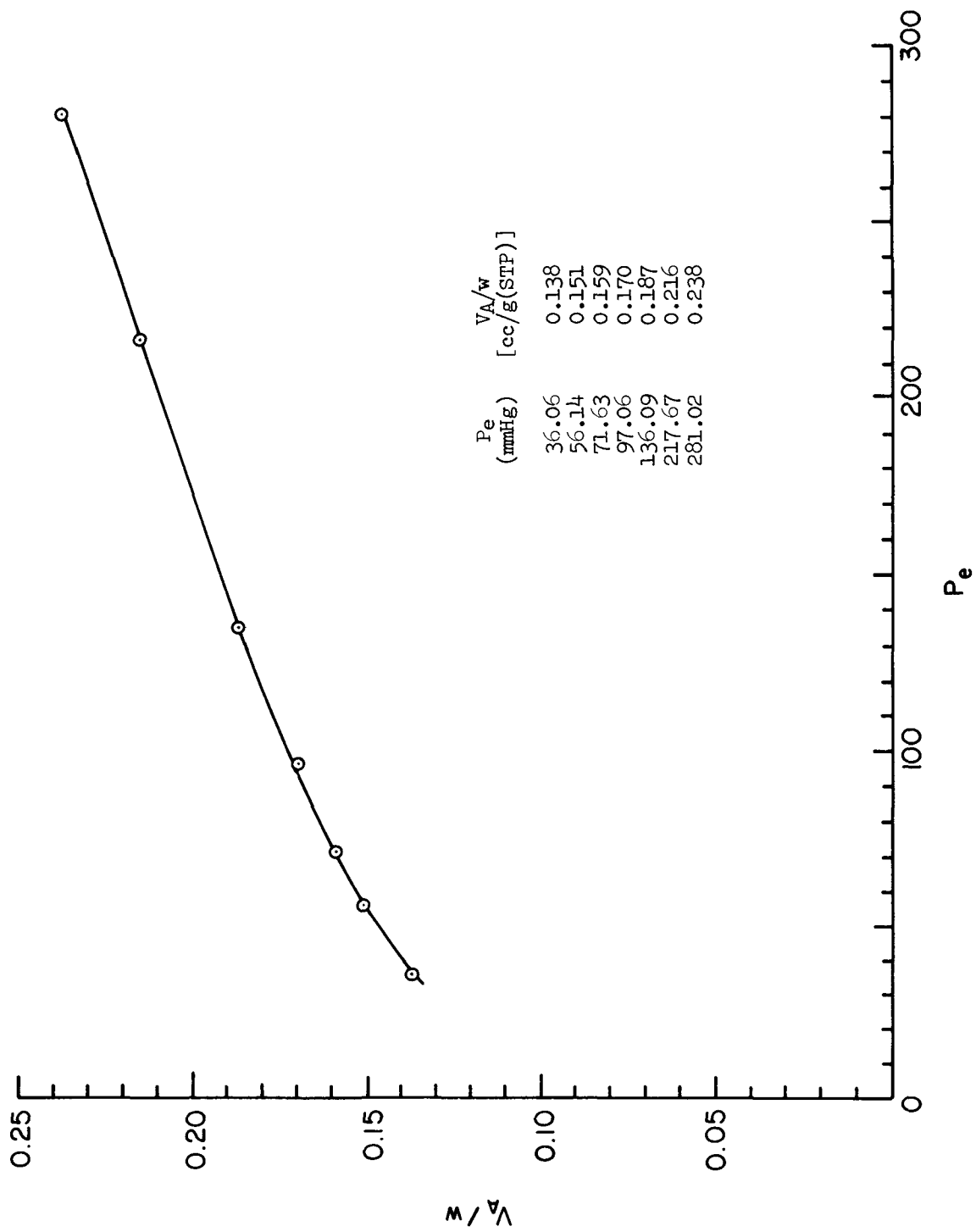


Fig. 31 -  $N_2$ -Adsorption Isotherm on "Museum Grade" Pyrite 100- $\infty$  Mesh at 77.3°K

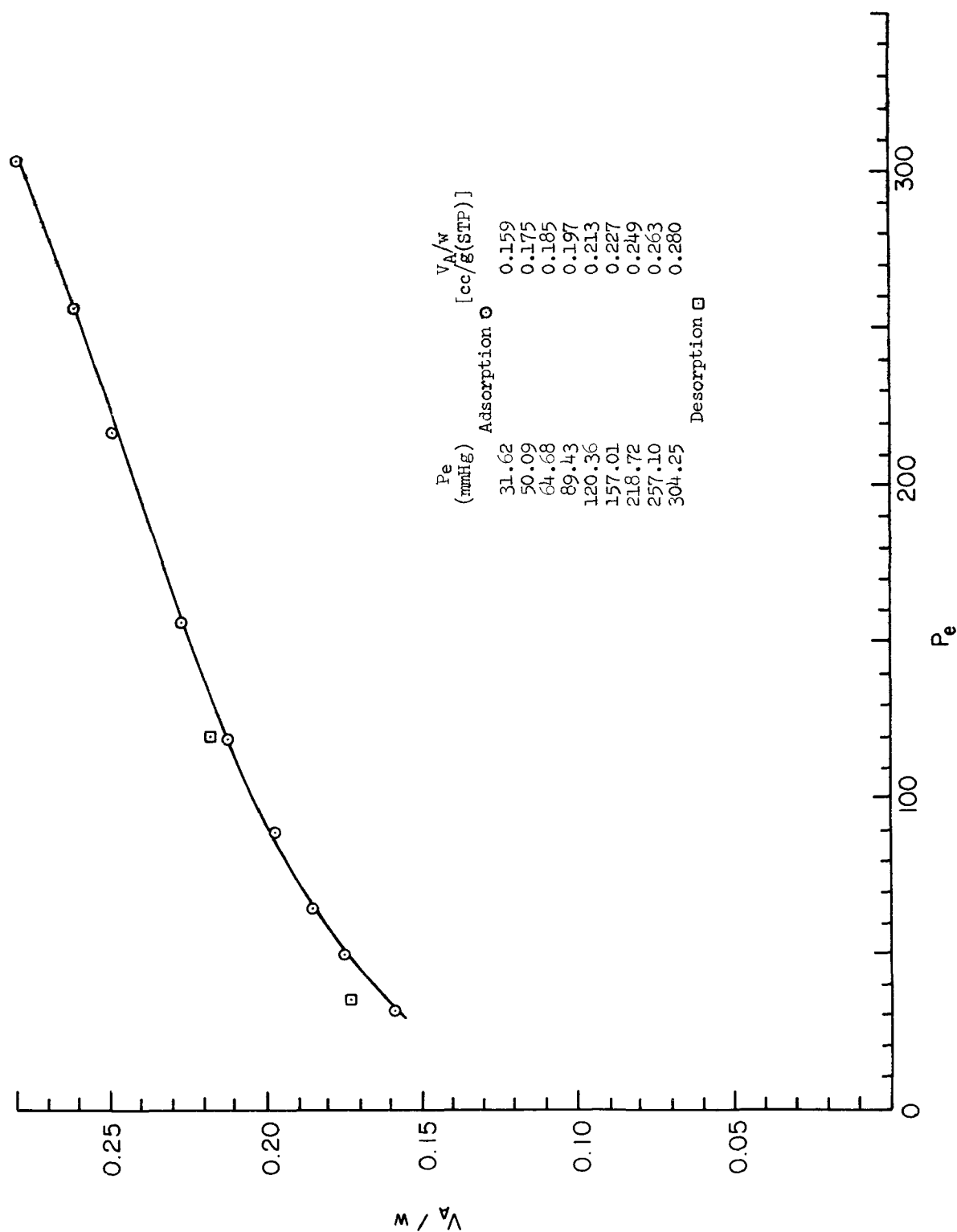


Fig. 32 -  $N_2$ -Adsorption Isotherm on "Sulfur Ball" 70-100 Mesh at 77.3°K  
Sample weight 25.5081 g

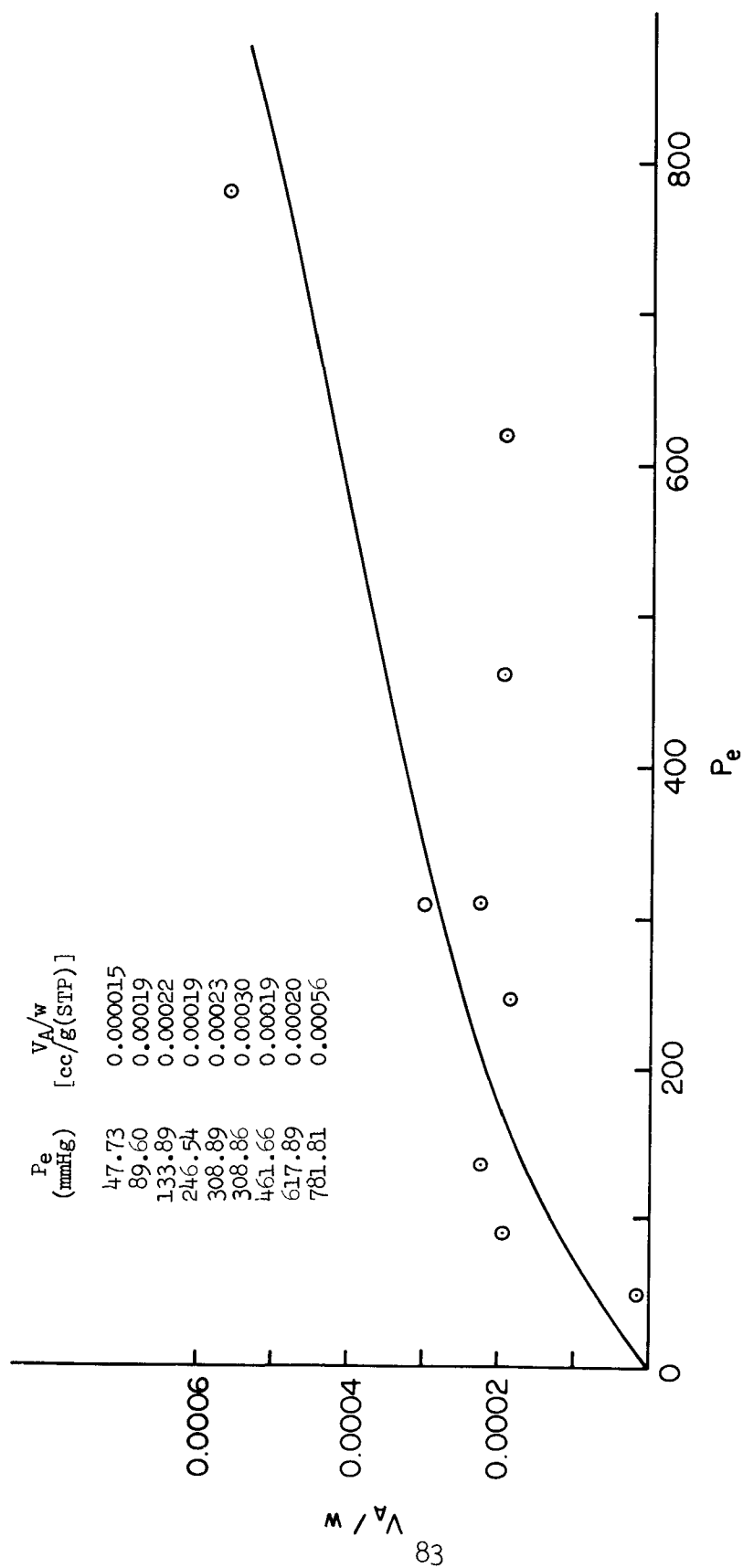


Fig. 33 -  $N_2$ -Adsorption Isotherm on "Museum Grade" Pyrite 100- $\infty$  Mesh  
at 25.0°C

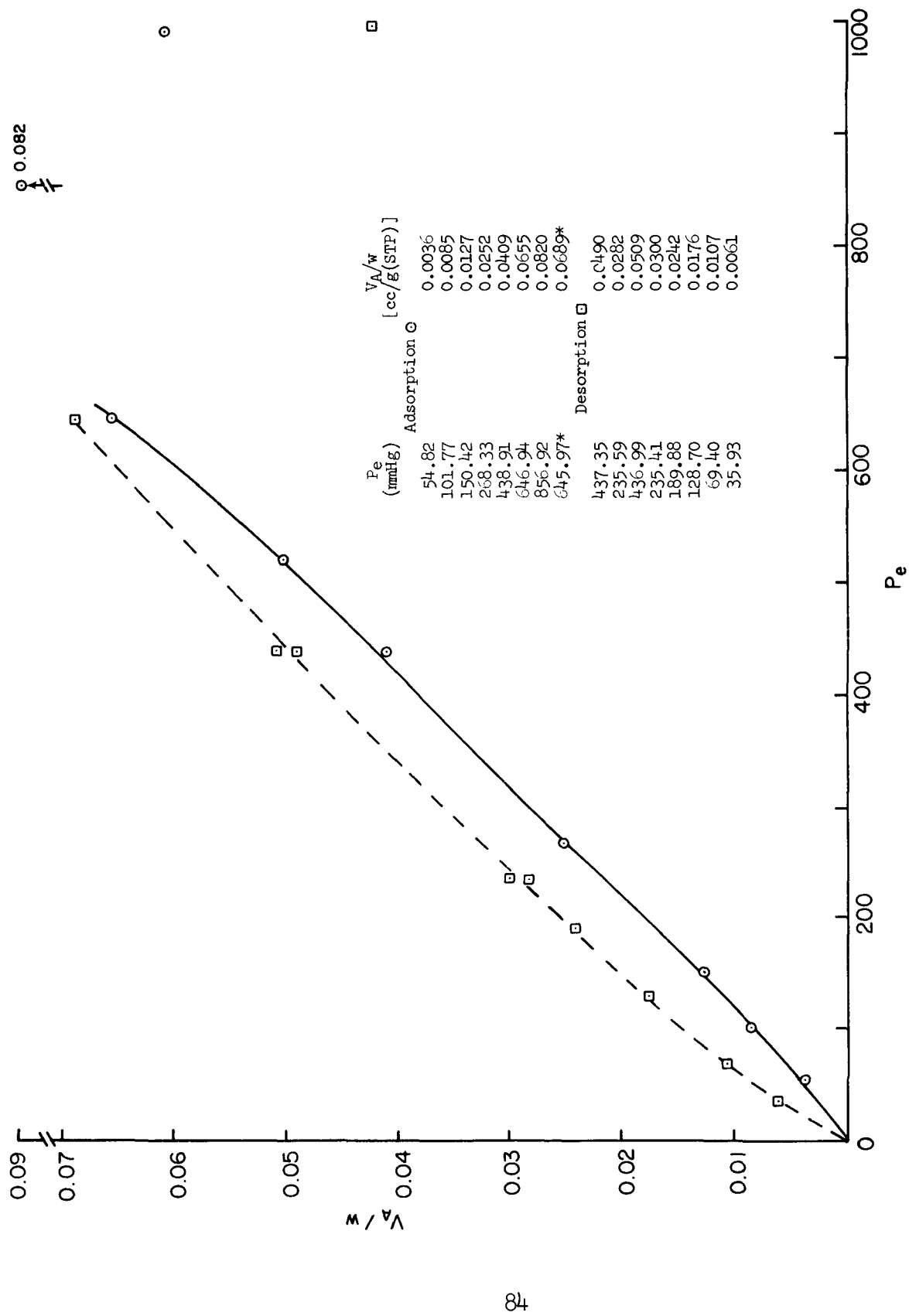


Fig. 34 -  $N_2$ -Adsorption Isotherm on "Sulfur Ball" 70-100 Mesh at 25.0°C

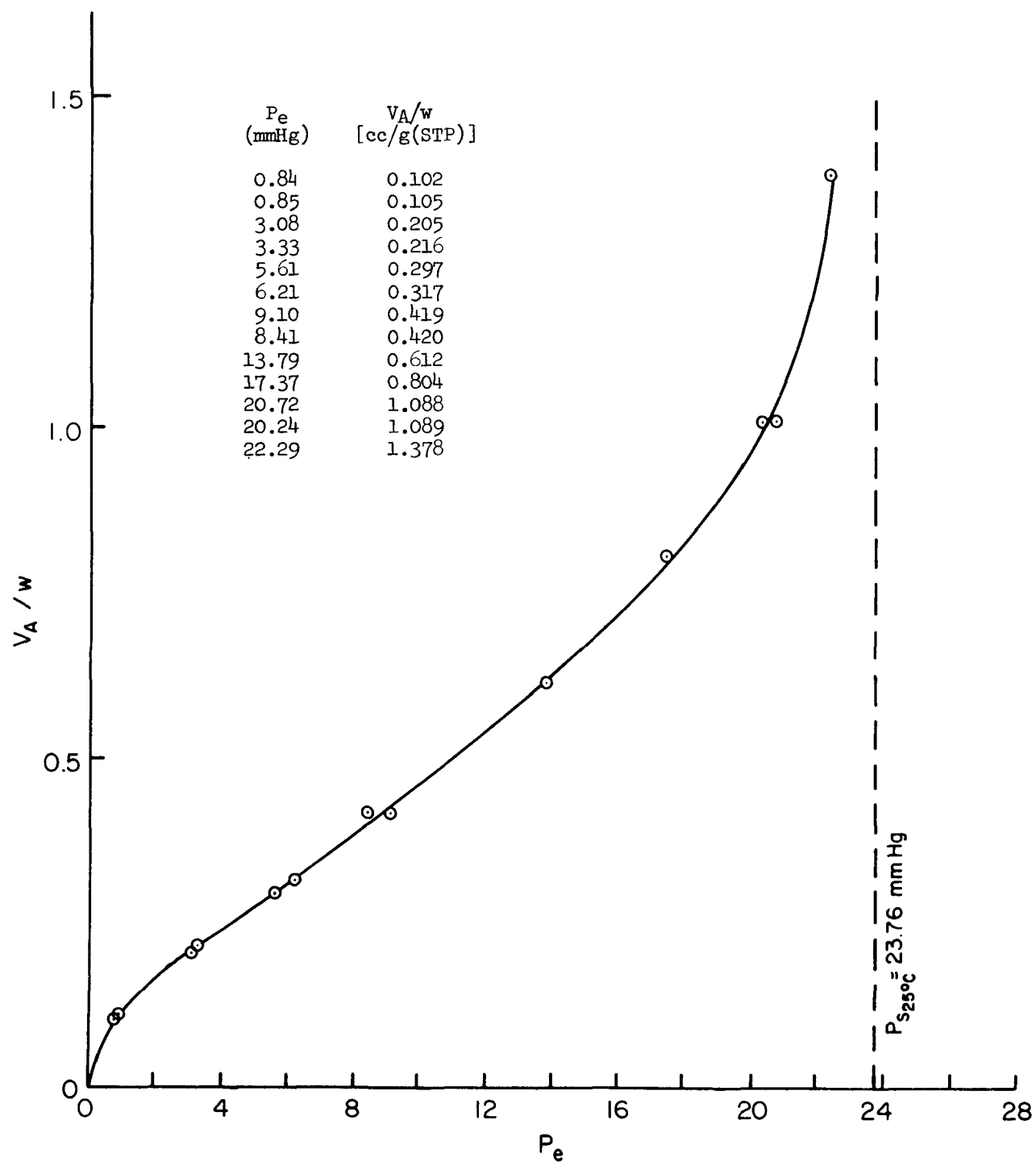


Fig. 35 -  $H_2O$ -Adsorption Isotherm on "Museum Grade" Pyrite 100-00 Mesh at 25.0°C

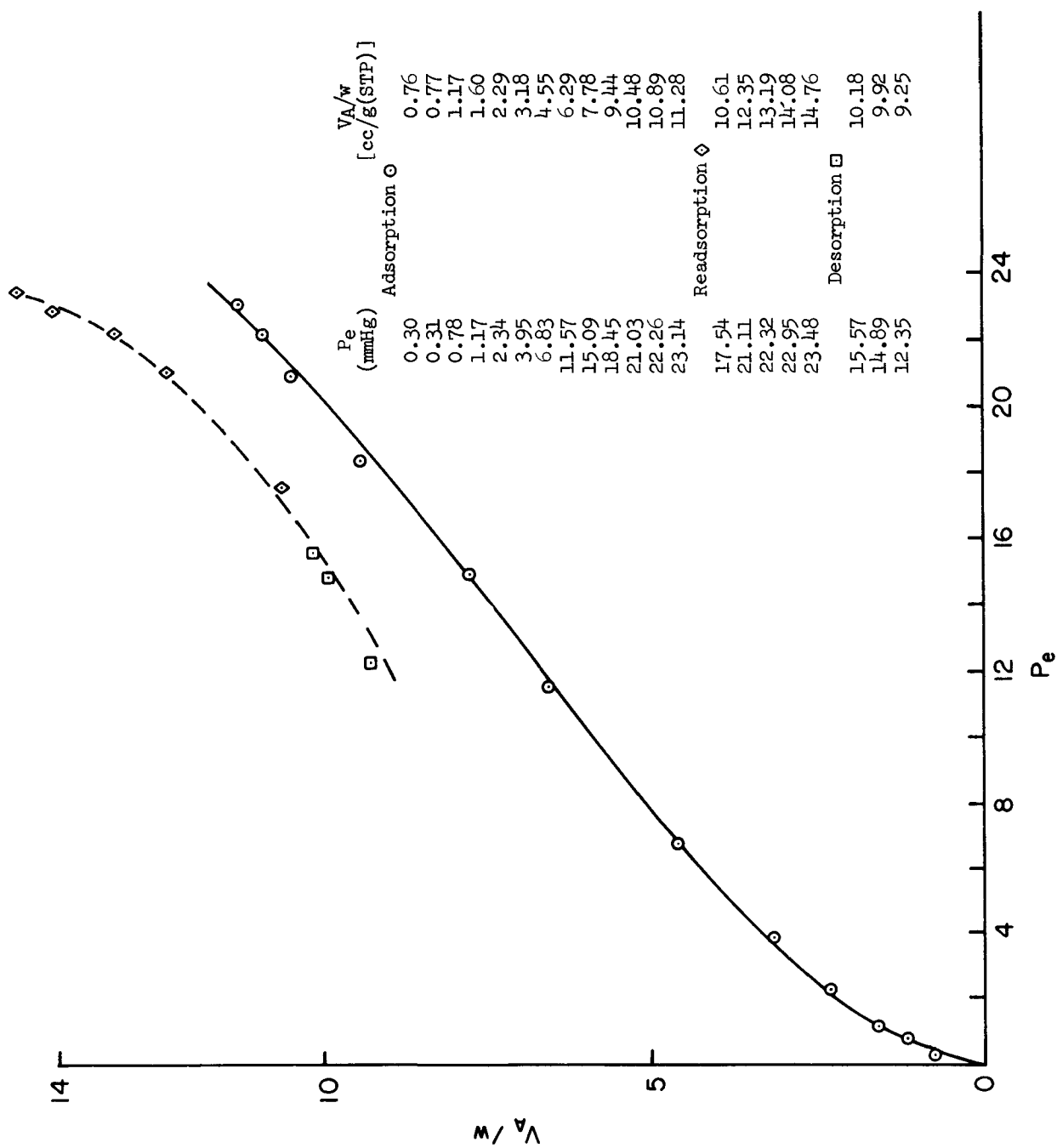


Fig. 36 -  $H_2O$ -Adsorption Isotherm on "Sulfur Ball" 70-100 Mesh at 25.0°C

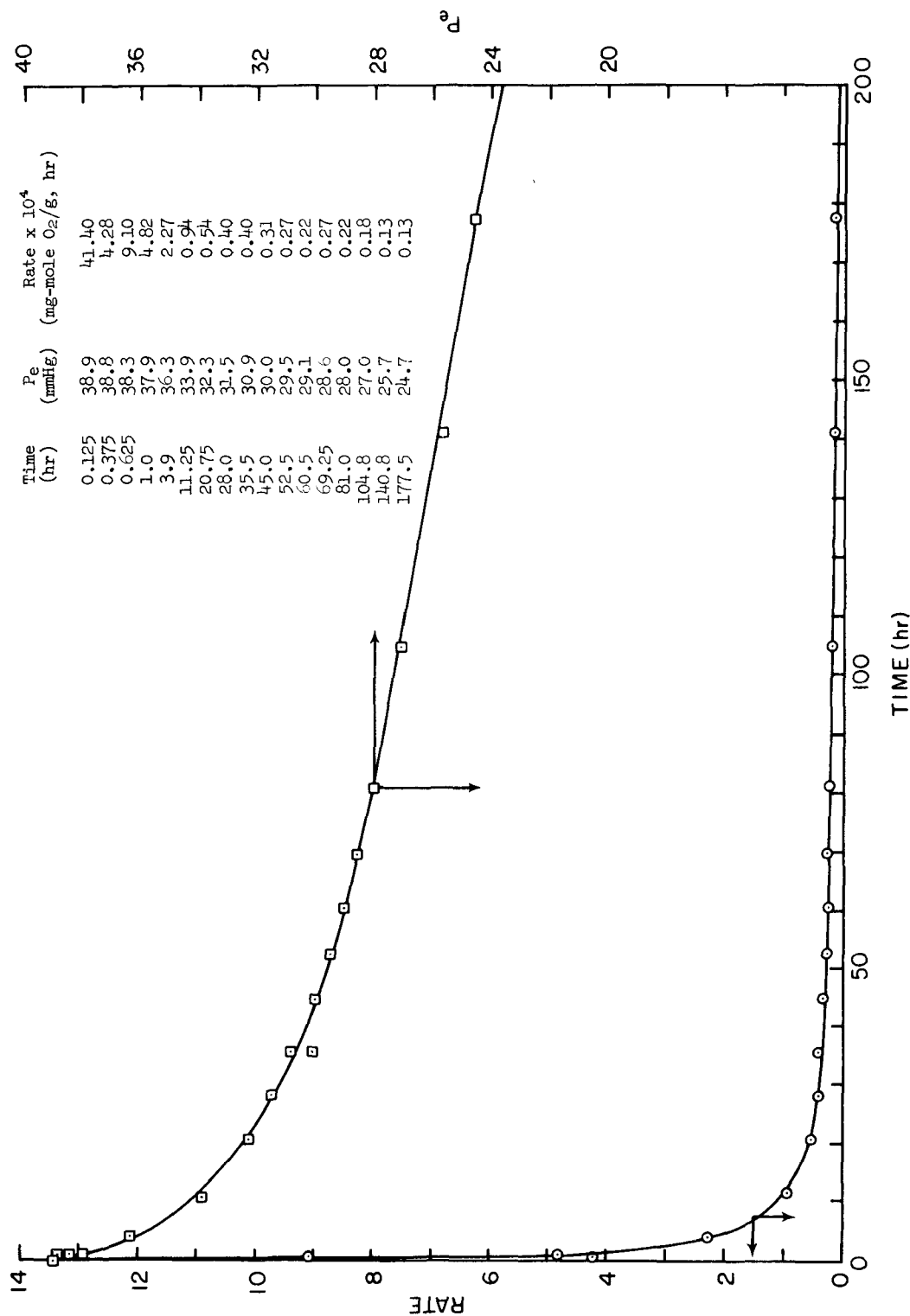


Fig. 37 - O<sub>2</sub>-Adsorption Rate on "Sulfur-Ball" 70-100 Mesh at 25.0°C  
O<sub>2</sub> Pressure from 40 to 24 mmHg

area than Museum Grade pyrite. Also note the hysteresis loop in Fig. 34, which could account for the nitrogen "contamination" reported on page 22.

Water adsorption isotherms are presented in Figs. 35 and 36. The adsorption isotherm for Sulfur Ball appear to have a hysteresis loop, but examination of desorption and re-adsorption data indicate that the initial adsorption cycle probably opened new capillaries and irreversibly increased adsorption capacity.

The oxygen adsorption data are particularly interesting since they can be interpreted in several ways. Physical adsorption is extremely rapid, and if it does occur it takes place in a few seconds (assuming no mass transfer limitations). The relatively slow uptake of oxygen shown in Fig. 37 and Table XIII could be attributed to chemisorption and/or chemical reaction.

Considering both these adsorption data and reaction kinetics of the oxygenation reaction when water is present, an adsorption-reaction mechanism can be described which explains the experimental observations below.

Assume that oxygen is first physically adsorbed; if adsorbed on a dual site the adsorbed oxygen dissociates and reacts with pyrite. When water is absent, oxidation products are not removed from reactive sites and the reaction rate decreases rapidly. When water is present, oxidation products are removed from reactive sites by dissolving in the surrounding aqueous phase.

The assumption that the initial adsorption of oxygen is physical can explain why nitrogen affects oxidation rate by competitive adsorption on reactive sites. Data of Table XIII show that a small but significant amount of oxygen was removed during the desorption cycle. This oxygen was physically rather than chemically adsorbed.



Table XIII. Oxygen Adsorption, Absorption, and Desorption on Sulfur Ball

	Equilibration Time (hr)	Equilibrium Pressure (mmHg)	$V_A/W$ (cc/g)
Adsorption ↓	0.5	44.04	0.00067
	1.0	43.93	0.00117
	2.0	43.81	0.00173
	3.0	43.69	0.00228
	19.0	43.18	0.00462
	20.0	43.18	0.00462
	0.5	80.93	0.00509
	3.0	80.82	0.00537
	0.5	120.63	0.00562
	2.0	120.55	0.00575
	0.5	221.79	0.00588
	1.0	221.68	0.00591
	21.0	217.39	0.00979
	45.0	214.46	0.01240
	70.0	211.83	0.01474
	17.0	694.65	0.01782
	24.0	691.91	0.01873
	45.0	691.70	0.02143
Desorption ↓	0.1	184.30	0.02036
	20.0	184.09	0.02132
	78.0	183.47	0.02417

## APPENDIX II

### CALCULATION OF EXPERIMENTAL DATA FOR FERRIC IRON OXIDATION

Derivation of Eqs. (11)-(16) may be found in the dissertation of S. Sasmajo.<sup>18</sup> The notation below is used.

$r$  = rate of pyrite oxidation (g-mole/hr-g pyrite)

$v$  = volumetric rate of titration ( $\ell$ /hr)

$C_3$  = concentration of ferric ions (g-mole/ $\ell$ )

$C_2$  = concentration of ferrous ions (g-mole/ $\ell$ )

$C_t$  = concentration of total iron (g-mole/ $\ell$ )

$R$  = ferric-ferrous ratio

$\bar{R}$  = average ferric-ferrous ratio between the inlet and outlet of the packed bed

$N$  = normality of  $\text{KMnO}_4$  (g equivalent/ $\ell$ ) or concentration of ferric ion of titrant (g-mole/ $\ell$ )

$q$  = volumetric flow rate of the reaction solution through the reactor ( $\ell$ /hr)

$t$  = time (hr)

$V$  = total volume of the reaction solution

$m$  = mass of pyrite sample (g)

$r^* = rm$

Conditions at time  $t = 0$  will be denoted by a subscript 0. Conditions at the inlet of the pyrite-packed bed will be denoted by a superscript  $i$  and at the outlet of the packed bed by a superscript  $o$ .

Reaction Rate ("r") with Potassium Permanganate as Titrant

$$r = \frac{Nv(R + 1)}{(15R + 1)(m)} \quad (11)$$

Normality of  $\text{KMnO}_4$  Solution to Maintain Constant  
Total Iron Concentration ( $C_t$ )

$$N = \frac{(15R + 14)(C_{t,o})}{R + 1} \quad (12)$$

Reaction Rate with Ferric Ion Solution as Titrant

$$r = \frac{Nv}{(15R + 14)(m)} \quad (13)$$

Normality of Ferric Ion Solution to Maintain Constant  
Total Iron Concentration

$$N = (C_{t,o}) \left( 1 + \frac{1}{15(R + 1)} \right) \quad (14)$$

Calculation of Average Ferric/Ferrous Ratio

For large changes in R:

$$\bar{R} = \frac{C_t^i}{C_t^o - C_t^i} \left\{ \frac{14}{15} \ln \frac{(15R^o + 14)}{(15R^i + 14)} - \ln \frac{(R^o + 1)}{(R^i + 1)} \right\} \quad (15)$$

where

$$R^o = \frac{(C_{t,q}^i R^i) / (R^i + 1) - (14r^*)}{(C_{t,q}^i) / (R^i + 1) - (15r^*)}$$

$$C_t^o = C_t^i + \frac{r^*}{q}$$

$$r^* = rm$$

For small changes in R:

$$\bar{R} = \frac{R^i + R^o}{2} \quad (16)$$

# APPENDIX III

## CALCULATION OF IONIC COMPOSITION

The method of calculation to determine the concentration of free  $\text{Fe}^{+++}$  ions and free  $\text{Fe}^{++}$  ions and their complexes, as well as major anions that are present in the solution, are described in this appendix. Separate descriptions for sulfate solution and for chloride solution are given below.

### Sulfate Solution

In our sulfate solution, the following chemical equilibria between the ionic species were considered:

1.  $\text{Fe}^{+++} + \text{SO}_4^{--} = \text{FeSO}_4^+$
2.  $\text{Fe}^{+++} + \text{HSO}_4^- = \text{FeHSO}_4^{++}$
3.  $\text{FeSO}_4^+ + \text{SO}_4^{--} = \text{Fe}(\text{SO}_4)_2^-$
4.  $\text{HSO}_4^- = \text{H}^+ + \text{SO}_4^{--}$
5.  $\text{Fe}^{+++} + \text{H}_2\text{O} = \text{Fe}(\text{OH})^{++} + \text{H}^+$
6.  $\text{Fe}^{++} + \text{SO}_4^{--} = \text{FeSO}_4$
7.  $\text{Na}^+ + \text{SO}_4^{--} = \text{NaSO}_4^-$

If  $Q_1$ ,  $Q_2$ ,  $Q_3$ , etc. are the stability constants for each of the equilibrium reactions listed above, we have the following equilibrium conditions:

$$Q_1 = \frac{(\text{FeSO}_4^+)}{(\text{Fe}^{+++})(\text{SO}_4^{--})} \quad (17)$$

$$Q_2 = \frac{(\text{FeHSO}_4^{++})}{(\text{Fe}^{+++})(\text{HSO}_4^-)} \quad (18)$$

$$Q_3 = \frac{(\text{Fe}(\text{SO}_4)_2^-)}{(\text{FeSO}_4^+)(\text{SO}_4^{--})} \quad (19)$$

$$Q_4 = \frac{(\text{SO}_4^{--})(\text{H}^+)}{(\text{HSO}_4^-)} \quad (20)$$

$$Q_5 = \frac{(\text{Fe}(\text{OH})^{++})(\text{H}^+)}{(\text{Fe}^{+++})} \quad (21)$$

$$Q_6 = \frac{(\text{FeSO}_4)}{(\text{Fe}^{++})(\text{SO}_4^{--})} \quad (22)$$

$$Q_7 = \frac{(\text{NaSO}_4^-)}{(\text{Na}^+)(\text{SO}_4^{--})} \quad (23)$$

Using Eqs. (17)-(23), the ionic composition in the solution can be determined. The calculation procedure is described below.

#### Determination of $\text{H}^+$ Concentration

The  $\text{H}^+$  concentration may be determined as the difference between the total hydrogen added to the solution (from a charge balance) and the hydrogen combined as  $\text{HSO}_4^-$ , or,

$$\text{H}^+ = \text{H}_T - \text{HSO}_4^- \quad , \quad (24)$$

where, from charge balance, total hydrogen added ( $\text{H}_T$ ) equals

$$\text{H}_T = 2(\text{SO}_4^{--})_T - 3(\text{Fe}^{\text{III}}) - 2(\text{Fe}^{\text{II}}) - \text{Na}^{\text{I}} \quad (25)$$

#### Calculation of $\text{HSO}_4^-$ Concentration

The equation to calculate the  $\text{HSO}_4^-$  concentration is derived below. To simplify the expressions, the following notations will be used:

- $\text{Fe}^{\text{III}}$  = total ferric ion concentration
- $\text{Fe}^{\text{II}}$  = total ferrous ion concentration
- $\text{Fe}^{+++}$  = concentration of free ferric ions
- $\text{Fe}^{++}$  = concentration of free ferrous ions
- $\text{L}$  = concentration of anion; in this case,  
L is the sulfate ion concentration
- $\text{H}$  = concentration of hydrogen ion
- $\text{HL}$  = concentration of  $\text{HSO}_4^-$  ions

The total sulfate ions in the solution is equal to the sum of free  $\text{SO}_4^{--}$  and all the  $\text{SO}_4^{--}$  ions that are associated. Therefore,

$$(\text{L})_{\text{total}} = \text{L} + \text{HL} + \text{Fe}^{+++}\text{L} + 2\text{Fe}^{+++}\text{L}_2 + \text{Fe}^{+++} + \text{Fe}^{++}\text{L} . \quad (26)$$

A balance for ferric ion concentration gives

$$\text{Fe}^{\text{III}} = \text{Fe}^{+++} + \text{Fe}^{+++}\text{L} + \text{Fe}^{+++}\text{L}_2 + \text{Fe}^{+++}\text{HL} + \text{Fe}^{+++}\text{OH} \quad (27)$$

Using the equilibrium relations, Eqs. (17)-(23), Eqs. (26) and (27) can be transformed to

$$(\text{L})_{\text{total}} = (\text{HL})(1 + G_0) + \text{Fe}^{+++} \left( \sum_{i=1}^3 g_i G_i (\text{HL})^{g_i} \right) + \text{Fe}^{++} \cdot G_5 (\text{HL}) \quad (28)$$

and

$$\text{Fe}^{+++} = \frac{\text{Fe}^{\text{III}}}{1 + \sum_{i=1}^4 G_i (\text{HL})^{g_i}} \quad (29)$$

where

$$G_0 = Q_4/H$$

$$G_1 = Q_1 Q_4/H$$

$$G_2 = Q_2$$

$$G_3 = Q_1 Q_3 Q_4^2/H^2$$

$$G_4 = Q_5/H$$

and

$$G_5 = Q_6 Q_4/H$$

The values of the  $g_i$ 's are

$$g_1 = 1$$

$$g_2 = 1$$

$$g_3 = 2$$

$$g_4 = 0$$

and

$$g_5 = 1$$

Combining Eqs. (28) and (29), we obtain

$$HL = \frac{(L)_{\text{total}} - G_a \text{Fe}^{\text{III}} - G_b \text{Fe}^{\text{II}}}{(1 + G_o)} \quad (30)$$

where

$$G_a = \frac{\sum_{i=1}^3 g_i G_i (HL)^{g_i}}{1 + \sum_{i=1}^4 G_i (HL)^{g_i}} \quad (31)$$

$$G_b = \frac{G_5(HL)}{1 + G_5(HL)} \quad (32)$$

and

$$G_c = \frac{G_6(HL)}{1 + G_6(HL)} \quad (33)$$

From a knowledge of (1) total sulfate  $[L_T]$ , (2) total ferric ion  $[\text{Fe}^{\text{III}}]$ , (3) total ferrous ion  $[\text{Fe}^{\text{II}}]$ , and (4) total sodium  $[\text{Na}^{\text{I}}]$  as obtained from analysis of solution or from inventory of quantities added to the solution, the ionic concentration can be calculated using the following procedure:

- A. Assume  $H^+ = 1/2 H_T$ ,  $HL = 1/2 H_T$ , and calculate  $G_i$ 's.
- B. Solve for  $G_a$ ,  $G_b$ , and  $G_c$ ; substitute into Eq. (30) and solve for HL.
- C. Using relation,  $H^+ = H_T - H_L$ , recalculate  $G_i$ 's using new  $H^+$  value.
- D. Again solve for  $G_a$ ,  $G_b$ , and  $G_c$  using corrected values for HL and  $G_i$ 's; substitute in Eq. (30) and solve for new HL.
- E. Repeat Steps C and D until HL values agree.
- F. When HL and  $H^+$  values are known, ionic composition can be calculated from stability constant equations.

# Calculation of $\text{Fe}^{+++}$ , $\text{Fe}^{++}$ and Their Complexes

After the  $\text{HSO}_4^-$  and  $\text{H}^+$  concentrations are known, the values of  $\text{Fe}^{+++}$ ,  $\text{Fe}^{++}$  and their complexes can be calculated from Eqs. (17)-(23).

In order to perform the calculations as outlined above, values of stability constants should be known. Table XIV summarizes the values of stability constants used in the calculation.

Table XIV. Stability Constants for Sulfate Solution<sup>20</sup>

Constants	Values of $\log (Q_i)$	Ionic Strength
$Q_1$	2.23	1.2
$Q_2$	0.78	1.2
$Q_3$	0.97	1.0
$Q_4$	-1.99	1.2
$Q_5$	-2.43	0.0
$Q_6$	0.04	1.1

Since the ionic strengths of the solutions used are not the same as those listed in Table XIV, corrections are needed. The calculation method to correct the stability constant is as follows:

(1) Calculate the values of the  $Q$ 's at zero ionic strength from the values given in Table XIV, using the relation

$$Q_1 = Q_{0,i} Q_{f,i} \quad (34)$$

where

$Q_i$  = stability constant at a given ionic strength  
for equilibrium reaction  $i$ ,

$Q_{0,i}$  = stability constant at zero ionic strength for  
equilibrium reaction  $i$ , and

$Q_{f,i}$  = activity coefficient quotient in terms of activ-  
ity coefficients for the equilibrium reaction  $i$ .



(2) To obtain the value of  $Q_{f,i}$ , the activity coefficients should be known. Values of activity coefficients were estimated from the empirical relation proposed by Davies<sup>4</sup>; i.e.,

$$- \log f_i = 0.50 z_i^2 [I^{1/2}/(1+I^{1/2}) - 0.20 I] \quad (35)$$

where

$f_i$  = activity coefficient of ionic species  $i$

$z_i$  = valence of the ionic species  $i$ , and

$I$  = ionic strength of the solution.

(3) Calculate the value of  $Q_1$  at any ionic strength from Eq. (34), using the value of  $Q_{O,i}$  obtained in step 1.

#### Chloride Solution

In chloride solution, the following chemical equilibria between the ionic species are considered:

1.  $\text{Fe}^{+++} + \text{Cl}^- = \text{FeCl}^{++}$
2.  $\text{FeCl}^{++} + \text{Cl}^- = \text{FeCl}_2^+$
3.  $\text{FeCl}_2^+ + \text{Cl}^- = \text{FeCl}_3$
4.  $\text{Fe}^{+++} + \text{H}_2\text{O} = \text{FeOH}^{++} + \text{H}^+$
5.  $\text{Fe}^{++} + \text{Cl}^- = \text{FeCl}^+$
6.  $\text{FeCl}^+ + \text{Cl}^- = \text{FeCl}_2$

The equilibrium relations for the above equations are

$$Q_1 = \frac{(\text{FeCl}^{++})}{(\text{Fe}^{+++})(\text{Cl}^-)} \quad (36)$$

$$Q_2 = \frac{(\text{FeCl}_2^+)}{(\text{FeCl}^{++})(\text{Cl}^-)} \quad (37)$$

$$Q_3 = \frac{(\text{FeCl}_3)}{(\text{FeCl}_2^+)(\text{Cl}^-)} \quad (38)$$

$$Q_4 = \frac{(\text{FeOH}^{++})(\text{H}^+)}{(\text{Fe}^{+++})} \quad (39)$$

$$Q_5 = \frac{(\text{FeCl}^+)}{(\text{Fe}^{++})(\text{Cl}^-)} \quad (40)$$

$$Q_6 = \frac{(\text{FeCl}_2)}{(\text{FeCl}^+)(\text{Cl}^-)} \quad (41)$$

The Q's in the above equations are the stability constants.

The calculation procedure to determine the ionic composition in the solution is similar to that in sulfate solution. Only a brief outline will therefore be given.

#### Determination of $\text{H}^+$ Concentration

The hydrogen ion concentration was calculated in the same manner as in the case of sulfate solution [Eqs. (24) and (25)].

#### Calculation of $\text{Cl}^-$ Concentration

Following a similar method as that used in calculating  $\text{HSO}_4^-$ , and also using the same notations, the following equations can be derived:

$$(\text{L})_{\text{total}} = (\text{L}) + \text{Fe}^{+++} \left[ \sum_{i=1}^3 g_i G_i (\text{L})^{g_i} \right] + \text{Fe}^{++} \left[ \sum_{i=5}^6 g_i G_i (\text{L})^{g_i} \right] \quad (42)$$

$$\text{Fe}^{+++} = \frac{\text{Fe}^{\text{III}}}{1 + \sum_{i=1}^4 G_i (\text{L})^{g_i}}, \quad \text{and} \quad (43)$$

$$\text{Fe}^{++} = \frac{\text{Fe}^{\text{III}}}{1 + \sum_{i=5}^6 G_i (\text{L})^{g_i}} \quad (44)$$

where

$L$  = chloride ion concentration;

$$G_1 = Q_1, g_1 = 1$$

$$G_2 = Q_1 Q_2, g_2 = 2$$

$$G_3 = Q_1 Q_2 Q_3, g_3 = 3$$

$$G_4 = Q_4/H, g_4 = 0$$

$$G_5 = Q_5, g_5 = 1$$

$$G_6 = Q_5 Q_6, g_6 = 2$$

Combining,

$$L = (L)_{\text{total}} - G_a \text{Fe}^{\text{III}} - G_b \text{Fe}^{\text{II}} \quad (45)$$

where

$$G_a = \frac{\sum_{i=1}^3 g_i G_i (L)^{g_i}}{1 + \sum_{i=1}^4 G_i (L)^{g_i}} \quad (46)$$

and

$$G_b = \frac{\sum_{i=5}^6 g_i G_i (L)^{g_i}}{1 + \sum_{i=5}^6 G_i (L)^{g_i}} \quad (47)$$

Iterative calculation similar to that used to calculate the  $\text{HSO}_4^-$  concentration will give the  $\text{Cl}^-$  concentration. Note that in Eqs. (42)-(47)  $L$  is used to represent  $\text{Cl}^-$  concentration.

Calculation of  $\text{Fe}^{+++}$ ,  $\text{Fe}^{++}$ , and their Complexes

The calculation for iron ions and their complexes in chloride solution is exactly the same as that for sulfate solution.

The stability constants for the complexes in chloride solution are given in Table XV. Corrections for stability constants due to

ionic strength were made in exactly the same manner as in sulfate solution.

Table XV. Stability Constants in Chloride Solution<sup>20</sup>

Constants	Values of $\log (Q_i)$	Ionic Strength
$Q_1$	1.48	0.0
$Q_2$	0.65	0.0
$Q_3$	-1.0	0.0
$Q_4$	-2.43	0.0
$Q_5$	0.36	2.0
$Q_6$	0.04	2.0

## APPENDIX IV

### TABLE HEADINGS

RUN	- run number
PH	- solution pH
EMF	- measured EMF of solution (volts)
EMF CORR	- corrected EMF (volts)
IRON CONC.	- total iron concentration $\times 10^2$ ; multiply tabulated values by $10^{-2}$ to obtain iron concentration in g-moles/l
GRAM SAMPLE	- weight of sample (grams)
FLOW RATE	- flow rate of recirculated solution (l/hr.)
RATE	- oxidation rate; multiply tabulated values by $10^{-6}$ to obtain reaction rate in g-mole pyrite oxidized per hour per gram of pyrite sample (g-mole/hr, gm)

# RUN DATA, FERRIC ION OXIDATION

Table XVI(\*)

RUN	PH	EMF	EMF CORR.	IRON CONC.	GRAM SAMPLE	FLOW RATE	RATE
F018 B	0.50	0.450	0.450	0.991	17.30	41.4	1.10
F019 B	0.50	0.440	0.439	1.013	17.30	41.4	0.68
F020 B	0.50	0.425	0.425	1.013	17.30	41.4	0.52
F021 B	0.50	0.400	0.399	1.091	17.30	41.4	0.32
F022 B	0.50	0.375	0.374	1.045	17.30	41.4	0.16
F023 B	0.50	0.460	0.459	1.000	17.30	41.4	1.43
F024 B	0.50	0.470	0.469	0.987	17.30	41.4	2.06
F051	0.50	0.450	0.445	0.971	17.30	41.4	1.13
F051 B	0.50	0.450	0.445	1.041	17.30	39.6	1.12
RR	0.50	0.450	0.448	1.041	17.30	41.4	1.23
RR1	0.50	0.450	0.448	1.023	17.30	41.4	1.12
RR2	0.50	0.450	0.448	1.023	17.30	41.4	1.19
STD1	0.50	0.450	0.442	1.068	17.30	41.4	1.31
STD2	0.50	0.450	0.444	1.068	17.30	41.4	0.85
STD3	0.50	0.450	0.451	1.091	17.30	41.4	1.12
F056	0.50	0.400	0.392	1.060	17.30	41.4	0.26
F057	0.50	0.425	0.422	1.045	17.30	41.4	0.42
F094 B	0.50	0.600	0.597	1.182	4.50	52.3	7.07
F097 B	0.50	0.450	0.445	0.983	4.50	52.3	0.80
F099 B	0.50	0.550	0.549	0.967	4.50	52.3	5.79
F0100B	0.50	0.575	0.573	0.999	4.50	52.3	6.52
F0101	0.50	0.750	0.669	0.999	4.50	50.3	8.35
F0102	0.50	0.700	0.656	0.972	4.50	50.3	7.74
F0103	0.50	0.650	0.633	0.956	4.50	51.7	7.60
F0104	0.50	0.475	0.475	0.983	4.50	52.3	1.37
F0105	0.50	0.500	0.500	0.959	4.50	52.3	2.84
F0106	0.50	0.525	0.525	0.975	4.50	52.3	4.90
F025	1.00	0.361	0.349	1.016	17.30	41.4	0.09
F026	1.00	0.385	0.390	1.091	17.30	43.9	0.27
F027	1.00	0.409	0.410	1.038	17.30	43.9	0.41
F028	1.00	0.424	0.425	1.038	17.30	43.9	0.70
F029	1.00	0.435	0.433	1.038	17.30	43.9	0.92
F030	1.00	0.443	0.446	0.978	17.30	43.9	1.19
F031	1.00	0.453	0.459	1.061	17.30	43.9	1.66
F032	1.00	0.458	0.460	1.056	17.30	43.9	1.85
F052	1.00	0.458	0.463	0.952	17.30	41.4	1.53
F052 B	1.00	0.458	0.456	1.005	17.30	39.0	2.08

(\*) SEE EXPLANATION AT THE BEGINING OF THIS APPENDIX

Table XVI(\*) - Continued

RUN	PH	EMF	EMF CORR.	IRON CONC.	GRAM SAMPLE	FLOW RATE	RATE
F033	2.00	0.345	0.347	1.041	17.30	41.4	0.17
F034	2.00	0.367	0.363	1.036	17.30	41.4	0.23
F035	2.00	0.390	0.385	1.034	17.30	41.4	0.53
F036	2.00	0.403	0.402	1.039	17.30	41.4	0.68
F037	2.00	0.413	0.411	1.030	17.30	41.4	0.84
F038	2.00	0.421	0.416	1.018	17.30	41.4	1.20
F039	2.00	0.430	0.425	1.039	17.30	41.4	1.92
F040	2.00	0.435	0.434	1.036	17.30	41.4	1.85
F041	2.00	0.445	0.445	1.036	17.30	41.4	2.39
F042	2.00	0.458	0.451	0.912	17.30	41.4	4.69
F053	2.00	0.445	0.434	0.984	17.30	37.8	2.95
F058	2.00	0.400	0.390	1.081	17.30	37.8	0.69
F059	2.00	0.425	0.415	1.078	17.30	39.0	1.07
F060	2.00	0.450	0.443	1.048	17.30	39.0	2.33
F0120	2.00	0.750	0.667	2.231	4.50	46.0	18.96
F0125	2.00	0.445	0.439	1.005	4.50	45.3	2.33
F0125B	2.00	0.445	0.437	1.005	4.50	45.3	1.92
F0126	2.00	0.460	0.460	0.991	4.50	46.0	5.03
F0127	2.00	0.700	0.637	0.997	4.50	46.0	18.69
F0128	2.00	0.650	0.623	0.986	4.50	46.7	14.44
F0129	2.00	0.600	0.592	0.997	4.50	46.7	14.89
F0130	2.00	0.575	0.571	0.975	4.50	46.7	13.95
F0131	2.00	0.550	0.548	0.980	4.50	46.7	13.69
F0132	2.00	0.525	0.524	0.983	4.50	46.7	11.70
F0133	2.00	0.475	0.475	1.011	4.50	46.7	5.62
F0134	2.00	0.500	0.500	0.983	4.50	45.3	8.77
F0135	2.00	0.650	0.622	1.016	4.50	45.3	15.78
F043	2.50	0.347	0.354	1.041	17.30	41.4	0.44
F044	2.50	0.366	0.369	1.034	17.30	41.4	0.67
F045	2.50	0.384	0.382	1.018	17.30	41.4	1.01
F046	2.50	0.397	0.395	1.018	17.30	41.4	1.31
F047	2.50	0.410	0.412	1.018	17.30	41.4	1.92
F048	2.50	0.421	0.422	1.029	17.30	41.4	2.58
F049	2.50	0.439	0.445	1.047	17.30	41.4	4.16
F050	2.50	0.450	0.453	1.047	17.30	41.4	6.04
F054	2.50	0.439	0.441	0.970	17.30	37.8	5.35

(\*) SEE EXPLANATION AT THE BEGINING OF THIS APPENDIX

Table XVII(\*)

RATE DATA, SULFATE SOLUTION  
WITHOUT ADDITION OF SODIUM SULFATE  
IRON CONC. VARIES

RUN	PH	EMF	EMF CORR.	IRON CONC.	GRAM SAMPLE	FLOW RATE	RATE
F0111	0.50	0.800	0.705	4.471	4.50	52.3	12.44
F0112	0.50	0.800	0.699	2.866	4.50	52.3	10.32
F0113	0.50	0.800	0.695	1.994	4.50	52.3	8.50
F0114	0.50	0.800	0.690	1.300	4.50	52.3	7.03
F0115	0.50	0.800	0.685	0.897	4.50	52.3	5.94
F0116	0.50	0.800	0.680	0.608	4.50	52.3	4.97
F0117	0.50	0.800	0.676	0.402	4.50	52.3	3.95
F0118	0.50	0.800	0.670	0.249	4.50	52.3	3.16
F0107	0.50	0.750	0.672	0.956	4.50	52.3	7.26
F0108	0.50	0.750	0.665	0.580	4.50	52.3	5.99
F0109	0.50	0.750	0.661	0.405	4.50	52.3	5.00
F0110	0.50	0.750	0.656	0.258	4.50	52.3	4.04
F0119	2.00	0.800	0.698	3.266	4.50	47.2	11.18
F0120	2.00	0.750	0.595	0.110	4.50	46.0	18.96
F0121	2.00	0.750	0.575	0.040	4.50	46.0	15.63
F0122	2.00	0.750	0.583	0.053	4.50	46.0	14.99
F0123	2.00	0.750	0.596	0.090	4.50	44.7	14.41
F0124	2.00	0.750	0.606	0.112	4.50	45.3	12.40

(\*) SEE EXPLANATION AT THE BEGINING OF THIS APPENDIX

Table XVIII(\*)

RATE DATA, SULFATE SOLUTION  
SODIUM SULFATE 0.20 GM-MOLES/L  
IRON CONC. 0.01 GM-MOLES/L

RUN	PH	EMF	EMF CORR.	IRON CONC.	GRAM SAMPLE	FLOW RATE	RATE
F061	0.50	0.400	0.402	1.051	17.30	43.9	0.08
F062	0.50	0.425	0.430	1.066	17.30	43.9	0.31
F063	0.50	0.450	0.456	1.084	17.30	42.6	0.72
F064	0.50	0.445	0.444	0.997	17.30	43.9	0.58
F065	2.00	0.400	0.436	1.016	17.30	41.5	0.77
F066	2.00	0.350	0.381	1.084	17.30	41.4	0.18
F067	2.00	0.375	0.411	1.124	17.30	41.4	0.35
F068	2.00	0.418	0.451	1.057	17.30	41.4	1.29

(\*) SEE EXPLANATION AT THE BEGINING OF THIS APPENDIX



Table XIX<sup>(\*)</sup>

RATE DATA, CHLORIDE SOLUTION IRON CONC. 0.01 GM-MOLES/L							
RUN	PH	EMF	EMF CORR.	IRON CONC.	GRAM SAMPLE	FLOW RATE	RATE
F076	0.50	0.400	0.393	0.983	17.30	41.4	0.21
F077 R	0.50	0.425	0.438	0.983	17.30	41.4	0.36
F078	0.50	0.470	0.463	0.991	17.30	41.4	1.40
F079	0.50	0.440	0.447	0.997	17.30	41.4	0.65
F080	0.50	0.450	0.452	1.013	17.30	41.4	0.75
F081	0.50	0.460	0.459	1.025	17.30	41.4	0.92
F082	0.50	0.475	0.467	1.016	17.30	41.4	1.28
F089	0.50	0.450	0.451	0.912	17.30	41.4	0.71
F070	2.00	0.425	0.428	1.069	17.30	41.4	0.99
F071	2.00	0.440	0.441	1.072	17.30	41.4	1.53
F072	2.00	0.450	0.444	1.069	17.30	37.8	2.00
F073	2.00	0.475	0.479	1.078	17.30	41.4	4.31
F074	2.00	0.460	0.459	1.087	17.30	41.4	2.86
F075	2.00	0.470	0.467	1.084	17.30	41.4	3.59

(\*) SEE EXPLANATION AT THE BEGINING OF THIS APPENDIX

Table XX<sup>(\*)</sup>

RATE DATA, CHLORIDE SOLUTION IRON CONC. VARIES							
RUN	PH	EMF	EMF CORR.	IRON CONC.	GRAM SAMPLE	FLOW RATE	RATE
F090	0.50	0.450	0.450	0.578	17.30	41.4	0.81
F091	0.50	0.450	0.450	0.344	17.30	41.4	0.76
F092	0.50	0.450	0.450	0.225	17.30	41.4	0.58
F093	0.50	0.450	0.450	0.186	17.30	41.4	0.58

(\*) SEE EXPLANATION AT THE BEGINING OF THIS APPENDIX

# APPENDIX V. Characteristics of Pyrite Samples

	Sample Designation			
	Museum Grade	Sulfur Ball #1	Sulfur Ball #2	McDaniel's Sulfur Ball
Mesh Size	60-100	60-100	60-100	60-100
Reactivity**	0.03	1.0	2.0	3.5
Chemical Analysis				
Fe	43.2	41.65	-	35.1*
S	49.7	46.72	-	38.5*
SiO <sub>2</sub>	6.0	2.3	-	6.0*
Al <sub>2</sub> O <sub>3</sub>		1.4	-	1.85*
Carbonaceous		6.5	-	17.9*(by diff.)

\*Chemical analysis on a 35-50 mesh sample

\*\*Note: Reactivity given in term of oxygenation rate (as  $\mu\text{g-mole}$  of pyrite oxidized per hour per gram of pyrite) in 100% oxygen for the mesh size listed. Other particlesizes of the same type of pyrite were used as noted in the text.

The reactivities are nominal values. Reactivities vary by as much as 50% from one reactor loading to the next, depending on how well the "fines," which formed in storage and handling, were washed from the charge to the reactor bed. Also, method of packing the bed affected reactivity. When interpreting experimental data taken from different series of runs comparative rather than absolute rate data must be used. In many cases a reliable basis for comparison is not available.

## ACKNOWLEDGEMENTS

A large number of faculty, staff, and students at The Ohio State University have contributed to this report.

The co-supervisor of the project for the last several years and co-author of this report Dr. Kenesaw S. Shumate, Associate Professor, Department of Civil Engineering, The Ohio State University, is responsible for the microbiological studies conducted during the course of this project and the written discussion of this phase of work.

Dr. Karlis Svanks, Assistant Professor, Department of Chemical Engineering, developed equipment and procedures for the ferric ion oxidation studies and made the adsorption isotherm determinations.

Dr. Ernest Ehlers, Professor, Department of Mineralogy supervised the mineralogical investigations.

The many hours of stimulating discussions with Professors P. R. Dugan and C. I. Randles of the Department of Microbiology; and Russell Brant, Geologist, The Ohio River Valley Water Sanitation Commission, were very helpful in developing the program and interpreting results.

A major contribution was made by the graduate students who worked on the project. These students and the title of their theses are listed on page 113. Birle, Kim, Morth, Konecik, Jutte, Wendschuh, Halko, and Sasmojo were in the Department of Chemical Engineering. Bailey was in the Department of Civil Engineering with Dr. Shumate as advisor.

The financial support of the Federal Water Pollution Control Administration, and formerly the Department of Health, Education, and Welfare, through Research Grant WP-00340 is gratefully acknowledged.

## REFERENCES

1. Bailey, J. R., "Biological Oxidation of Pyrite," M. S. Thesis, The Ohio State University (1968).
2. Birle, J. D., "Sulfide to Sulfate Reaction Mechanism in Pyrite Materials," M. S. Thesis, The Ohio State University (1963).
3. Braley, S. A., Research Summary Report on Fellowship No. 326B to Mellon Institute (1953).
4. Davies, C. W., "The Extent of Dissociation of Salts in Water, Part VIII," J. Chem. Soc., (1938), 2093.
5. Delchamps, E. W., and Temple, K. L., "Autotrophic Bacteria and the Formation of Acid in Bituminous Coal Mines," Applied Microbiol. 1 (1953), 255.
6. Dugan, P. R., and Randles, C. I., "The Microbial Flora of Acid Mine Water and Its Relationship to Formation and Removal of Acid," Project A-002-OHIO Completion Report, The Ohio State University Water Resources Center, (Oct. 1968).
7. Ehlers, E. G., and Stiles, D. V., "Melanterite-Rozenith Equilibrium," Am. Mineralogist 50 (1965), 1457.
8. Gale, N. L., and Beck, J. V., "Evidence for Calvin Cycle and Hexose Monophosphate Pathway in Thiobacillus ferrooxidans," J. Bacteriol. 94 (1967), 1059.
9. Garrels, R. M., and Thompson, M. E., "Oxidation of Pyrite by Iron Sulfate Solutions," Am. J. Sci., Bradley Volume 258A (1960), 57.
10. Hougen, O. A., and Watson, K. M., Chemical Processes Principles, Vol. III, John Wiley & Sons, Inc., New York (1947).
11. Kim, H. W., "Vapor Phase Oxidation of Pyrite," M. S. Thesis, The Ohio State University (1966).
12. Konicek, M. G., "The Biological Oxidation of Pyrite," M. S. Thesis, The Ohio State University (1966).
13. Lister, M. W., and Rivington, D. E., "Ferric Halide Complexes," Canad. J. Chem. 33 (1955), 1603.
14. Nancolas, G. H., Interactions in Electrolyte Solutions, Elsevier, Amsterdam (1966).
15. Orr, C., and Dallavalle, J. M., Fine Particle Measurement: Size, Surface, and Pore Volume, MacMillan (1959).

16. Parsons, R., Modern Aspects of Electrochemistry, (J. O. M. Brockris, editor), Butterworth, London (1954).
17. Rabinowitch, E., and Stockmeyer, W. H., "Association of Ferric Ions with Chloride, Bromide and Hydroxyl Ions," J. Am. Chem. Soc. 64, (1942), 335.
18. Sasmojo, S., "Oxidation Kinetics of Pyritic Materials in Aqueous Media," Ph.D. Dissertation, The Ohio State University (1969).
19. Schaeffer, W. I.; Holbert, P. E.; and Umbreit, W. W., "Attachment of *Thiobacillus thiooxidans* to Sulfur Crystals," J. Bacteriol. 85 (1963), 137.
20. Sillen, L. G., and Martell, E., "Stability Constants of Metal Ion Complexes," Special Publication No. 17, The Chemical Society, London (1964).
21. Silverman, M. P., "Mechanism of Bacterial Pyrite Oxidation," J. Bacteriol. 94 (1967), 1046.
22. Silverman, M. P., and Lundgren, D. G., "Studies on the Chemoautotrophic Iron Bacterium *Ferrobacillus ferrooxidans* - I. An Improved Medium and Harvesting Procedure for Securing High Cell Yields," J. Bacteriol. 77, (1959), 642.
23. Standard Methods for the Examination of Water and Waste Water, 12th Ed., Am Public Health Assoc., New York, New York (1965).
24. Stokes, H. N., "On Pyrite and Marcasite," U.S.G.S. Bulletin 186, (1901).
25. Sykes, K. W., "The Structure and Reactivity of the Complexes of Ferric Ions with Some Simple Anions," Chem. Soc. (London) Spec. Publ., No. 1 (1954), 64.
26. Wendschuh, P. H., "The Use of the Potentiostat to Study the Sulfide to Sulfate Reaction Mechanism," M. S. Thesis, The Ohio State University (1967).
27. Whiteker, R. A., and Davidson, N., "Iron (III) Sulfate Complex Ions: Ion-Exchange and Spectra," J. Am. Chem. Soc. 75 (1953), 3081.

## LIST OF PUBLICATIONS

### Master of Science Theses

- Birle, J. D., "Sulfide to Sulfate Reaction Mechanism in Pyritic Materials," The Ohio State University (1963).
- Kim, H. W., "Vapor Phase Oxidation of Pyrite," The Ohio State University (1964).
- Morth, A. H., "Reaction Mechanism of the Oxidation of Iron Pyrite," The Ohio State University (1965).
- Konicek, M. G., "The Biological Oxidation of Pyrite," The Ohio State University (1966).
- Jutte, B. B. Jr., "Effect of Oxygen and Nitrogen in Aqueous Solution on the Kinetics of the Sulfide-to-Sulfate Reaction," The Ohio State University (1966).
- Wendschuh, P. H., "The Use of the Potentiostat to Study the Sulfide to Sulfate Reaction Mechanism," The Ohio State University (1967).
- Bailey, J. R., "Biological Oxidation of Pyrite," The Ohio State University (1968).
- Halko, E., "Aerobic-Anaerobic Oxidation of Pyrites," The Ohio State University (1968).

### Ph.D. Dissertation

- Sasmojo, S., "Oxidation Kinetics of Pyritic Materials in Aqueous Media," The Ohio State University (1969).

### Papers

- Ehlers, E. G., and Birle, J. D., "Electropolishing of Pyrite," Am. Mineralogist 49 (1964), 800.
- Ehlers, E. G.; Stiles, D. V.; and Birle, J. D., "Fossil Bacteria on Pyrite," Science 148 (1965), 1719.
- Schopf, J. M.; Ehlers, E. G.; Stiles, D. V.; and Birle, J. D., "Fossil Iron Bacteria Preserved in Pyrite," Proc. Am. Phil. Soc. 109 (1965), 288.
- Ehlers, E. G., and Stiles, D. V., "Melanterite-Rozenith Equilibrium," Am. Mineralogist 50 (1965), 1457.

Morth, A. H., and Smith, E. E., "Kinetics of the Sulfide-to-Sulfate Reaction," Paper to 151st National Meeting, Am. Chem. Soc., Pittsburgh, Pa. (March, 1966).

Smith, E. E., "Engineering Aspects of Acid Mine Drainage," Proc. Second Annual Symposium, Water Resources Research, The Ohio State University (1966).

Smith, E. E., "Acid Mine Drainage Research at the Ohio State University," Proc. 22nd Purdue Industrial Waste Conference (May, 1967).

Smith, E. E.; Svanks, K.; and Shumate, K. S., "Sulfide to Sulfate Reaction Studies," Second Symposium on Coal Mine Drainage Research, Mellon Inst., Pittsburgh, Pa. (May, 1968).

Smith, E. E.; Svanks, K.; and Halko, E., "Aerobic-Anaerobic Oxidation of Pyrite," 157th National Meeting, Am. Chem. Soc., Division of Fuel Chemistry, Minneapolis, Minn. (April, 1969).

## GLOSSARY OF TERMS

EMF - Electromotive Force (voltage) as observed using a Platinum-Saturated Calomel electrode pair for oxidation-reduction potential measurements.

Ferric Ion Oxidation - Oxidation of pyrite where immediate oxidizing agent is the ferric ion. The ultimate electron acceptor in natural systems is oxygen.

Free Ferric Ion - Non-complexed ferric ion in solution.

Museum Grade Pyrite - Large crystalline mass of pyrite, usually from igneous deposits; the type obtained from mineral supply houses.

Oxygenation - Oxidation of pyrite by direct reaction with oxygen.

Sulfur Ball - Pyritic material found in coal measures; present in finely disseminated particles up to massive agglomerates.



BIBLIOGRAPHIC: The Ohio State University  
Research Foundation.  
A Study of the Sulphide-to-Sulphate Reaction  
Mechanism. FWPC Publication No. WP-

ACCESSION NO:

KEY WORDS:

A detailed study of the mechanisms and kinetics of the chemical reactions responsible for acid mine drainage has been made. The mineralogical features of the solid phase reactant (pyrite) that determine its reactivity were described. The rate-limiting reactions and variables affecting the rate of these reactions were identified.

It was found that two basic oxidation modes are important: oxygenation, in which oxygen is the immediate oxidizing agent; and ferric ion (or microbiologically catalyzed) oxidation, in which ferric ions are the oxidants. From a knowledge of the dissolved oxygen, ferric/ferrous ratio, and total iron ion content at the reaction site,

Mine Drainage  
Coal Mine Drainage  
Sulfides  
Iron Sulfides  
Pyrite  
Ferrobacillus  
Pollution Abatement  
Industrial Wastes  
Reaction Kinetics

BIBLIOGRAPHIC: The Ohio State University  
Research Foundation.  
A Study of the Sulphide-to-Sulphate Reaction  
Mechanism. FWPC Publication No. WP-

ACCESSION NO:

KEY WORDS:

A detailed study of the mechanisms and kinetics of the chemical reactions responsible for acid mine drainage has been made. The mineralogical features of the solid phase reactant (pyrite) that determine its reactivity were described. The rate-limiting reactions and variables affecting the rate of these reactions were identified.

It was found that two basic oxidation modes are important: oxygenation, in which oxygen is the immediate oxidizing agent; and ferric ion (or microbiologically catalyzed) oxidation, in which ferric ions are the oxidants. From a knowledge of the dissolved oxygen, ferric/ferrous ratio, and total iron ion content at the reaction site,

Mine Drainage  
Coal Mine Drainage  
Sulfides  
Iron Sulfides  
Pyrite  
Ferrobacillus  
Pollution Abatement  
Industrial Wastes  
Reaction Kinetics

BIBLIOGRAPHIC: The Ohio State University  
Research Foundation.  
A Study of the Sulphide-to-Sulphate Reaction  
Mechanism. FWPC Publication No. WP-

ACCESSION NO:

KEY WORDS:

A detailed study of the mechanisms and kinetics of the chemical reactions responsible for acid mine drainage has been made. The mineralogical features of the solid phase reactant (pyrite) that determine its reactivity were described. The rate-limiting reactions and variables affecting the rate of these reactions were identified.

It was found that two basic oxidation modes are important: oxygenation, in which oxygen is the immediate oxidizing agent; and ferric ion (or microbiologically catalyzed) oxidation, in which ferric ions are the oxidants. From a knowledge of the dissolved oxygen, ferric/ferrous ratio, and total iron ion content at the reaction site,

Mine Drainage  
Coal Mine Drainage  
Sulfides  
Iron Sulfides  
Pyrite  
Ferrobacillus  
Pollution Abatement  
Industrial Wastes  
Reaction Kinetics

the reaction regime can be determined.

Kinetic equations were derived for both reaction modes. From these basic relationships the oxidation rate in real pyritic systems can be accurately predicted when conditions at the reaction site are known.

For a given pyrite surface oxygenation rate is, for all practical purposes, dependent only on the oxygen concentration in the aqueous phase surrounding the reactive site on the pyrite surface. Ferric ion oxidation rate is determined by the ferric/ferrous ratio and free ferric ion concentration in solution, and is not affected by dissolved oxygen.

In a real system, the ferric/ferrous ratio is determined by a "relative" microbial activity; i.e., the number of bacteria per exposed pyrite surface. Bacteria concentration is limited by pH and oxygen concentration as well as nutrient levels.

the reaction regime can be determined.

Kinetic equations were derived for both reaction modes. From these basic relationships the oxidation rate in real pyritic systems can be accurately predicted when conditions at the reaction site are known.

For a given pyrite surface oxygenation rate is, for all practical purposes, dependent only on the oxygen concentration in the aqueous phase surrounding the reactive site on the pyrite surface. Ferric ion oxidation rate is determined by the ferric/ferrous ratio and free ferric ion concentration in solution, and is not affected by dissolved oxygen.

In a real system, the ferric/ferrous ratio is determined by a "relative" microbial activity; i.e., the number of bacteria per exposed pyrite surface. Bacteria concentration is limited by pH and oxygen concentration as well as nutrient levels.

the reaction regime can be determined.

Kinetic equations were derived for both reaction modes. From these basic relationships the oxidation rate in real pyritic systems can be accurately predicted when conditions at the reaction site are known.

For a given pyrite surface oxygenation rate is, for all practical purposes, dependent only on the oxygen concentration in the aqueous phase surrounding the reactive site on the pyrite surface. Ferric ion oxidation rate is determined by the ferric/ferrous ratio and free ferric ion concentration in solution, and is not affected by dissolved oxygen.

In a real system, the ferric/ferrous ratio is determined by a "relative" microbial activity; i.e., the number of bacteria per exposed pyrite surface. Bacteria concentration is limited by pH and oxygen concentration as well as nutrient levels.